

05

111

E75 10266

CR-14264



"Made available under NASA sponsorship  
in the interest of early and wide dis-  
semination of Earth Resources Survey  
Program information and without liability  
for any use made thereof."

(E75-10266) PRINCIPAL SOURCES AND DISPERSAL PATTERNS OF SUSPENDED PARTICULATE MATTER IN NEARSHORE SURFACE WATERS OF THE NORTHEAST PACIFIC OCEAN Final Report, 1 Sep. 1972 - 1 Jan. 1974 (Geological Survey) 145 p HC	N75-22877  Unclas G3/43 00266
--	--

1209A

RECEIVED

FEB 21 1975

SIS/902.6

Original photography may be purchased from:  
EROS Data Center  
10th and Dakota Avenue  
Sioux Falls, SD 57198

JSC

PRINCIPAL SOURCES AND DISPERSAL PATTERNS  
OF SUSPENDED PARTICULATE MATTER  
IN NEARSHORE SURFACE WATERS OF  
THE NORTHEAST PACIFIC OCEAN

Paul R. Carlson, T. John Conomos, Richard J. Janda, and David H. Peterson

U.S. Geological Survey  
345 Middlefield Road  
Menlo Park, California 94025

February 10, 1975

Final Report

1 September 1972 - 1 January 1974

Prepared for:

NASA  
Goddard Space Flight Center  
Greenbelt, Maryland 20771

TECHNICAL REPORT STANDARD TITLE PAGE

1. Report No.	2. Government Accession No.	3. Recipient's Catalog No.	
4. Title and Subtitle Principal sources and dispersal patterns of suspended particulate matter in nearshore surface waters of the northeast Pacific Ocean		5. Report Date February 10, 1975	6. Performing Organization Code
		8. Performing Organization Report No.	
7. Author(s) Carlson, Paul R., Conomos, T. John, Janda, Richard J., and Peterson, David H.		10. Work Unit No.	
9. Performing Organization Name and Address U.S. Geological Survey 345 Middlefield Road Menlo Park, California 94025		11. Contract or Grant No. SR 209	
		13. Type of Report and Period Covered Type III Final Report 1 Sept. 72 - 1 Jan. 74	
12. Sponsoring Agency Name and Address Edward W. Crump Goddard Space Flight Center Greenbelt, Maryland 20771		14. Sponsoring Agency Code	
		15. Supplementary Notes	
16. Abstract. Nearshore, near-surface currents off California, Oregon and Washington, as monitored with ERTS imagery, undergo seasonal changes similar to models of oceanic currents over the outer continental shelf off these western states. The flow directions are southward during March-October (California Current) reversing to northward during November-February (Davidson Current). In nearshore waters of the northeastern Gulf of Alaska, however, a counterclockwise current flow prevails throughout the year. This flow moves suspended sediment from the Copper River into Prince William Sound and would do likewise with oil spilled in the northeastern Gulf of Alaska. Suspended sediment from the Yukon River is carried north along the eastern edge of the Bering Sea and some may eventually reach the Chukchi Sea via Bering Strait. In all regions, local variations were seen and must be considered in coastal zone planning.			
<p>In estuaries (e.g. San Francisco Bay), ERTS imagery provides supplementary circulation data, but resolution and repetition are marginal for small, rapidly changing features. Conventional aerial photography (e.g. U-2) provides more useable coverage of circulation patterns of turbid water.</p> <p>Resolution of ERTS imagery proved to be a problem in detailed geologic mapping of the northern Olympic Peninsula, however, satellite imagery does provide an overview of major features important to regional interpretations.</p> <p>Comparison of ERTS imagery with older maps of Icy Bay, Alaska shows the glaciers have retreated at a rate of 5 km<sup>2</sup>/yr since 1952. ERTS imagery provides a means of mapping receding ice fronts and documenting coastal changes in relatively inaccessible regions.</p>			
17. Key Words Suggested by Author Suspended sediment plumes Nearshore, near-surface circulation Seasonal changes in coastal currents Estuarine suspended matter		18. Distribution Statement	
19. Security Classif. (of this report)	20. Security Classif. (of this page)	21. No. of Pages 139	22. Price

Figure 2A. Technical Report Standard Title Page. This page provides the data elements required by DoD Form DI-1473, HEW Form OE-6000 (ERIC), and similar forms.

## CONTENTS

CHAPTER		PAGE
1	INTRODUCTION	1
2	THE EVOLUTION OF ICY BAY, ALASKA, by Tau Rho Alpha	4
3	CIRCULATION OF NEARSHORE SURFACE WATER IN THE GULF OF ALASKA, by Erk Reimnitz and Paul R. Carlson	10
4	ERTS IMAGERY AND DISPERSAL OF YUKON AND KUSKOKWIM RIVER SEDIMENTS IN THE NORTHEASTERN BERING SEA, by C. Hans Nelson, Bradley R. Larsen and Robert W. Rowland	26
5	APPLICATION OF ERTS IMAGERY TO THE INTERPRETATION OF THE GEOLOGIC FRAMEWORK OF THE NORTHWESTERN OLYMPIC PENINSULA, WASHINGTON AND THE SOUTH SIDE OF VANCOUVER ISLAND, BRITISH COLUMBIA, by Parke D. Snively, Jr., and Norman S. MacLeod	41
6	SEASONAL DISTRIBUTION OF THE COLUMBIA RIVER EFFLUENT by Paul R. Carlson and T. John Conomos	46
7.	DISTRIBUTION, ABUNDANCE, AND COMPOSITION OF SUSPENDED PARTICLES IN THE SAN FRANCISCO BAY SYSTEM, APRIL AND JULY 1973, by Paul R. Carlson, T. John Conomos, Harley J. Knebel, David H. Peterson, E. Peter Scrivani, Richard E. Smith, William C. Todd, and Sally M. Wienke	58
8	A FIELD EVALUATION OF A NEPHELOMETER FOR THE DETECTION OF TURBIDITY VARIATIONS IN SAN FRANCISCO BAY AND THE GULF OF THE FARALLONES by Laurence E. Schemel	92
9	ERTS OBSERVATIONS OF SURFACE CURRENTS ALONG THE PACIFIC COAST OF THE UNITED STATES, by Paul R. Carlson and Deborah R. Harden	100

CHAPTER		PAGE
10	ERTS IMAGERY OF THE WEST-CENTRAL COASTAL ZONE OF MEXICO, by Deborah R. Harden, Erk Reimnitz, and Paul R. Carlson	127
11	CONCLUSIONS	134
12	APPENDIX (Papers associated with ERTS experiment)	136

## INTRODUCTION

This experiment was conceived as the result of preliminary aerial and shipboard observations of turbid surface water patterns in estuary and nearshore waters, largely of the San Francisco Bay system (Carlson and others, 1970; Carlson, 1971). San Francisco Bay was emphasized for this study because of the extensive investigations underway involving physical and chemical characteristics of water and suspended sediment (McCulloch and others, 1970). The synoptic, small-scale coverage provided by ERTS encouraged us to expand the study over the western coastline of North America from Alaska to Mexico (Fig. 1). We feel that this study have given us insight into coastal processes of this region that would have been virtually unattainable any other way.

Due to the varied nature of the region and the investigations, the studies are divided into individual chapters in this report. The areas and the respective chapters are shown on Figure 1. The first chapters deal with Alaska and adjacent waters. Subsequent chapters proceed south along the west coast from the Olympic Peninsula to San Francisco Bay. The report concludes with a short note about the Mexican coastal zone.

The principal objectives have been to evaluate sources and dispersal patterns of suspended sediment in the nearshore zone, to obtain an overview of nearshore circulation along the west coast, and to determine the resolution of ERTS imagery and the resultant application to studies of coastal sedimentation problems and processes.

This experiment was most successful in obtaining seasonal information about nearshore surface water circulation. The synoptic view of the turbid coastal waters afforded by ERTS will be valuable for (1) choosing the location of waste discharge effluents and dredge spoil disposal sites, (2) determining actions which will minimize harmful effects of oil spills and (3) facilitating coastal zone planning and management.

The most difficult task attempted in this study was to relate "water truth" to ERTS imagery. Many complications arose: (1) excessive clouds or haze, (2) heavy seas, (3) dense, underexposed, positive transparencies, (4) rapidly changing water properties which could not be related to features observable on the imagery, (5) scale problems (resolution was limited to features >50-100 meters) and (6) the lag time between the date an area was flown over by the satellite and the date the image was received by the investigators.

### Acknowledgements

Helpful discussions about various aspects of the study were held with: Robert Thompson, James Gast, and George Crandall, Oceanog. Dept. Calif. St. Univ., Humboldt; Stephens Tucker, Naval Post Graduate School; Douglas Pirie, U.S. Army Corps of Engineers; David Stellar, Geosource.

ORIGINAL PAGE IS  
OF POOR QUALITY

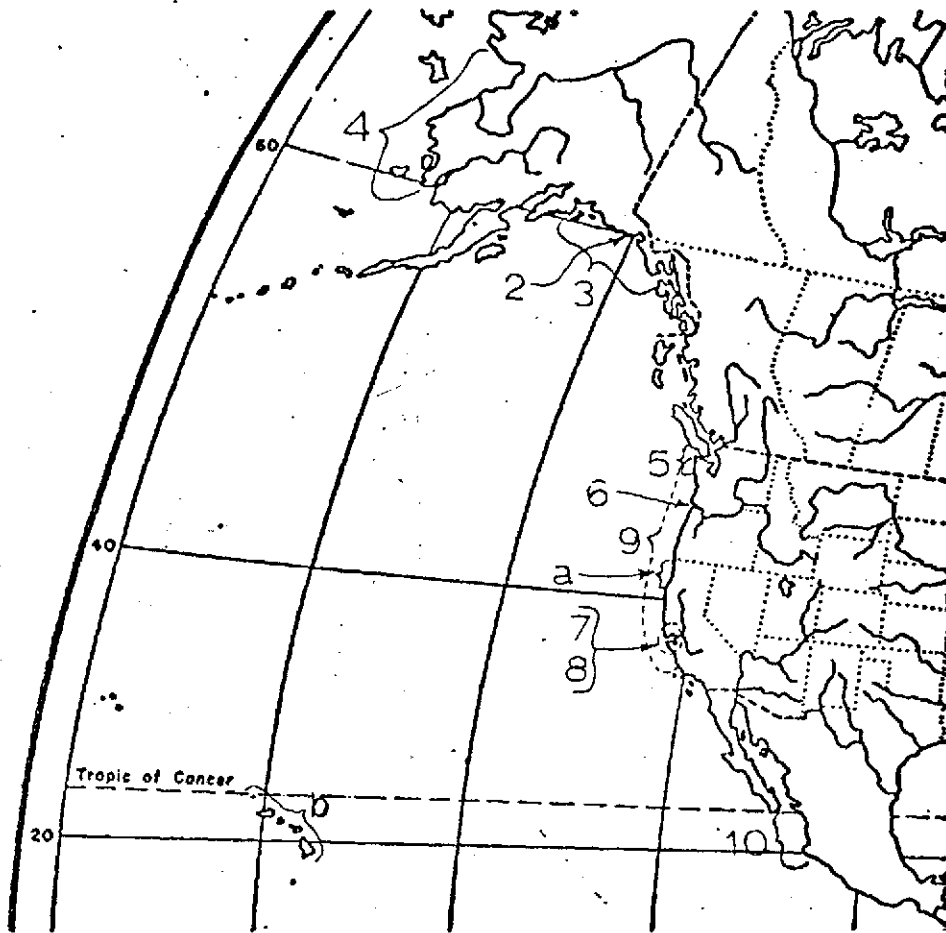


Figure 1. Index map of study areas. Numbers indicate chapters pertaining to the areas. Letters (a and b) mark study areas not in report but to be appended.

ORIGINAL PAGE IS  
OF POOR QUALITY

International; Donald Ross, International Imaging Systems; Robert Heller, Robert Aldrich, and Robert Dana, U.S. Forest Service; V. Klemas, Marine Studies, University of Delaware and numerous colleagues at the U.S. Geological Survey.

James Gast and his students provided assistance at sea and Gast and Robert Thompson provided additional oceanographic data. Stephens Tucker furnished Secchi disc data for the offshore waters. James Baker, Stanford University was instrumental in obtaining computer output of ERTS digitized data. NASA (Ames) personnel associated with the U-2 program provided useful and timely aerial coverage.

#### References Cited

- Carlson, P. R., 1971, Remote sensing in marine geology: Arctic to Caribbean, in third annual earth resources program review: Ntl. Aeronautics and Space Admin., Houston, Texas, vol. I, p. 17-1 - 17-17.
- Carlson, P. R., Peterson, D. H., Conomos, T. J., and McCulloch, D. S., 1970, Aerial and in situ observations of a fresh-water plume in San Francisco Bay and adjacent Pacific Ocean: Trans., Am. Geophys. Union, v. 51, p. 767.
- McCulloch, D. S., Peterson, D. H., Carlson, P. R., and Conomos, T. J., 1970, Some effects of fresh water inflow on the flushing of South San Francisco Bay: A preliminary report: U.S. Geol. Survey Circ. 637A, p. A1-A27.

ORIGINAL PAGE IS  
OF POOR QUALITY

## THE EVOLUTION OF ICY BAY, ALASKA

by

Tau Rho Alpha

A comparison of early sketch maps, Alaskan topographic maps and ERTS imagery, suggests that Icy Bay developed in the past 175 years as the ice front of Guyot and Tyndall glaciers receded. Icy Bay lies at the foot of Mt. St. Elias in southeastern Alaska (Fig. 1) and is bordered by three large glaciers: Guyot to the west, Tyndall to the north and Malaspina, the largest glacier in North America to the east (Fig. 2-5) (Shepard and Wanless, 1971, p. 411).

The present Icy Bay was named in 1913 by Tarr and Martin (1914); however, as early as 1794 this area was visited by Vancouver (1798). Vancouver's sketch map and the reports of Tebenkof (1852) and Topham (1889) suggest that a bay existed to the east of the present Icy Bay at the former outlet of the Yahtse River (Figs. 2 and 3). The configuration of this bay, as depicted in figure 2, was based on these early reports, the onshore landforms of the former delta of the Yahtse River, the well-defined sand barriers and spits and the lateral moraines of the combined Guyot and Tyndall glaciers (Plafker and Miller, 1958). These morphologic features, particularly the sand barriers and spits, are visible on ERTS imagery (Fig. 5). The maximum extent of the Guyot and Tyndall glaciers was based on a submarine shoal and on the distribution of a glacial moraine adjacent to the present Icy Bay (Fig. 1). This crescent-shaped submarine shoal has a relief of 50 feet and is located just beyond the mouth of Icy Bay. From acoustic seismic profiles taken in 1974 there is evidence that this shoal is composed of morainal material (Terry Bruns, 1974, personal comm.).

The development of Icy Bay parallels the recession of the combined Guyot and Tyndall glaciers. The estimated withdrawal of the ice from its maximum extent, as indicated by the submarine moraine, until the 1950-52 period created 280 sq. km. of bay. This withdrawal reached a point in the 1950's where the two glaciers were no longer combined (Fig. 3).

The Icy Bay of Vancouver presumably was filled into elevations above sea level by glacial outwash from the Malaspina glacier through the delta of the Yahtse River and by sandspits built into the east side of the bay by the prevailing westerly longshore currents (Shepard and Wanless, 1971, p. 416). The 1974 acoustic seismic profiles of the Icy Bay area show no evidence for isostatic changes, glacial rebound, or active tectonism that could account for the retreat of the Guyot and Tyndall glaciers (Terry Bruns, 1974, personal comm.; George Plafker, 1974, personal comm.).

ORIGINAL PAGE IS  
OF POOR QUALITY

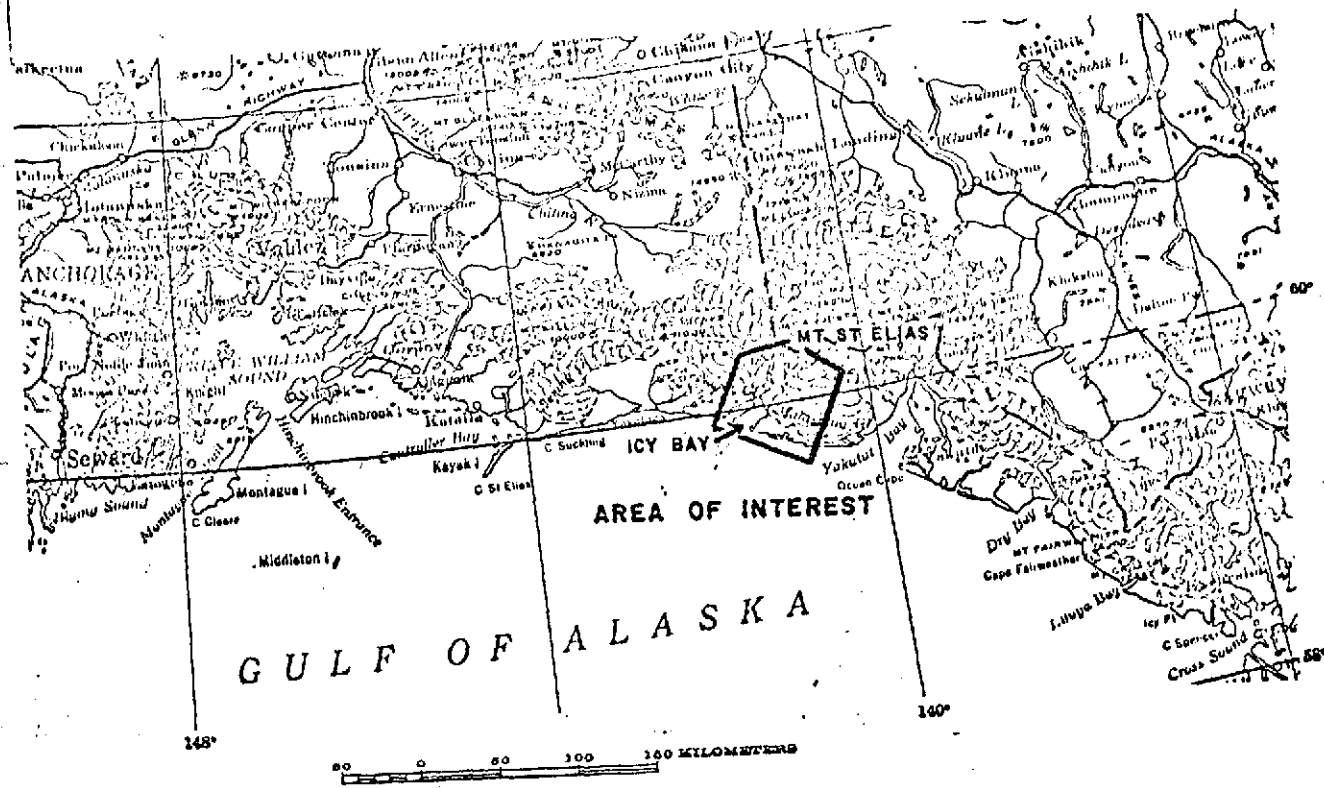


Figure 1. Location map for Icy Bay, Alaska, a portion of U.S. Geological Survey 1:1,584,000 Scale Map 1955.

ORIGINAL PAGE IS  
OF POOR QUALITY

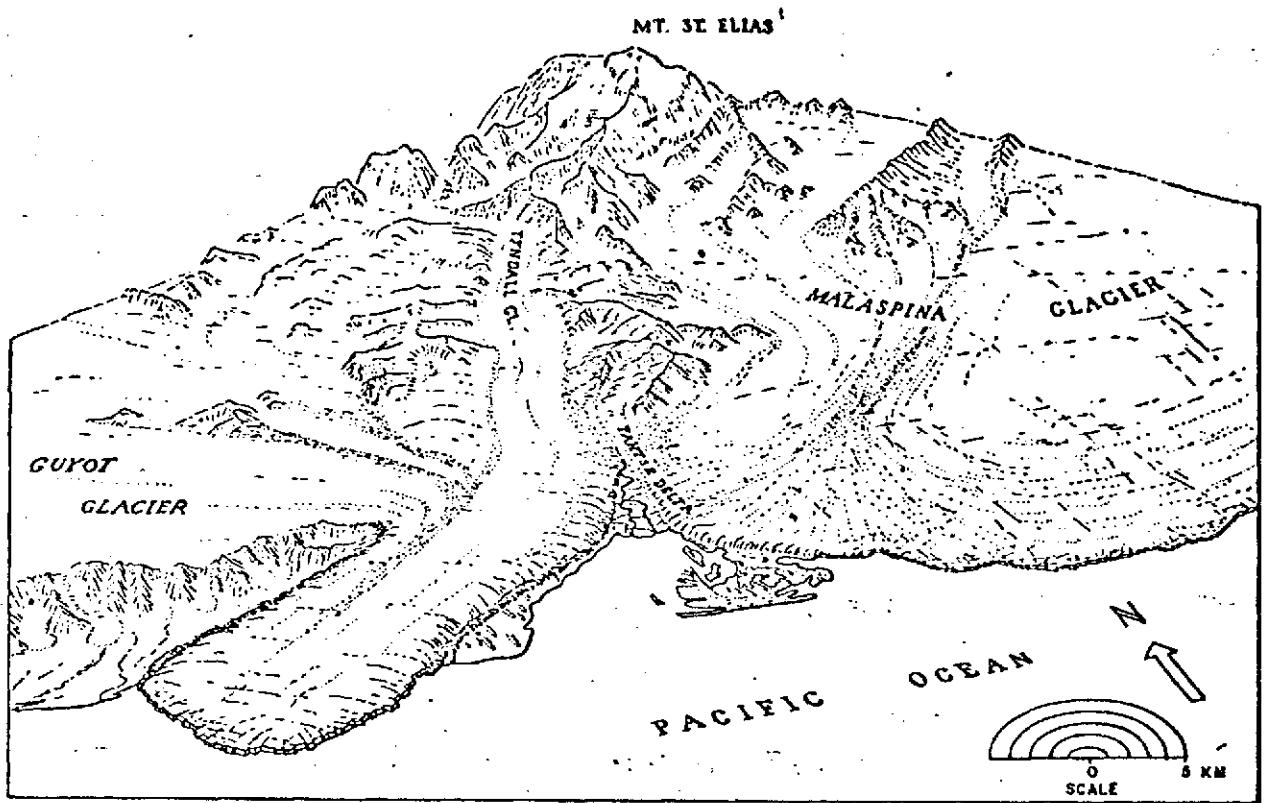


Figure 2. The unnamed bay. Based on the visits of Vancouver (1798,) Tebenkof (1852), and Topham (1889).

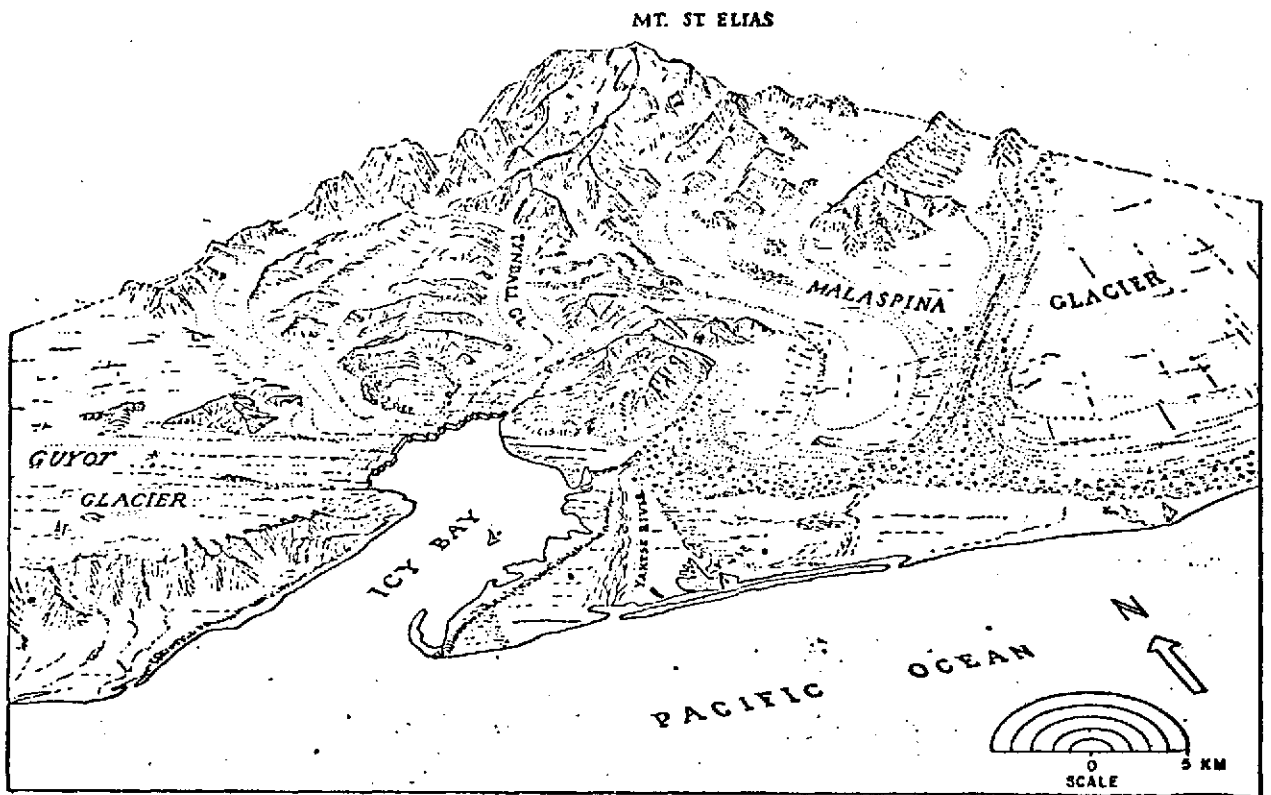


Figure 3. Icy Bay as it appeared in 1950-1952. Based on four maps of the U.S. Geological Survey, Alaska Topographic Series 1:250,000 (Bering Glacier, 1950; Icy Bay, 1950; Mt. St. Elias, 1952, and Yakutat, 1952).

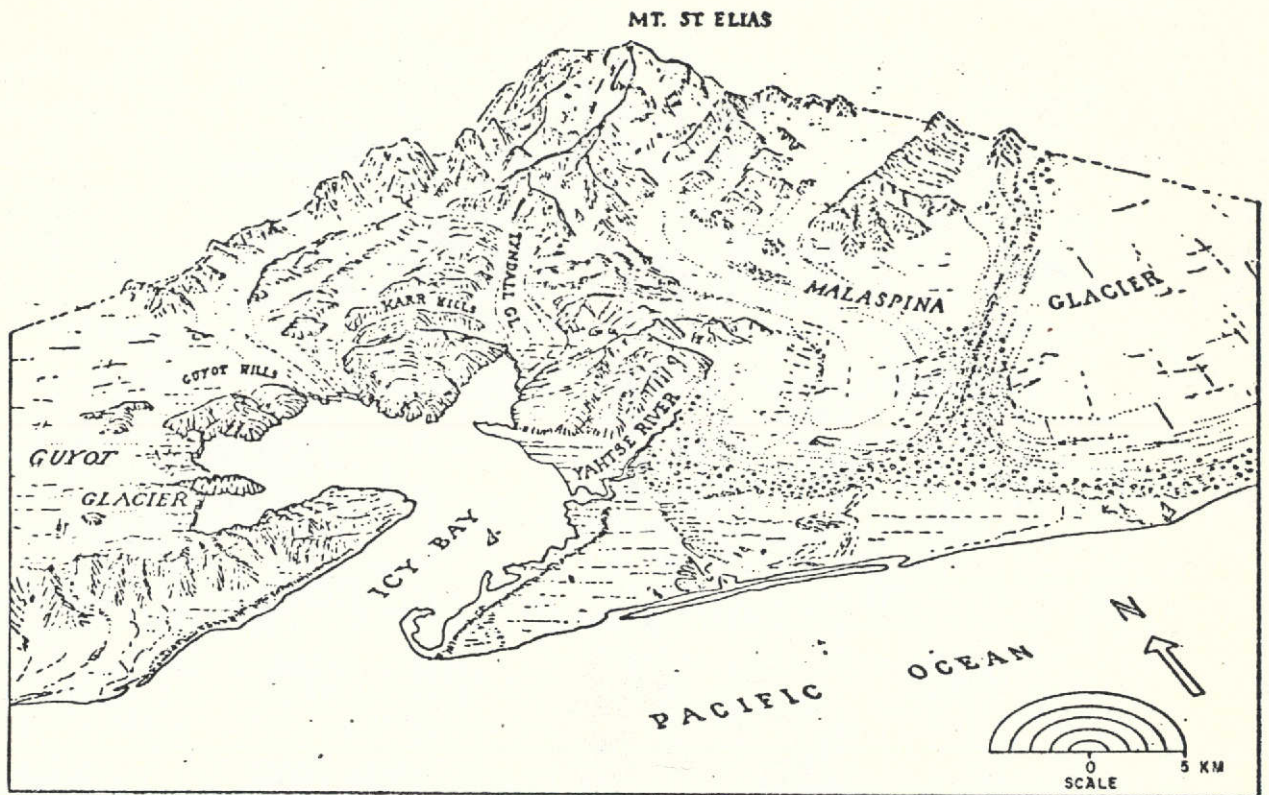


Figure 4. Icy Bay as it appeared in 1972. Based on ERTS imagery of 21 September 1972 MSS-7 1060 20111.

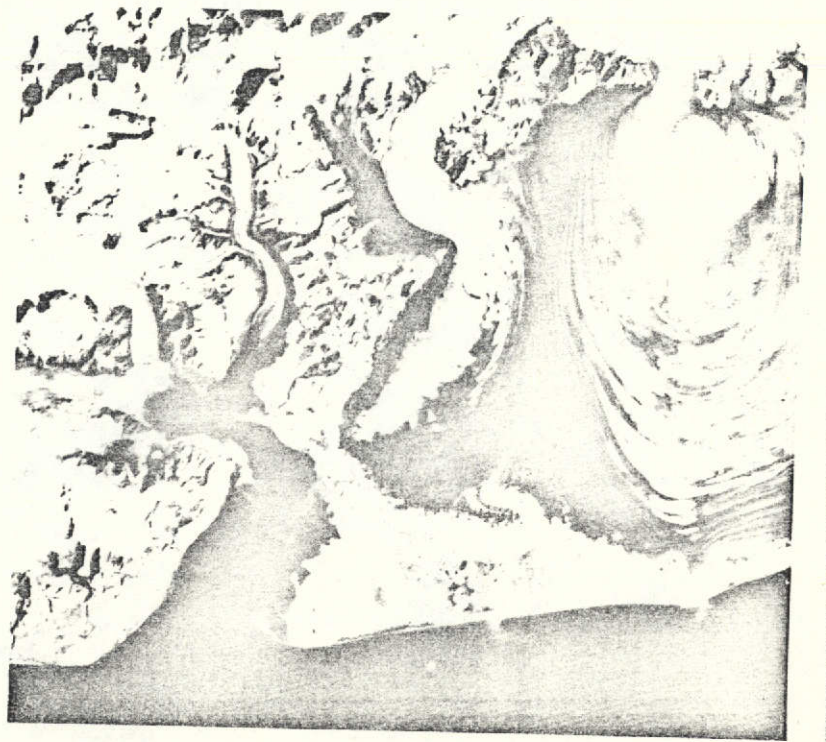


Figure 5. ERTS imagery of 21 September 1972 MSS-7 1060 20111. Illustrating maximum retreat of ice front up to 1972.

ERTS imagery of 1972 (Fig. 5) and 1973 depicts Icy Bay as having developed four distinct inlets due to the recession of an estimated  $5 \text{ km}^2/\text{yr} \approx 100 \text{ sq. km}$  of ice since 1950-1952 (compare figs. 3 and 4). The two inlets to the west have developed from that part of the ice front of Guyot glacier that is west of the Guyot Hills. There is a lobe of Guyot glacier that flows on the east side of the Guyot Hills that has developed into the smallest of the new inlets in Icy Bay. The fourth inlet of Icy Bay has developed at the mouth of Tyndall glacier at the base of Mt. St. Elias. Along with the development of the new inlets, new headlands have been exposed as the ice front receded. Except for the Karr Hills and the Guyot Hills, all of the other headlands had been covered with ice previous to 1972 (compare figs. 3 and 4). Another change illustrated by ERTS imagery is that the Yahtse River flows directly into Icy Bay and no longer flows toward the earlier unnamed bay which is now completely filled up (Fig. 4). This infilling process has left high and dry the sand barriers and spits which were near the mouth of Vancouver's Icy Bay. In the ERTS imagery the stagnant ice front of Malaspina glacier which terminates onshore is not as spectacular as the abrupt tidewater fronts of Guyot and Tyndall glaciers because the front of the Malaspina is low and covered with pitted moraine and vegetation (Plafker and Miller, 1958). Some of the larger pitholes and ice-margin lakes are visible in the imagery.

ERTS imagery of southeastern Alaska was used by M. F. Meier (1973) to calculate a  $3 \text{ sq. km}$  ice loss in an 18-day period at the terminus of Hubbard glacier. This loss is the largest observed in an Alaskan glacier in so short a time (Meier, 1973). Thus large scale ice retreats which averaged  $5 \text{ km}^2/\text{yr}$  during the evolution of Icy Bay are reasonable.

An estimated growth of  $380 \text{ sq km}$  of bay has been documented by early explorers, modern planimetric mapping and by ERTS imagery. ERTS imagery provides a low cost, convenient means of mapping the receding ice front and documenting the rapidly changing coastal landforms in this relatively inaccessible region.

ORIGINAL PAGE IS  
OF POOR QUALITY

#### REFERENCES CITED

- Meier, M. F., 1973, Evaluation of ERTS imagery for mapping and detection of changes of snowcover on land and on glaciers, in Symposium on significant results obtained from the Earth Resources Technology Satellite-1, Vol. 1; Technical Presentations Section A: Natl. Aeronautics and Space Adm., p. 862-875.
- Plafker, George, and Miller, D. J., 1958, Glacial feature and surficial deposits of the Malaspina District, Alaska: U.S. Geol. Survey Misc. Geol. Inv. Map I-271, scale 1:125,000.
- Shepard, F. P., and Wanless, H. R., 1971, Our changing coastlines: McGraw-Hill Book Company, New York, 579 p.
- Tarr, R. S., and Martin, Lawrence, 1914, Alaskan glacier studies: Natl. Geog. Soc., Washington, 498 p.
- Tebenkof, Michael, 1852, Hydrographic atlas and observations: with 48 charts, St. Petersburg (map published in Tarr and Martin, 1914).
- Topham, H. W., 1889, An expedition to Mount St. Elias: Alpine Jour., v. 14, p. 345-371.
- U.S. Geological Survey, 1950, Bering Glacier: Alaskan Topog. Map, scale 1:250,000.
- \_\_\_\_\_, 1950, Icy Bay: Alaskan Topog. Map, scale 1:250,000.
- \_\_\_\_\_, 1952, Mount St. Elias: Alaskan Topog. Map, scale 1:250,000.
- \_\_\_\_\_, 1952, Yakutat: Alaskan Topog. Map, scale 1:250,000.
- Vancouver, George, 1798, Voyage of discovery to the North Pacific Ocean in the years 1790-1795: London, v. 3, atlas, printed for G. G. and J. Robinson, Paternoster-Row; J. Edwards, Pall-Mall (as referenced in Plafker and Miller, 1958).

ORIGINAL PAGE IS  
OF POOR QUALITY

## CIRCULATION OF NEARSHORE SURFACE WATER IN THE GULF OF ALASKA

Erk Reimnitz and Paul R. Carlson

As plans progress for increased use of nearshore waters in the Gulf of Alaska (Fig. 1), more information is urgently needed regarding water circulation. Potential areas of use and environmental conflict include transportation (oil tanker traffic from Valdez to lower 48 states), fisheries development and protection, and offshore drilling and related activities. Although general information has been published regarding the movement of oceanic surface water in the Gulf of Alaska (Fig. 2) data are sparse for the nearshore waters. Reasons are: relative inaccessability, formidable weather, and expense and difficulty in obtaining synoptic data for nearshore waters. However, ERTS provides a valuable tool for a reconnaissance of these nearshore waters.

The purpose of this chapter is to illustrate the usefulness of ERTS imagery for the study of circulation of nearsurface water and the dispersal of suspended sediment and detrimental pollutants such as oil in the nearshore waters of the northeastern Gulf of Alaska. The geographic area extends from Cross Sound and Glacier Bay in the southeast to Prince William Sound and Valdez Arm in the northwest (Fig. 1). This 750 km long stretch of glaciated coast will be discussed in two units: (1) Cross Sound to Kayak Island which contains small glacial streams and two large glaciers which reach the open coast and (2) the Copper River Delta region which dominates the coastline between Kayak Island and Prince William Sound. (Also, see Chapter 2 on Icy Bay by Alpha, this report.)

### Interpretive Techniques

Imagery of southcentral Alaska was obtained for intervals during the period of September 1972 to November 1973. Clouds, of course, obscured much of the scene on many passes; however, because a pass was made every 18 days several clear images were obtained of most of this coastal region in September of 1972 and 1973 and images of varying cloud cover and quality were obtained at other times of the year for various segments of the coastal waters.

Circulation patterns or flow directions of the near surface water are inferred from the configuration of patterns of turbid water which are especially prominent in the nearshore zone during times of high discharge from coastal rivers and streams. Along the coast of southcentral Alaska, discharge is highest during the summer and early fall (Fig. 3) when maximum glacial melt occurs and the glacially fed streams become brown due to the large quantities of glacial "flour" (fine silt and clay) suspended in the water. For example, Hoskins and Burrell (1972) reported a suspended sediment load of more than 1,000 mg/l in Glacier Bay

**ORIGINAL PAGE IS  
OF POOR QUALITY**



Figure 1. ERTS study area of southeastern Alaska. Portion of U.S.G.S. 1:1,584,000 scale map, 1955.

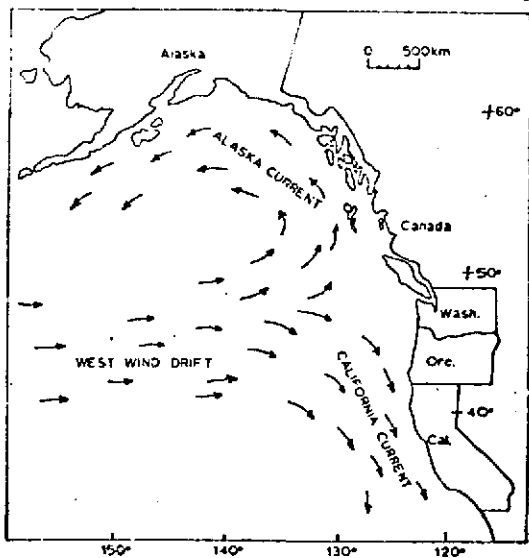


Figure 2. Surface currents of the Northeast Pacific Ocean (modified from Uda, 1963, and Dodimead and others, 1963).

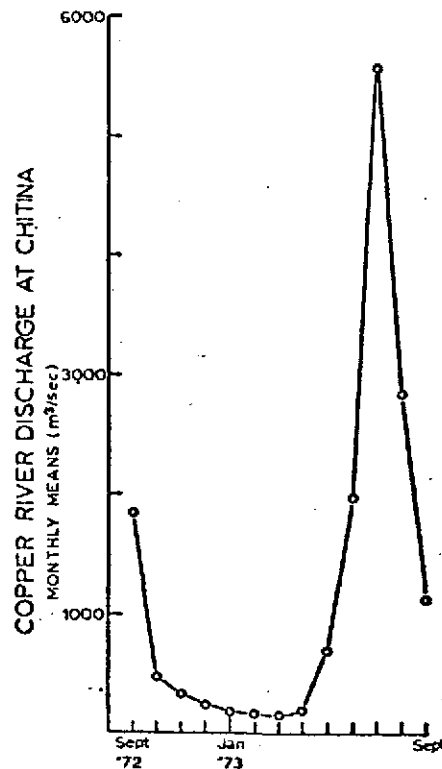


Figure 3. Discharge of the Copper River at Chitina, Alaska for the period September 1972-September 1973. Discharge data from U.S. Geological Survey (Larry S. Leveen, oral commun., 1974).

ORIGINAL PAGE IS  
OF POOR QUALITY

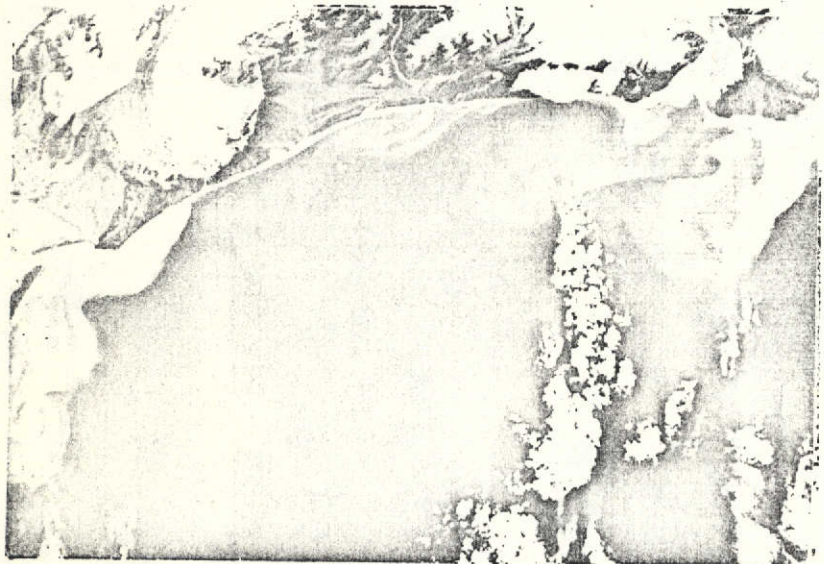
where glacial streams entered the fjord. At these times of high discharge, turbid water patterns are visible on ERTS imagery more than 50 km offshore (Fig. 4a). Each of the four bands of the multispectral scanner system provided information of value. The plume of suspended sediment discharged into the ocean is seen in greatest detail on the green band (0.5-0.6  $\mu\text{m}$ ) (Fig. 4a). The red band (0.6-0.7  $\mu\text{m}$ ) provides an outline of the main core of the plume (Fig. 4b), and the near infrared band (0.7-0.8  $\mu\text{m}$ ) shows only the immediate outlet position of the effluents with highest sediment concentrations. The infrared band (0.8-1.1  $\mu\text{m}$ ) (Fig. 4c) provides the best penetration through atmospheric haze and therefore most clearly delineates the shoreline. Use of all the bands permits good definition of the effluents and provides a means to determine distance and area covered by the plumes of suspended matter. These plumes can be traced on the green band to at least 50 km distance from the effluent. The greater water penetrating capability of the green wave lengths accounts for the larger plume area visible on the green band compared to the red band image, for as the suspended sediment moves farther from the effluent the sediment becomes more diffuse and settles deeper in the water column.

#### Surface Currents: Cross Sound to Kayak Island

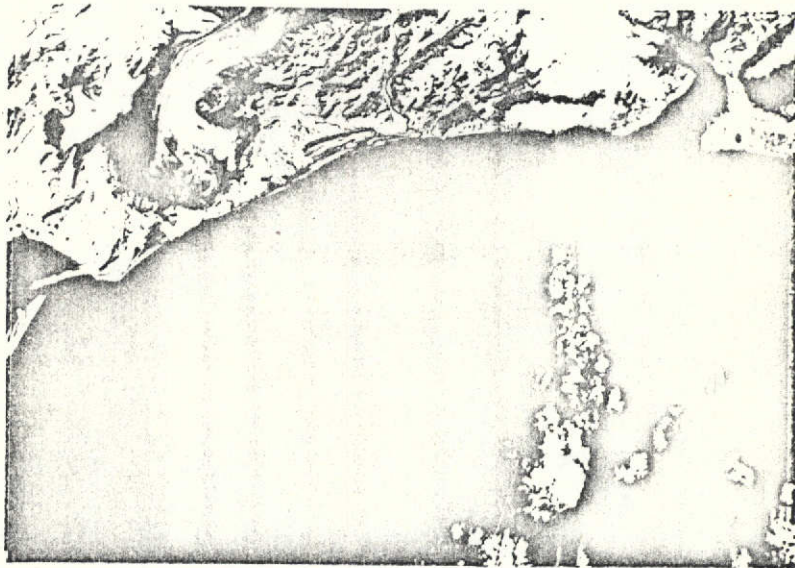
In addition to plume area and source, flow direction of surface currents can be inferred from the red and green bands of the ERTS imagery (Fig. 5). Satellite imagery from two successive days, with a side overlap of almost 50% at this latitude, shows plumes in the nearshore currents setting to the west, a direction consistent with the gyre made by the Alaskan current. The current movement, however, is complicated by changes in winds and tides and by coastal morphology. The complex gyre shown on the imagery of September 22, 1972 (Figs. 4a and 5) was produced by the disrupting influence of Kayak Island. Complications in the surface water flow can also be seen off the mouth of Icy Bay on the sketch made from the September 21, 1972 image (Fig. 5). Subsequent coverage of the nearshore zone off Icy Bay (Fig. 6) shows variations in the nearshore currents during other times of the year. Note particularly the current gyre off the Malaspina Glacier on October 9, 1972, resulting in an easterly flow about 30 km offshore and the confused flow patterns near Icy Bay on May 13, 1973.

Imagery of the coastal zone from Cross Sound to Prince William Sound was obtained on eight successive, nearly cloud-free days in mid-September of 1972 and five successive days in 1973 (Fig. 7). The nearshore patterns of suspended sediment in this area suggest a zone of convergence as the flow direction is toward the southeast along the coast northwest of Lituya Bay, but westerly along the shoreline southeast of the bay. However, this pattern varies at other times of the year (Fig. 8). The influence of islands such as Kayak, Hinchinbrook, and Montague Island can be readily seen on the sketch (Fig. 7). Note especially the complex gyres set up off Kayak Island. Evidence for the persistence, but changeability of this complex gyre can be seen by comparing the September sketches (Fig. 6) with ERTS images taken October 12, 1972 (Fig. 9), and August 14, 1973 (Fig. 10) of the Kayak Island gyre. Note that in September of both 1972

ORIGINAL PAGE IS  
OF POOR QUALITY



a.



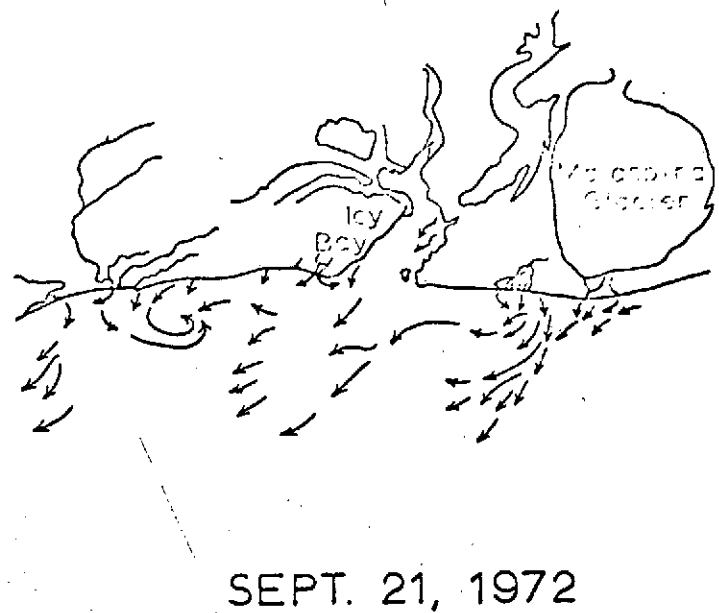
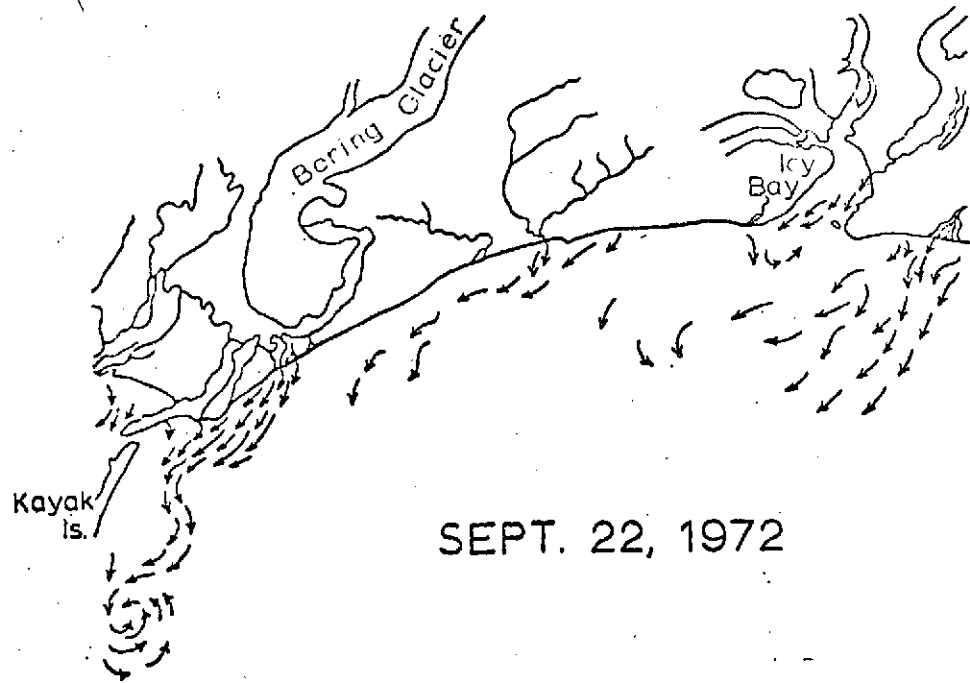
c.



b.

Figure 4. ERTS Multispectral scanner imagery of the southeastern Alaska coastal zone between the Bering Glacier (left) and Icy Bay (right). Image date September 22, 1972; no. 061-20165.

- a. Band 4 (0.5-0.6  $\mu\text{m}$ ). Note the complex gyres of the surface currents as shown by very turbid glacial melt water.
- b. Band 5 (0.6-0.7  $\mu\text{m}$ ).
- c. Band 7 (0.8-1.1  $\mu\text{m}$ ).



0 50km

Figure 5. Flow directions of surface currents in the nearshore waters of the Gulf of Alaska on two consecutive days. Numbers of the images used for the interpretation were September 21, 1972; no. 1060-20111 and September 22, 1972; no. 1061-20165 (see Fig. 4).

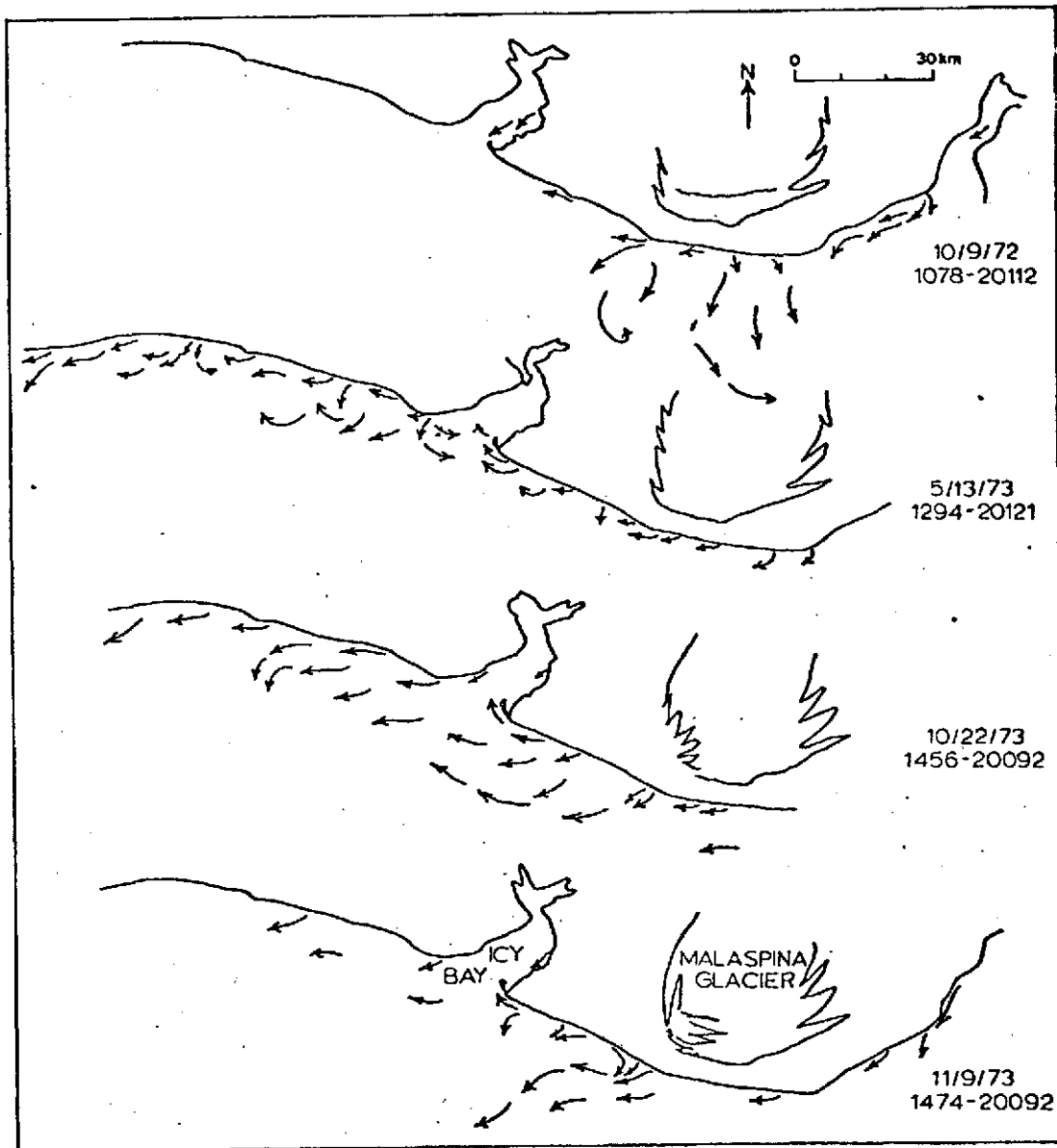


Figure 6. Surface current directions in nearshore waters of the Gulf of Alaska off Icy Bay and the Malaspina Glacier as interpreted from ERTS green band imagery. Dates and identification numbers of images are listed to the right of each panel.

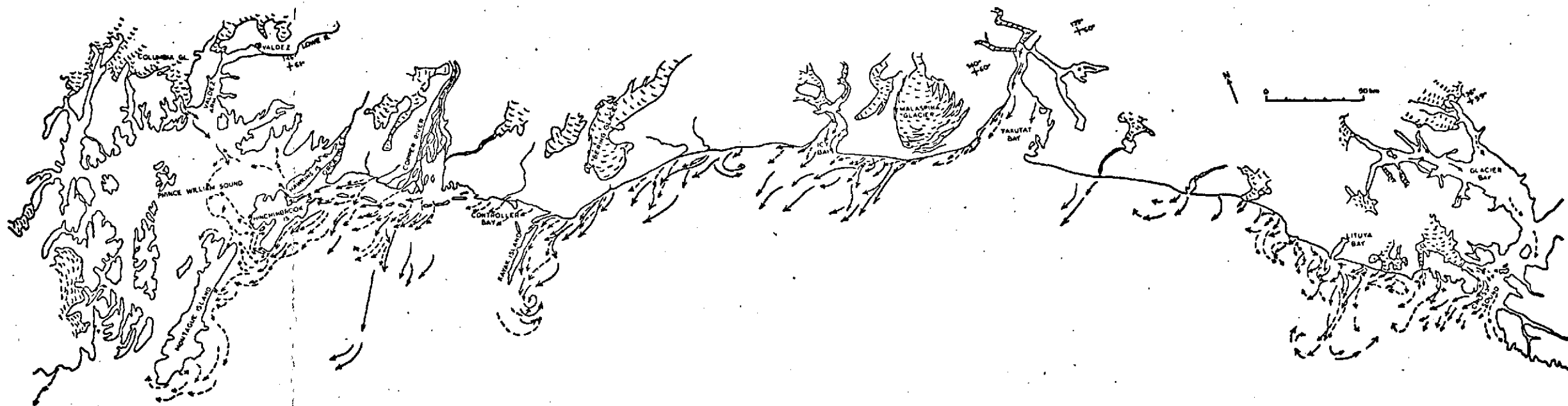


Figure 7. Near surface current directions in the Gulf of Alaska as interpreted from ERTS imagery of September 1972 (solid arrow) and September 1973 (dashed arrows). The green and red bands of the following dates and image numbers were used:

9-18-72	no. 1057-19542	9-12-73	no. 1416-19480
9-19	1058-20000	9-15	1419-20040
9-20	1059-20052	9-16	1420-20102
9-21	1060-20111	9-17	1421-20160
9-22	1061-20165	9-18	1422-20215
9-23	1062-20224	9-19-73	1423-20273
9-24	1063-20282		
9-25-72	1064-20340		

67

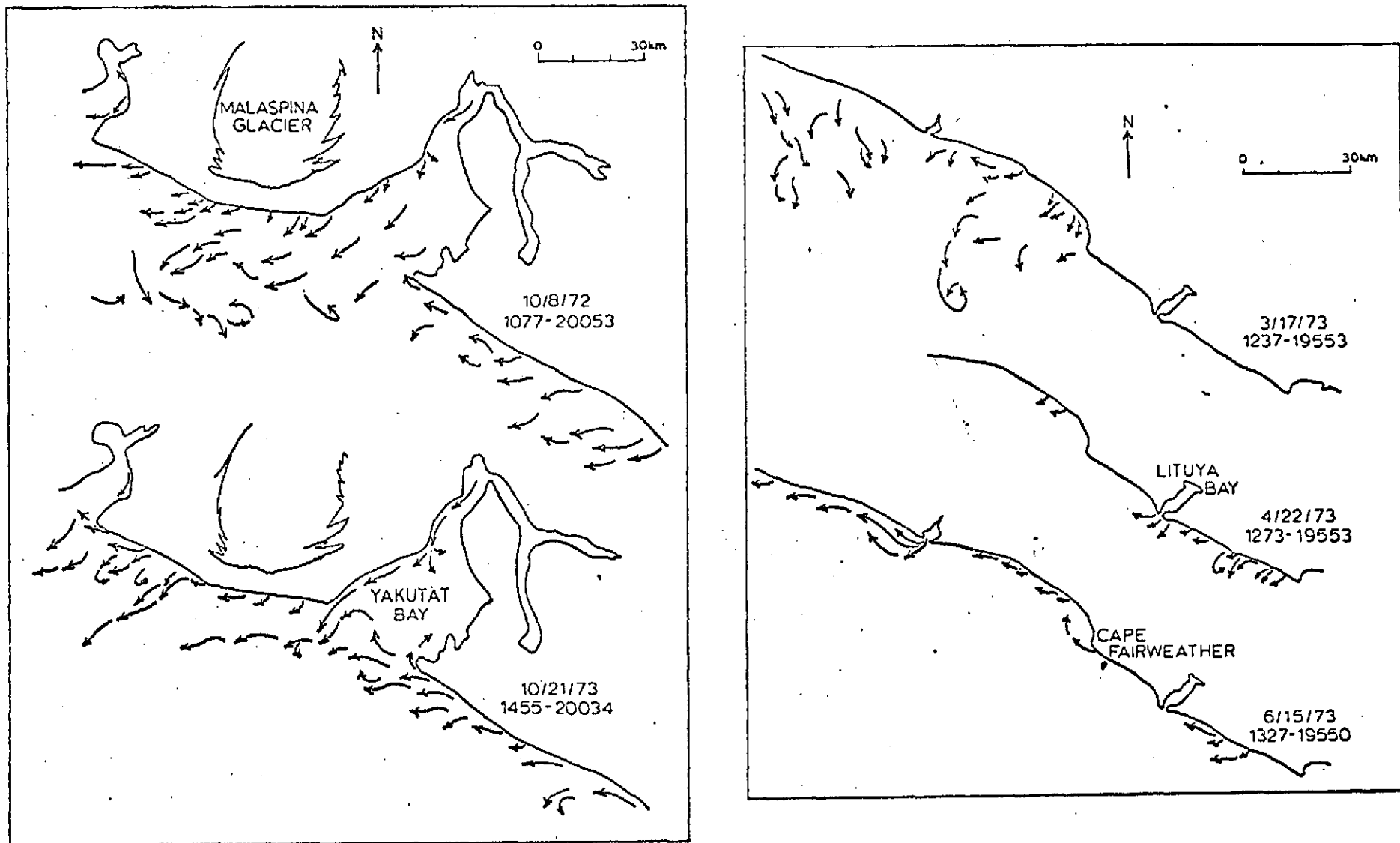


Figure 8. Surface current directions in nearshore waters of the Gulf of Alaska off Malaspina Glacier and Yakutat Bay (left) and Cape Fairweather and Lituya Bay (right) as interpreted from ERTS green band imagery. Dates and identification numbers of images are listed to the right of each panel.

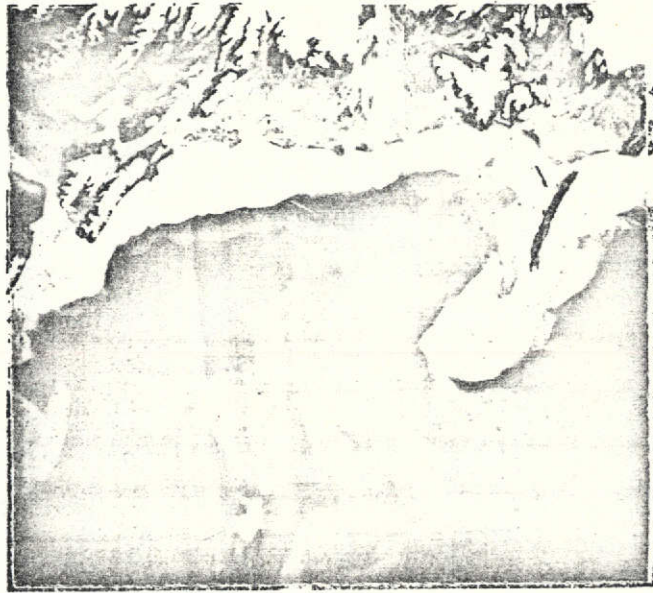
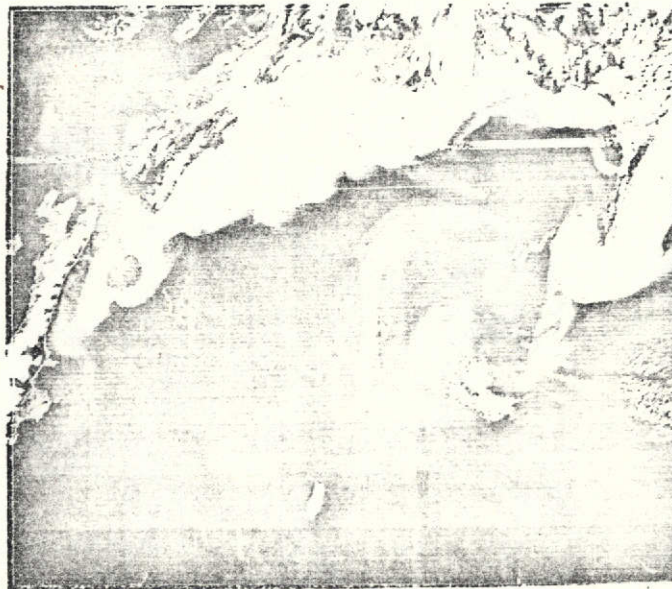


Figure 9. ERTS green band image of well defined plumes of turbid water off the Copper River (top center) and off Kayak Island (right center). Image date October 12, 1972; no. 1081-20284.



ORIGINAL PAGE IS  
OF POOR QUALITY

Figure 10. ERTS image (green band) of visually distinct plumes of turbid water off the Copper River (top center) and off Kayak Island (right center). Image date August 14, 1973, no. 1387-20281.

and 1973, the plumes are deflected by the island into a counterclockwise gyre and appear to be contained east of the island. However, in the October 12, 1972 image the plume of turbid water loops around the south end of the island in a clockwise motion toward Controller Bay. The flat side along the northwestern edge of the plume appears to be the result of a severe shear that had developed at that point in time. On the August 13, 1973 image the clockwise eddy again was well developed, but the prominent shear visible on the October 12, 1972 image was not apparent.

### Copper River Delta Region

ERTS imagery of the Copper River Delta region in the Gulf of Alaska provides information relating to (1) circulation of the nearshore, near surface water, (2) transport of suspended sediment and other pollutants such as oil, (3) interaction of other sediment sources with the river, (4) the effects of river-borne sediment on the nearby Prince William Sound, (5) delta changes due to the 1964 Alaska Earthquake. The imagery is interpreted in the light of background information available from previous studies in the area.

In spite of a relatively small drainage basin, the Copper River, with a sediment load of at least  $97 \times 10^9$  kg/yr (Reimnitz, 1966), is one of the Gulf of Alaska's major sediment sources. This is partly because it is an alpine type river with steep gradient, but more because all of its major tributaries are fed by glaciers, and much of the drainage basin is mantled by easily erodible glacial deposits. Since the 1964 Alaskan Earthquake, when the delta region was uplifted by 2 meters, the proportion of river-borne sediment entering the Gulf of Alaska may be higher than before, when the delta was undergoing slow subsidence (Reimnitz, 1966).

The best ERTS imagery available for this study represents conditions during the months of September and October. This is about 2 months after peak river discharge (Fig. 3), but during the time of highest precipitation in the coastal region.

Figure 11 is an ERTS Multispectral Scanner image of September 24, 1972 showing the delta and inner shelf. The turbid river water is largely restricted to the nearshore, and is isolated by clearer water from another turbid water plume to the east, originating from the Bering Glacier. Some suspended sediment can be traced in a plume from the central part of the delta toward the central shelf. Concentrations of suspended matter are highest over the western part of the delta (Fig. 11b), and can be seen extending westward into Prince William Sound. Using the approach outlined earlier, vectors were drawn that show the surface circulation patterns (Fig. 12). The currents in the nearshore region are generally westward, with a large eddy off the eastern delta, in the shelter of Kayak Island which projects far into the gulf. This diagram also shows that suspended river sediment is transported from the delta into the eastern part of Prince William Sound. Two tidal inlets in the eastern part of the delta show influx of relatively clear oceanic water into the tidal flat regions (see arrows, Fig. 11b; the image Fig. 11a represents the end of flood tide).

ORIGINAL PAGE IS  
OF POOR QUALITY

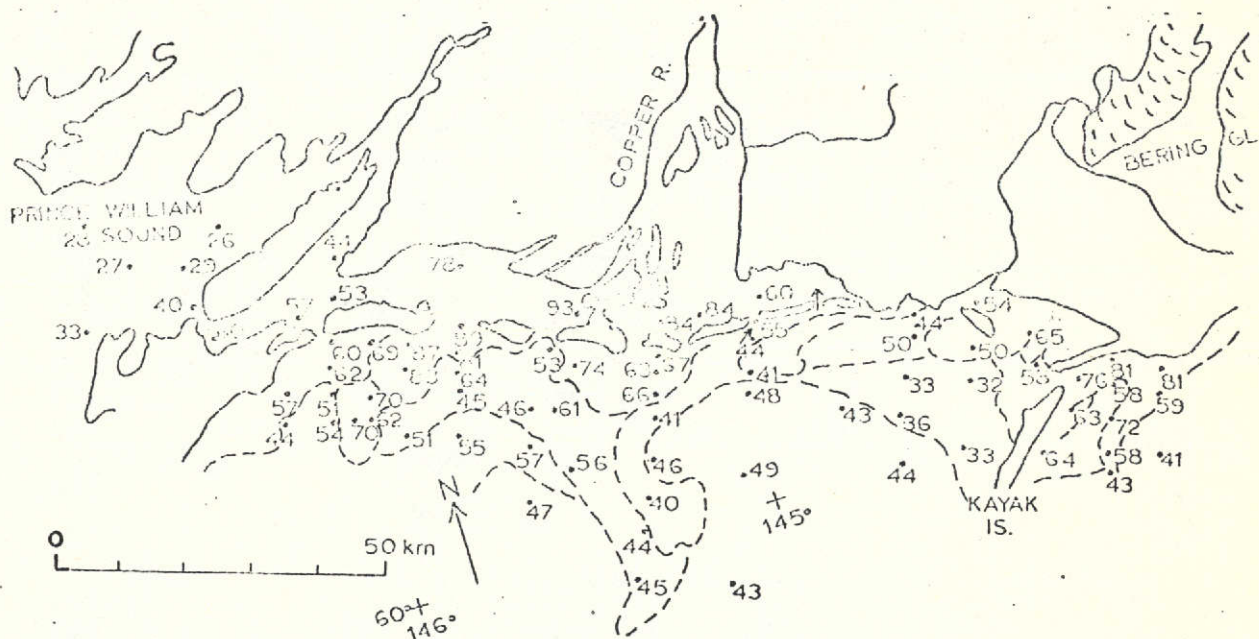


Figure 11. Suspended sediment off the Copper River Delta.

- a. Image date September 24, 1972; no. 1063-20282 (green band).
- b. Portrayal of density differences in the turbid water. I2S Digicol was used to obtain the numbers from a positive transparency of the image shown in a. The higher the numbers, the more turbid the water. The dashed lines outline plume contacts visible on the image.

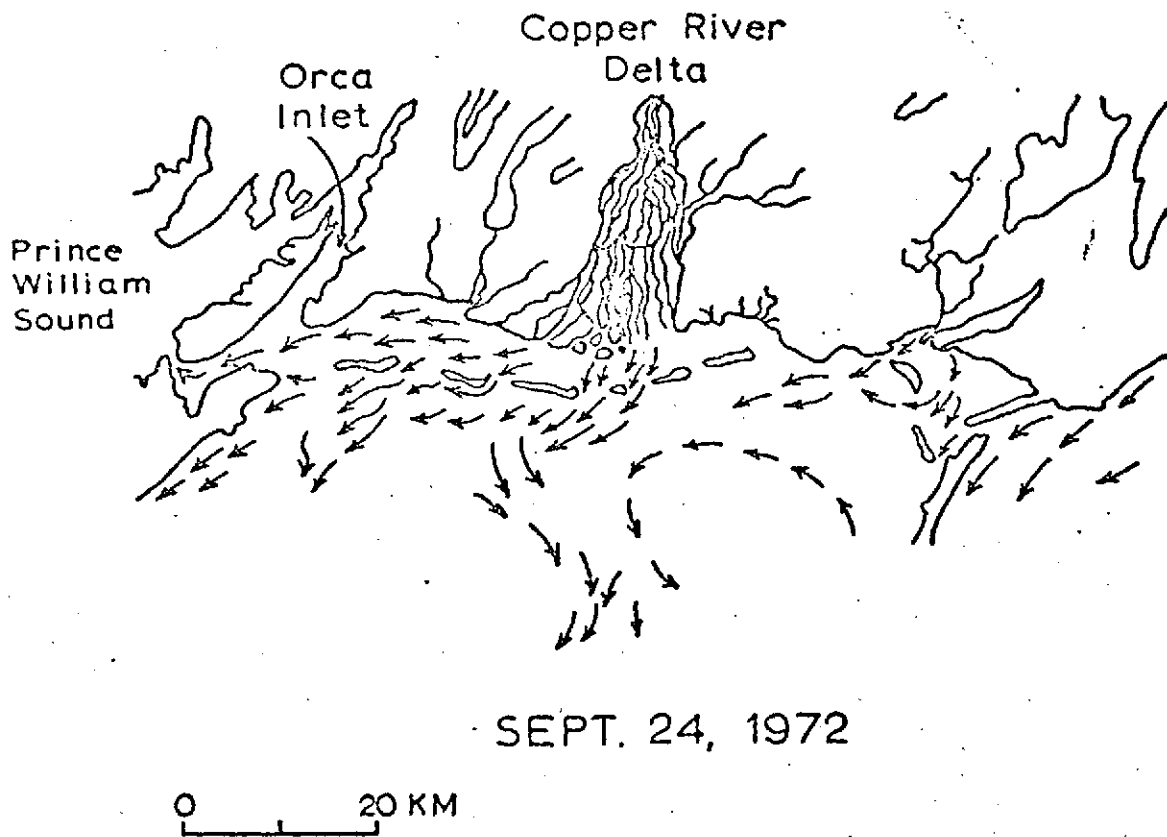


Figure 12. Westward setting nearshore currents in the Gulf of Alaska off the Copper River Delta. Interpreted from ERTS Multispectral Scanner imagery recorded September 24, 1972 (no. 1063-20282).

Figure 11 shows changes in the delta that are related to the 1964 Earthquake. Reimnitz (1972) reported that the main discharge of the river had shifted from a westerly to a central location on the delta after the earthquake. This is shown by highly turbid water, indicative of concentrations of suspended sediment, entering the Gulf through centrally located tidal inlets. Related to this shift in distributaries is a rapid buildup of tidal flats to an elevation that might lie above mean high tide line in the central delta. When comparing this image to 1964 data, a general accretion of the barrier islands is noted. This probably also is related to the uplift of the delta in 1964.

Figure 9 is an ERTS image of the same area taken on October 12, 1973. Conditions on this day are rather similar to those seen in the September 1972 image, except that the river supplied sediment is restricted to a narrower zone near shore, and the open shelf has very clear water. This image demonstrates two additional points that are of importance for the sedimentary environment of the region. Large amounts of suspended sediment supplied by the Bering Glacier east of this image, are deflected seaward by Kayak Island. This sediment source therefore has little influence on sedimentation in the Copper River Delta region, and deposits of sediments from the Bering Glacier may be found on the central shelf seaward of Kayak Island. Secondly, high concentrations of suspended sediment are being transported into Prince William Sound not only from the delta tidal flats directly, but also from the open shelf through Hinchinbrook Entrance.

Other images (Fig. 10) show rather similar dispersal patterns, except that under some conditions turbid water from the Copper River can extend as far as the central part of Prince William Sound, and westward past Hinchinbrook Entrance to the western end of Montague Island (Fig. 7). Local sources of suspended sediment in Prince William Sound apparently supply little sediment to the sound compared to the Copper River.

Band 7 of the ERTS imagery taken at low tide can be used to delineate channel patterns on the Copper River Flats. These channels are known to shift over short periods of time (Reimnitz, 1966), and bathymetric surveys in these areas are difficult to conduct. Suitable ERTS imagery therefore can be used as an aid in coastal navigation and fishing.

Modern sediment dispersal patterns seen on ERTS images agree well with major depocenters delineated by seismic reflection techniques. Figure 13 is an isopach map of the modern Copper River (Reimnitz, 1966). According to this diagram, deltaic sediments are restricted to the inner shelf, and Tarr Bank is reported to be an erosional surface (Reimnitz, 1966). Offshore the delta is thickest west of the rivermouths, in the direction of sediment transport. Orca Inlet, a former fjord basin, has been filled to tidal flat level, and a wedge of deltaic sediments has been built northward into Prince William Sound beyond Hinchinbrook and Hawkins Island. A seismic profile through Hinchinbrook Entrance (von Huene and others, 1967) shows a thick wedge of post-glacial sediments prograding from the open shelf into Prince William Sound. Reimnitz

**ORIGINAL PAGE IS  
OF POOR QUALITY**

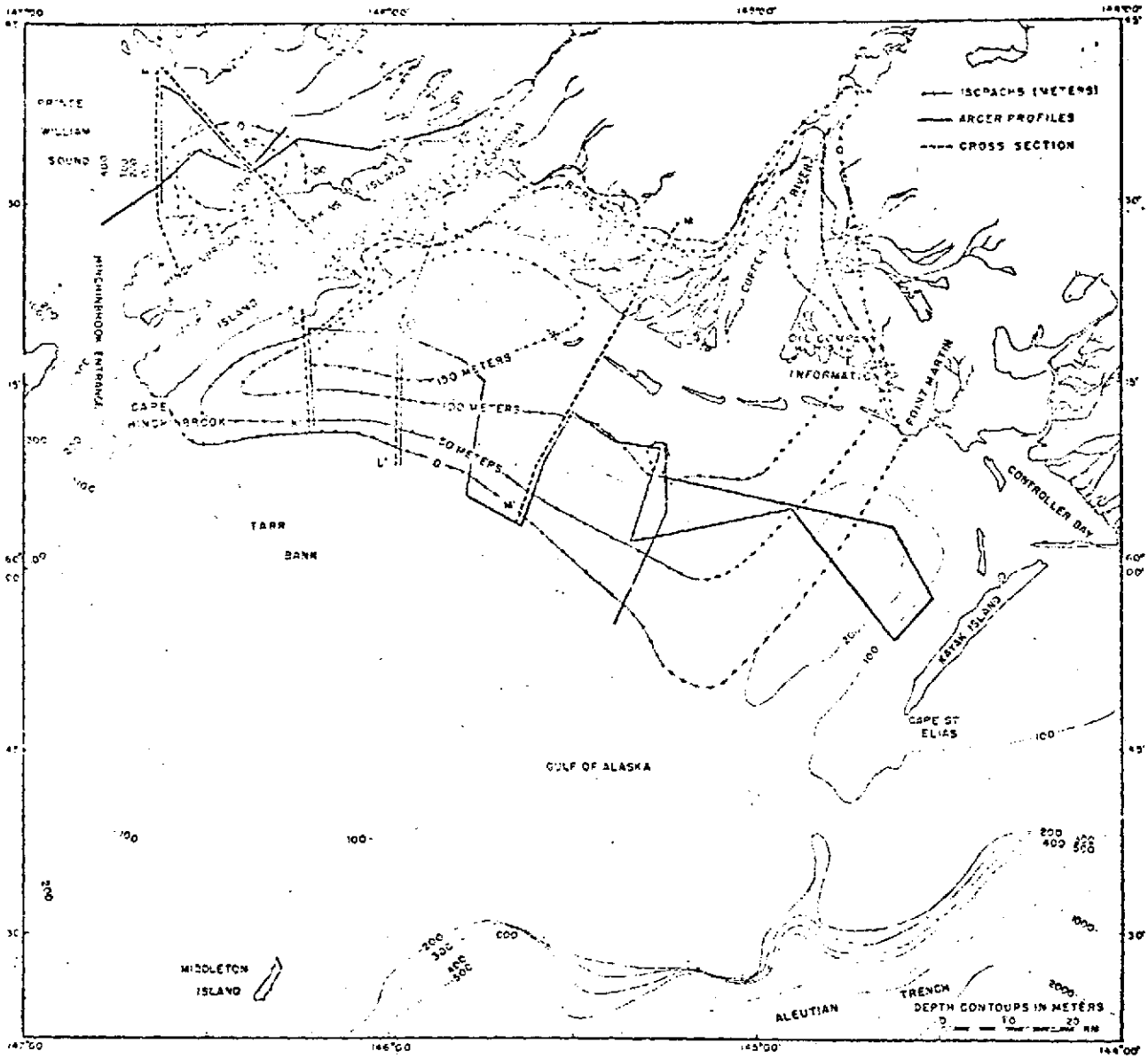


Figure 13. Isopach map of sediment thickness off the Copper River Delta (from Reimnitz, 1966). The sediment thickness was interpreted from continuous seismic profile records.

ORIGINAL PAGE IS  
OF POOR QUALITY

(1966) did not consider this sediment accumulation as part of the Copper River Delta. The ERTS imagery indicates that this sediment is part of the Copper River Delta, and that deltaic sediment accumulations can also be expected along the seaward side of Montague Island (Figs. 7, 9-12).

### Conclusions

(1) The synoptic coverage afforded by ERTS indicates that overall circulation in the nearshore near surface waters of the Gulf of Alaska is counterclockwise at least during clear weather -- consistent with the flow of the Alaskan gyre.

(2) The least cloud covered ERTS imagery of the southcentral Alaskan coastal zone was obtained during the period of August-October. The large number of cloudy days, the low sun angles in the winter, and the 18-day cycle of the satellite greatly restricted additional coverage which is necessary in order to obtain a more complete model of circulation. The results shown here represent the infrequent fair-weather conditions.

(3) Complicated flow patterns (flow reversals, complex gyres, and zone of convergence and divergence) develop within the nearshore zone and can be seen clearly on the green and red bands of ERTS images. These flow patterns are affected by tides, winds and topography.

(4) During times of high discharge (maximum glacial melt) turbid water is visible on the green band imagery more than 50 km offshore.

(5) ERTS imagery indicates that the Copper River Delta is building westward along the inner shelf, and is filling Prince William Sound: local sediment sources of Prince William Sound are small compared to the input of Copper River sediments.

(6) Major depocenters for post-glacial sediments agree with modern sediment dispersal patterns seen in ERTS imagery: very little of the modern continental sediment reaches the outer shelf today.

(7) Future spills of oil on the open shelf south of the Copper River may have detrimental effects on Prince William Sound fisheries, however, direction of surface current flow obtained from ERTS imagery will provide knowledge of the most likely dispersal patterns of spilled oil and make subsequent cleanup more efficient and effective.

(8) Changes in the Copper River delta related to the 1964 Alaska Earthquake can be detected in the ERTS imagery.

(9) Tidal channel patterns of the Copper River Flats can be delineated from ERTS imagery at low tide, and thus the imagery can be used as an aid to coastal navigation.

ORIGINAL PAGE IS  
OF POOR QUALITY

### References Cited

- Dodimead, A. J., Favorite, F., and Hirano, T., 1963, Review of oceanography of the Subarctic Pacific region: in Salmon of the North Pacific Ocean: International North Pacific Fisheries Com. Bull., 13, Part 2, 195 p.
- Hoskins, C. M., and Burrell D. C., 1972, Sediment transport and accumulation in a fjord basin, Glacier Bay, Alaska: Jour. Geology, v. 80, p. 539-551.
- Reimnitz, Erk, 1966, Late Quaternary history and sedimentation of the Copper River Delta and vicinity, Alaska (unpublished Ph.D. dissertation, La Jolla: California Univ., San Diego, 160 p.
- \_\_\_\_\_, 1972, Effects in the Copper River Delta: The Great Alaska Earthquake of 1964: Oceanography and Coastal Engineering, ISBN 0-309-1605-3, National Academy of Sciences, p. 290-309.
- Uda, M., 1963, Oceanography of the Subarctic Pacific Ocean: Jour. Fish. Res. Bd. Canada, v. 20, p. 119-179.
- von Huene, Roland, Shor, G. G., Jr., and Reimnitz, Erk, 1967, Geological interpretation of seismic profiles in Prince William Sound, Alaska: Geol. Soc. America Bull., v. 78, p. 259-268.

ORIGINAL PAGE IS  
OF POOR QUALITY

# ERTS IMAGERY AND DISPERSAL OF YUKON AND KUSKOWIM RIVER SEDIMENT IN THE NORTHEASTERN BERING SEA

C. Hans Nelson, Bradley R. Larsen and Robert W. Rowland  
U.S. Geological Survey, Menlo Park, California 94025

## INTRODUCTION

Ninety percent of the total river sediment carried to the Bering Sea enters from the Yukon and Kuskokwim Rivers. The Yukon annually contributes about 96% of this, or approximately 96 million metric tons of suspended and bedload sediment (Lisitsyn, 1966). Part of the Yukon-Kuskokwim sediment is deposited in a large delta complex (52,000 km<sup>2</sup>) that forms about 800 km of the Bering Sea coast between Kuskokwim Bay and Norton Sound (Fig. 1). The rest of the sediment is dispersed in a complex pattern of deposition and bypassing on the epicontinental shelf of the northeastern Bering Sea.

In this paper we present new data on the dispersal of modern sediment near the effluents of the Yukon and Kuskokwim Rivers during the ice-free season (June through October). These data include measurements of salinity and temperature, water turbidity, grain size and concentration of suspended sediment, and grain size of bottom sediment; these data are compared with Earth Resources Technology Satellite (ERTS) images showing sediment plumes of the Yukon and Kuskokwim Rivers (Figs. 1-6).

## OCEANOGRAPHIC SETTING

Sediment from the Yukon and Kuskokwim Rivers is mainly dispersed by the Alaskan Coastal Water. This water mass has low salinity (20-30 ‰) because it is generated primarily by Yukon and Kuskokwim runoff (Saur and others, 1954). The water mass parallels the eastern Bering Sea coast and generally extends offshore to a depth of about 30 m (Fig. 1); it also fills Norton Sound. The entire water mass has a net northward movement because of sea surface slope (Coachman and Aagaard, 1966).

Numerous non-synoptic measurements of current velocity taken during different weather conditions of the ice free season indicate that speed of the Alaskan Coastal Water is variable but movement generally is northward (Fig. 1). Typically, current speeds in the seaward areas of the Alaskan Coastal Water are 10 (bottom) to 20 (surface) cm/sec. whereas within 30 km of the shoreline the entire water column travels northward at velocities of 30-40 cm/sec. (Fleming and Heggarty, 1966; Husby, 1969; 1971; McManus and Smyth, 1970). The maximum current speeds are found where the Alaskan coast protrudes westward to constrict water flow at locations such as Bering and Etolin Straits; here velocities reach 180 cm/sec. and 90 cm/sec. respectively (Fleming and Heggarty, 1966; Fig. 1).

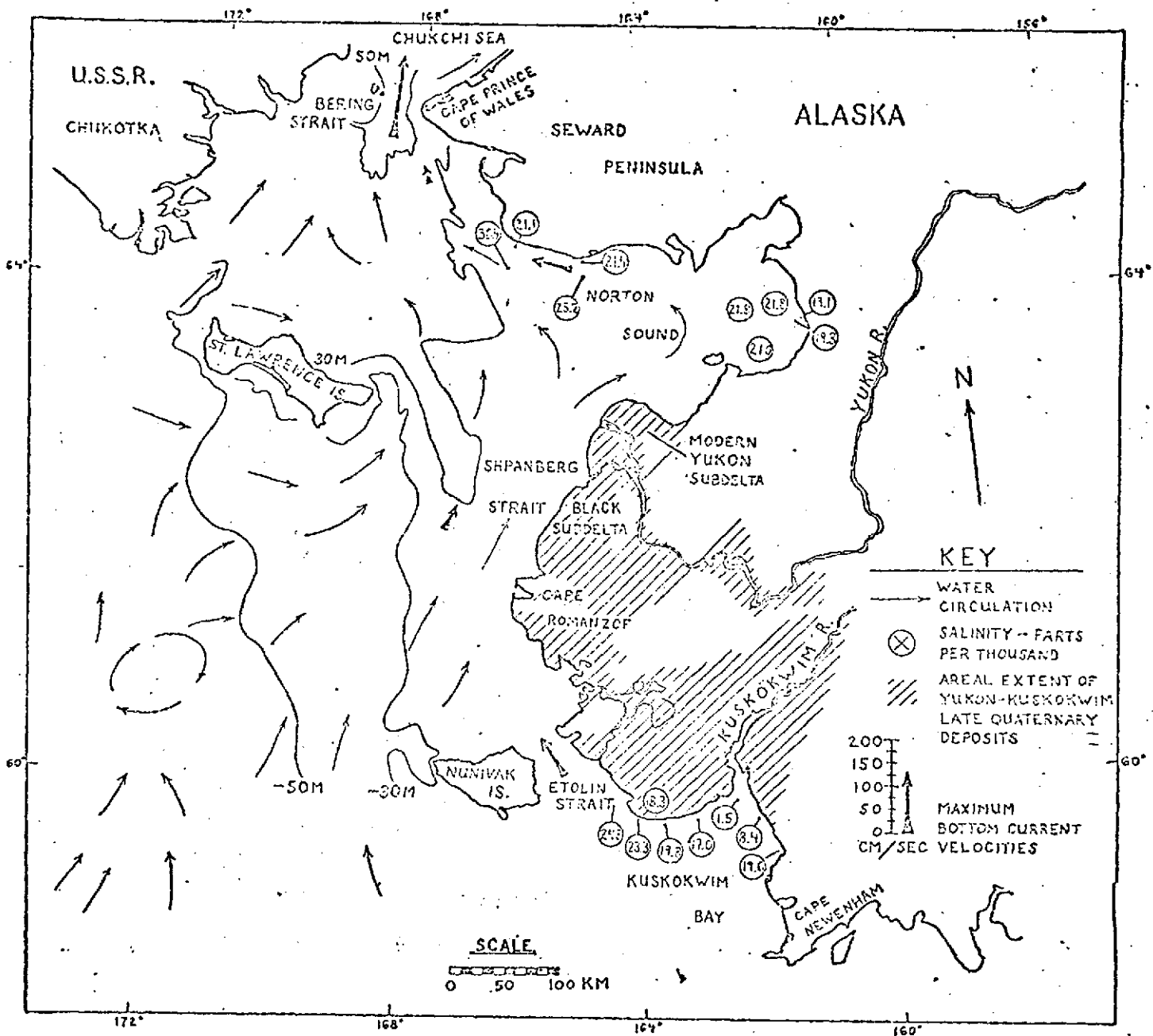


Figure 1. Northeastern Bering Sea study area showing late Quaternary deltaic and flood plain deposit in the Yukon-Kuskokwim delta complex, offshore water circulation (after Knebel and Creager, 1973; McManus and others, in press), and maximum bottom current velocities (selected from Fleming and Heggarty, 1966; Husby, 1969, 1971; Knebel, 1972; and Nelson and Hopkins, 1972). Surface salinities for Kuskokwim Bay water measured August 30 and 31, 1972, for elsewhere on September 1-7, 1972.

ORIGINAL PAGE IS  
OF POOR QUALITY

Disruption of the dominant northerly flow occurs at the landward and seaward fringes of the Alaskan Coastal Water. Reversals in current directions near the coast may result from local wind and tidal fluctuations; reversals in the slowly moving water of the seaward fringe appear to be caused by wind and tidal fluctuations and/or by movements of other nearby water masses (Nelson and Hopkins, 1972; Knebel and Creager, 1973; McManus and others, in preparation).

#### SUSPENDED SEDIMENT DISPERSAL

Discharge of suspended sediment from Arctic rivers takes place principally in the summer when the land surface is thawed (Lisitsyn, 1966). Therefore, although observations of suspended sediments have been restricted to the summer months, the available data presumably describe the bulk of the annual sediment discharge.

In the central Kuskokwim River, surface water contained suspended sediment concentrations of 100-200 mg/l during non-flood discharge conditions of late August, 1972 (Fig. 2). The concentrations dropped to below 50 mg/l in the lower river near the first occurrence of brackish water where there is a tidal effect (Fig. 1).

ERTS imagery of August 31 at the time of our coastal water sampling, shows that the main Kuskokwim River plume occupied the northern part of Kuskokwim Bay. The configuration of the plume seems to suggest a westward movement of surface water along the northern coastline of the bay and a general southerly movement of the plume in the eastern part of the bay (Figs. 4 & 5 and Table 1). Inspection of MSS Bands 5 and 6 indicate the greatest plume turbidity occurred along the eastern coast in the northern end of Kuskokwim Bay. The greatest sediment concentrations, coarsest suspended sediment, lowest salinities and shallowest secchi disc observations all were made in water along the northeastern coast of the bay (Figs. 1-3).

Other ERTS imagery suggests that this pattern may be persistent in Kuskokwim Bay. Images in May of 1973 show the northern end of the Bay filled by the sediment plume and also reveal a long westward extension of part of the sediment plume along the northern shoreline toward Cape Romanzof (Wright and Sharma, in press).

From Cape Romanzof north-northeast toward the Yukon subdelta and northwest toward St. Lawrence Island, patterns of currents, suspended sediment concentrations, and sediment plumes in ERTS imagery are diverse (Figs. 1, 2 & 4); these limited data suggest that suspended sediment movement is quite variable with time and water depth and that data is insufficient to determine the dominant pathway of suspended sediment dispersal in this area. Neiman (1961) reported a high concentration of suspended sediment in bottom water both to the north-northeast and northwest from Cape Romanzof (Fig. 2). Deposition from such northwestward excursions of sediment laden water may be partly

29

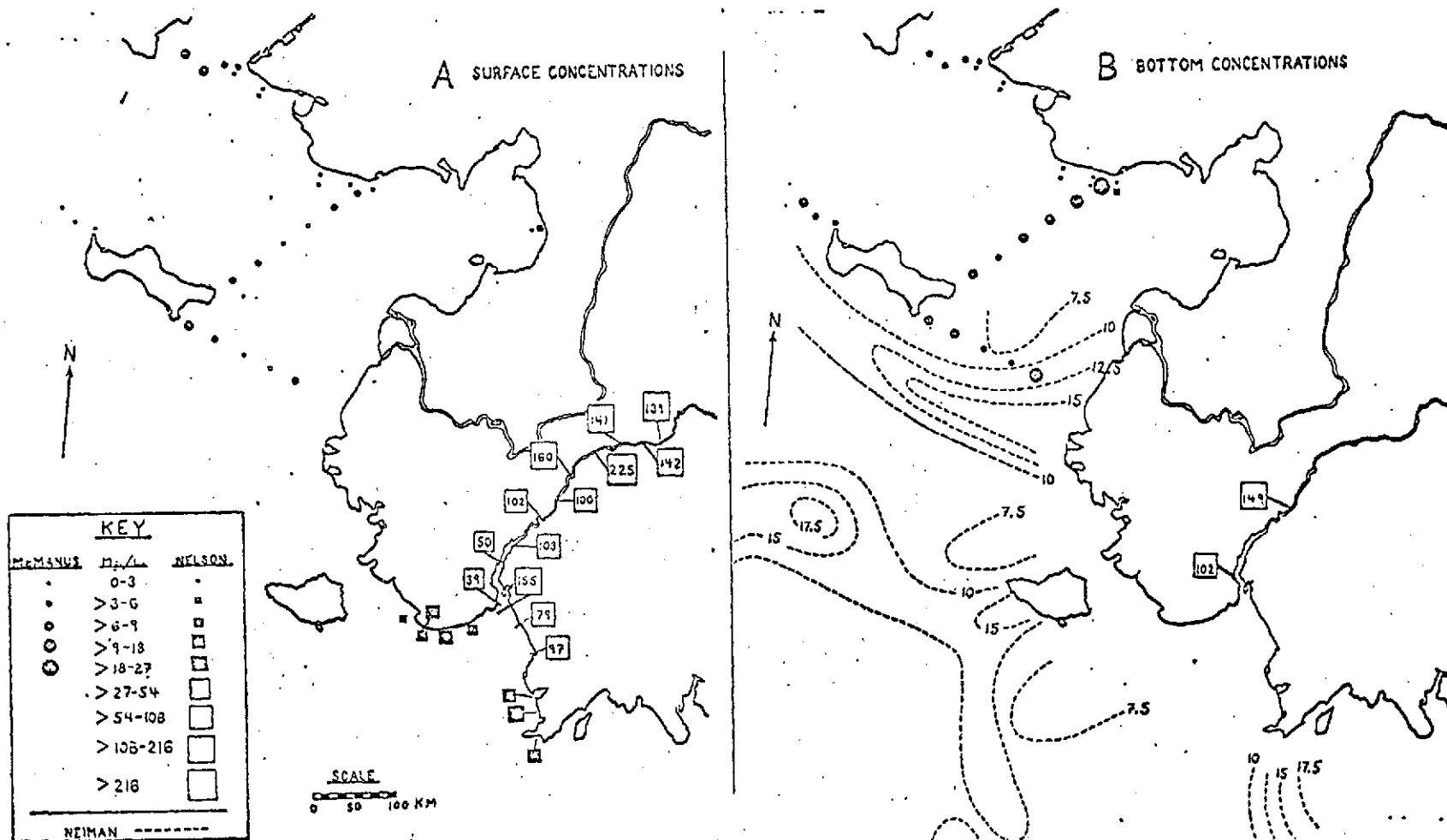


Figure 2. Distribution of suspended sediment in surface (A) and near bottom (B) water of northeastern Bering Sea and the Kuskokwim River. Selected data are included from Neiman (1961) and McManus and Smyth (1970). For her 50 samples, Neiman used membrane ultrafiltration at  $0.7 \mu$  on 1-4 l. of water (Lisitsyn, 1966, p. 167) in a method nearly identical to ours. Our grab samples were collected with Van Dorn bottles and our filter handling and weighing procedure was after Winneberger, Austin and Klett (1963). McManus and Smyth (1970) utilized a transmissometer to collect their data. Only our Kuskokwim data was synoptic; it was collected throughout the lower estuary from a helicopter on the day of the ERTS imagery in Figures 4 and 5.

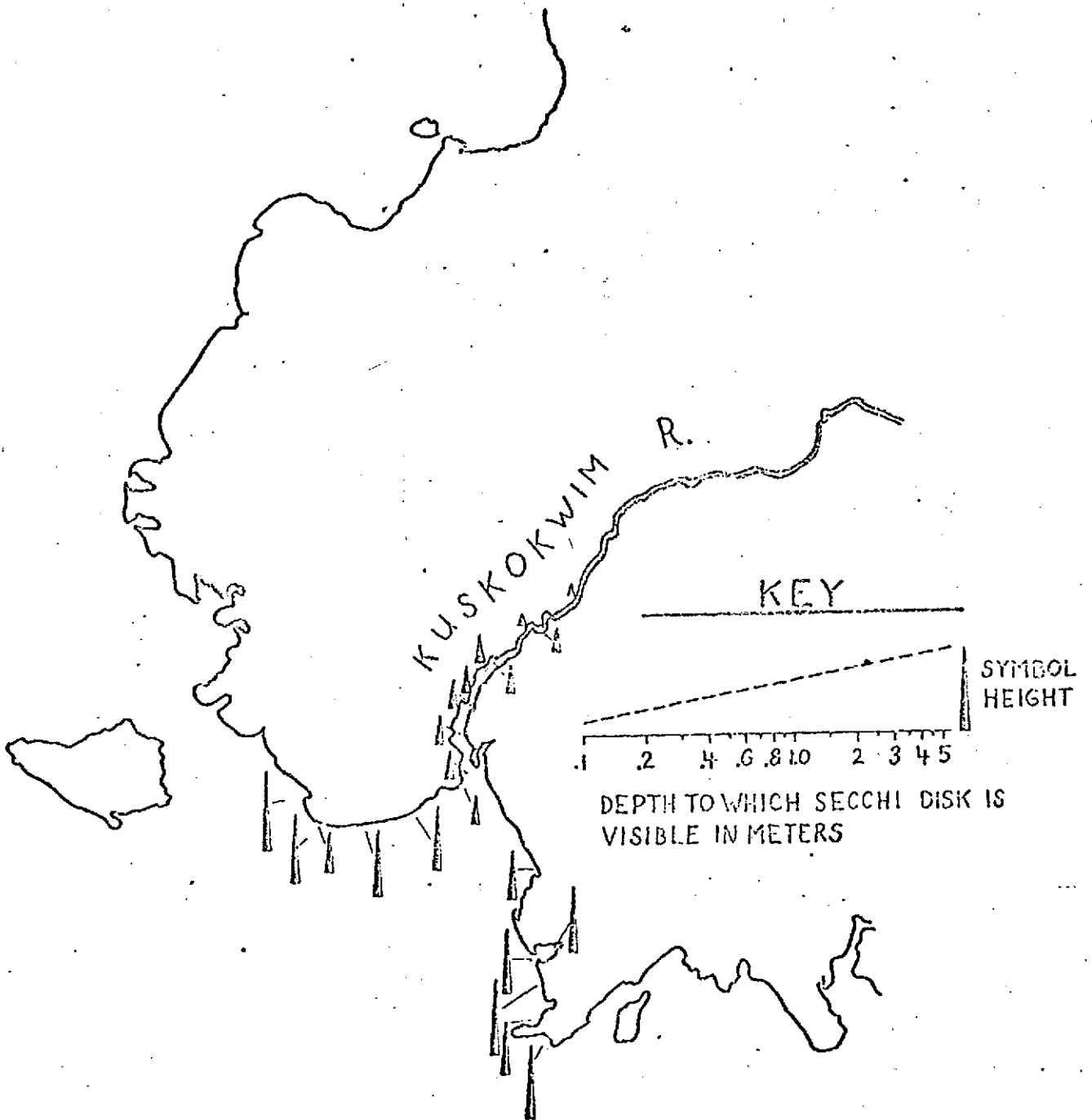
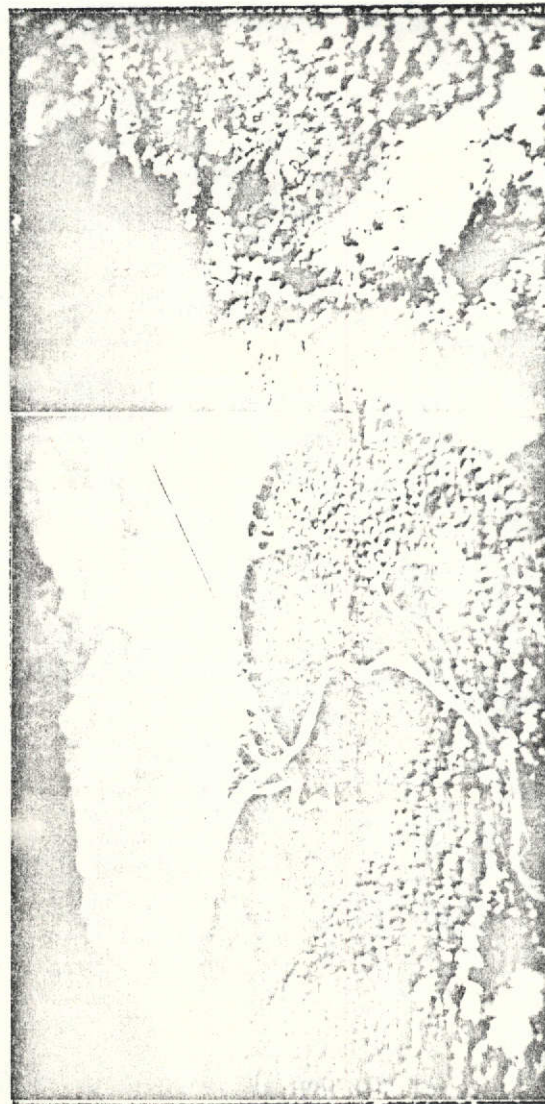


Figure 3. Visibility depth of 25 cm Secchi disc in lower Kuskokwim River and upper Kuskokwim Bay on August 30 and 31, 1972.



KUSKOKWIM DELTA



YUKON DELTA

ORIGINAL PAGE IS  
OF POOR QUALITY

Figure 4. Kuskokwim and Yukon River sediment plumes as interpreted from multispectral scanner band 4 imagery of the Earth Resources Technology Satellite (ERTS-1). All imagery was collected between 1100-1200 hrs. Bering Standard Time during mid to late ebb tides, except for plume areas along the western shoreline of the Yukon subdelta where mid to late flood tides were occurring.

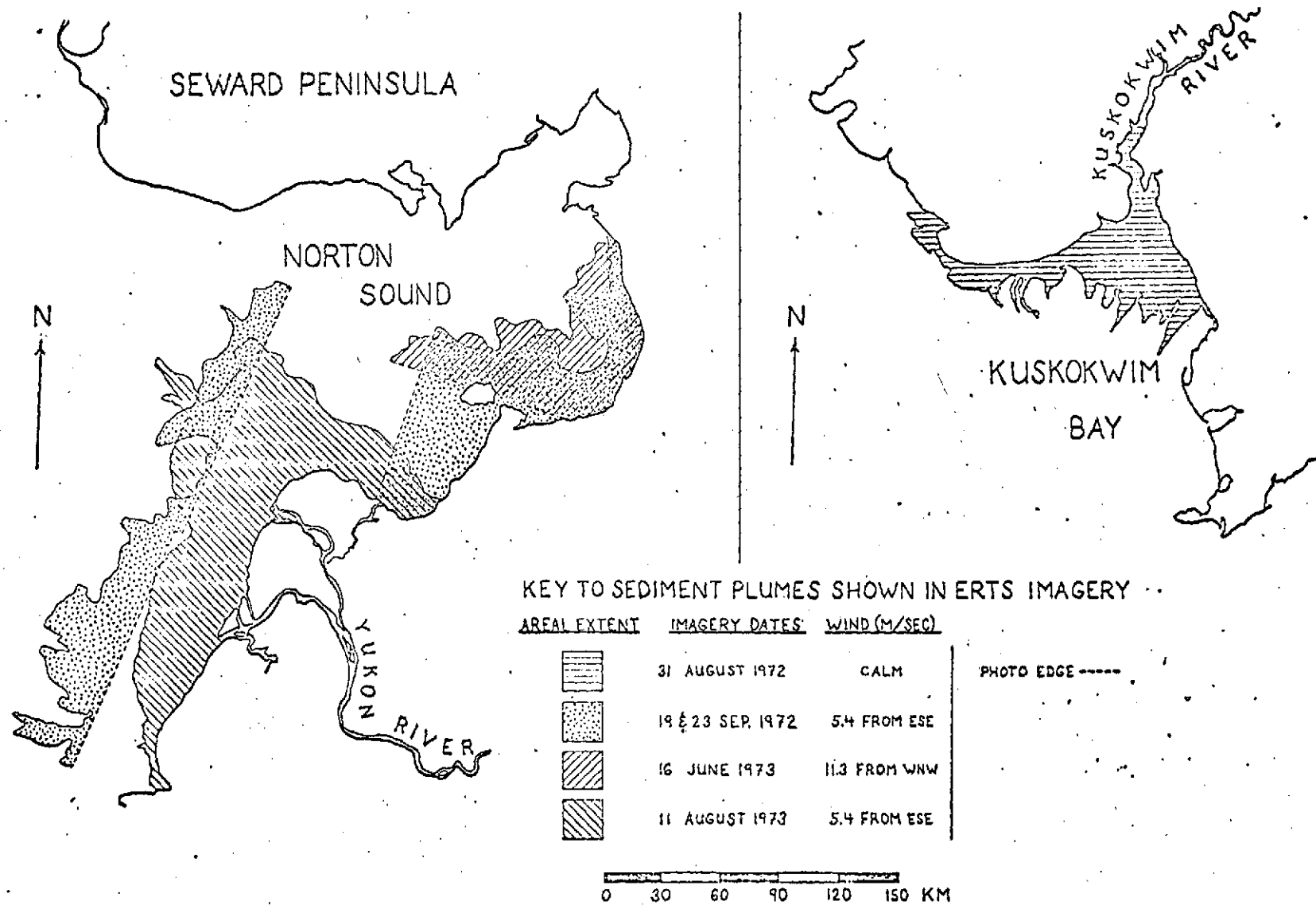


Figure 5. ERTS imagery MSS band 4 for Yukon River sediment plume of August 11, 1973, and MSS band 5 for Kuskokwim River sediment plume of August 31, 1972.

Table 1. Dispersions of the sediment plumes measured from the Kuskokwim River mouth and from the southwest distributary of the Yukon River, which is the primary sediment source shown in the ERTS Imagery (Fig. 5).

Distance to the furthest recognizable boundary of the lowest density part of plumes has been measured on MSS Band 4 of ERTS imagery. Distance to the boundary of the highest density part of plumes has been measured on MSS Band 6 of ERTS imagery.

	<u>ERTS Imagery</u>	<u>MSS 4</u>				<u>MSS 6</u>			
		<u>North</u>	<u>East</u>	<u>West</u>	<u>South</u>	<u>North</u>	<u>East</u>	<u>West</u>	<u>South</u>
W W Kuskokwim	1039-21371 (31 Aug 72)	-	35 km	120 km	105 km	-	20 km	20 km	52 km
Yukon	1384-21530 1384-21533 (11 Aug 73)	140 km	105 km	60 km	70 km	90 km	95 km	60 km	65 km

responsible for formation of St. Lawrence Bank, a shoal south of St. Lawrence Island (Knebel and Creager, 1973). McManus and Smyth (1970) believed northerly transport around the delta from the Kuskokwim, best explained the high quantity of suspended sediment they noted in bottom water north of Cape Romanzof. ERTS imagery, however, shows southwesterly movement of a small part of the Yukon River plume from the southwest distributary (Figs. 4 & 5). The dominant flow from this main distributary apparently causes some movement southwestward against the surface and bottom currents that generally flow northward (Figs. 1 & 4). Thus, the high concentration of suspended sediment in bottom water north of Cape Romanzof may originate both from dispersal of the Kuskokwim River plume northwestward and Yukon River plume southwestward along the delta margin.

Neither ERTS photos nor available suspended sediment data provide a clear cut picture of Kuskokwim sediment dispersal to the south and southwest. High suspended sediment concentrations noted by Neiman (1961) south of Kuskokwim Bay near Cape Newenham may have an origin in part from a continued southerly dispersal of the Kuskokwim plume (Fig. 2). However, these concentration gradients lead eastward toward Nushagak Bay where other ERTS imagery (Summer, 1972) and suspended sediment data (G. D. Sharma, Univ. Alaska, oral commun., 1974) reveals a well developed sediment plume moving from the Bay toward this region. Neiman's (1961) contours of suspended sediment concentration southwest of Nunivak Island, in addition, suggest that movement of Kuskokwim sediment plumes may continue westerly at depth away from the delta margin; but such a pattern is not visible on 1972 or 1973 ERTS imagery of surface waters. G. D. Sharma (University of Alaska, oral communication, 1974) also finds that chemical parameters of Kuskokwim water can be traced in this westerly to southwesterly direction.

The high suspended sediment concentrations in bottom water just north of St. Matthew Island coincide with a major current gyre and a relatively thick deposit of modern silt in that area (Fig. 1; Neiman, 1961; Knebel and Creager, 1973). It is speculative whether this concentration of suspended sediment can be attributed to the movement of Kuskokwim sediment into this central shelf area of sluggish water circulation or whether resuspension of shelf sediment contributes to these suspended sediment concentrations and modern silt deposits. More of the synoptic coverage provided by ERTS imagery and more measurements of water hydrography and chemistry are necessary before the major, variable dispersal paths of Kuskokwim derived sediment can be traced in the central and southern Bering shelf areas.

The pattern of suspended sediment dispersal can be more clearly defined for the Yukon River. ERTS imagery shows that turbid water typically surrounds the modern subdelta in a wide halo and appears to be carried northward and eastward within Norton Sound by a counter-clockwise current gyre (Figs. 1, 4, & 5; Table 1). The ERTS imagery from August 11, 1973, shows that although the wind drift is against this typical circulation gyre, the Yukon plume extends northward and eastward from the most southwesterly distributary, the main discharge point of the Yukon River (Figs. 4 & 5; Table 1).

**ORIGINAL PAGE IS  
OF POOR QUALITY**

The Yukon plume appears to disperse in two pathways through the northern Bering Sea. It may travel directly northward from the Yukon subdelta across the western side of Norton Sound to western Seward Peninsula (G. D. Sharma, University of Alaska, oral communication, 1974; McManus and others, in preparation) or it may follow the counterclockwise gyre that "hugs" the coast of Norton Sound (Fig. 4). The counterclockwise movement along the southern margins of Norton Sound and Seward Peninsula is suggested by salinity and temperature data (Fleming and Heggarty, 1966; Husby and Hufford, 1971; Fig. 1), by a core of turbid bottom water with Yukon derived silt that paralleled the coastline in a 0-20 km wide zone near Nome in the early summer (McManus and Smyth, 1970; Fig. 2) and by thicker deposits of Holocene silt at the margins of Norton Sound (Fig. 7). The low content of suspended sediment that we recently encountered near Nome in the late summer indicates that transport of large quantities of Yukon derived silt may be intermittent because of seasonal changes and/or storms (Fig. 2).

#### GEOLOGIC IMPLICATIONS

The sediment discharge from Arctic rivers consists predominately of silt (Hill and Tedrow, 1961; Lamar, 1966). Analyses of suspended sediment samples taken from the Kuskokwim River at the time of the August 21, 1972 ERTS imagery show that 75% of the suspended sediment is silt-sized throughout most of the river and the eastern nearshore areas of Kuskokwim Bay where the most turbid plume is shown on ERTS imagery (Figs. 4, 5, & 6; Table 1). To the west of the river mouth along the northern coast of Kuskokwim Bay where a less turbid river plume is evident, the concentration of silt drops to 50% (Figs. 2, 3, 5, & 6). The remainder of suspended material is made up of clay-size material and organic debris. The predominance of silt in suspended sediments of the drainage basins probably accounts for the high percentage of silt and the generally low percentage of clay both in the suspended sediment of the Alaskan Coastal Water and in the modern bottom sediment of the regions underlying the main sediment plumes shown in ERTS imagery (Figs. 4, 5, & 7).

In locations where the distribution patterns of bottom sediment are well defined, there appears to be good correlation with the distribution patterns of suspended sediment plumes that are shown in ERTS imagery. Along the southern margin of the Yukon-Kuskokwim delta complex where the Kuskokwim River plume parallels the shoreline, the bottom sediment is dominantly modern silt (Figs. 4-6). Seaward of the "silt belt", that underlies the main plume, waves shoal on discontinuous offshore bars of fine-grained sand (Fig. 5). In these shallower offshore regions silt and finer sized sediment apparently have been winnowed out, re-suspended, and carried off by the Alaskan Coastal Water.

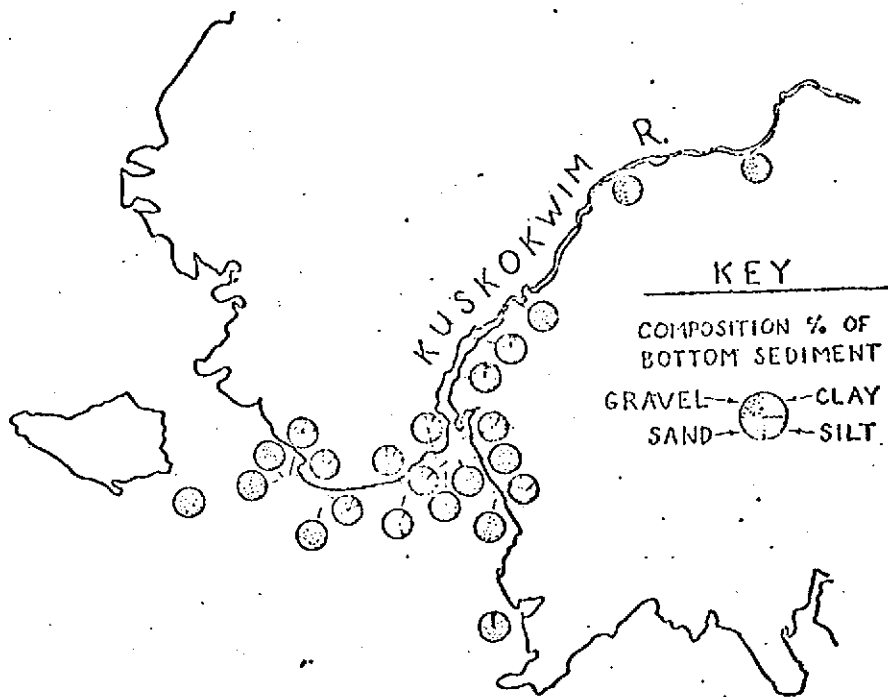
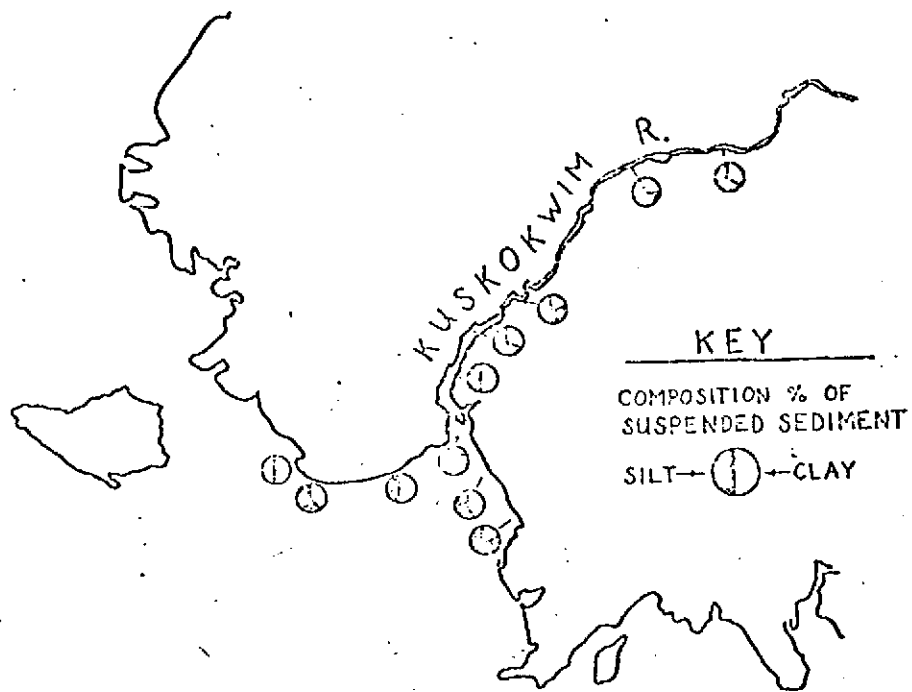


Figure 6. Grain-size composition of suspended and bottom sediments of the lower Kuskokwim River and upper Kuskokwim Bay collected August 30 and 31, 1972. Weight percent of the <.062 mm size fractions was determined by the hydrophotometer method of Jordan, Freyer, and Hermen (1971) and of the >.062 mm size fractions by sieving at .062 mm for sand and at 2 mm for gravel.

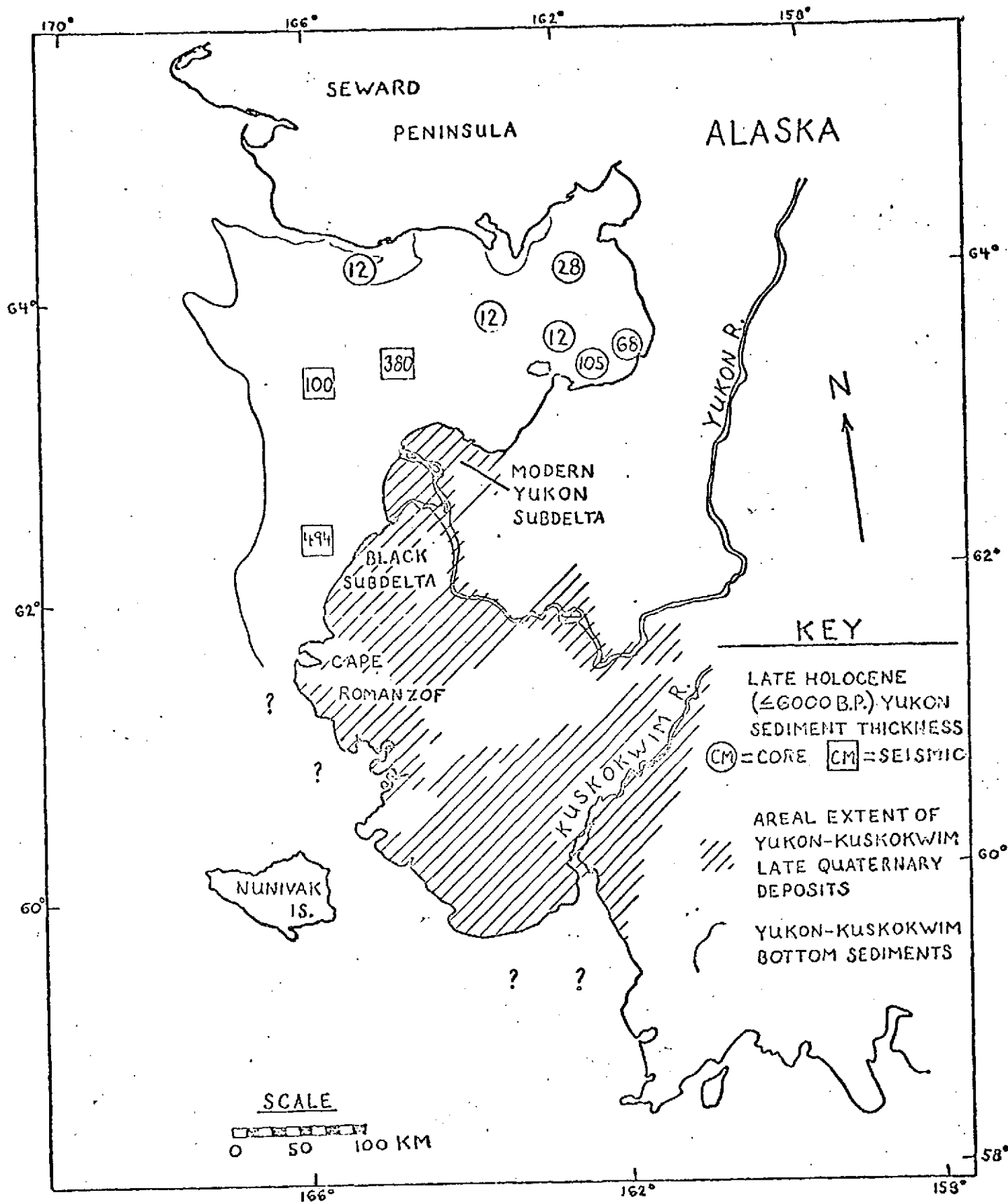


Figure 7. Distribution and thickness of late Holocene (<6,000 BP) sandy silt derived from the Yukon River. Sediment distribution pattern after McManus and others (in press) and thickness data from unpublished seismic reflection profiling records and core stratigraphy determined by radiocarbon chronology (C. H. Nelson, U.S. Geological Survey, Menlo Park, California).

ERTS images confirm the persistent movement of part of the suspended sediment plumes with the Alaskan Coastal Water as it travels westward between the Kuskokwim delta margin and the offshore bars (Figs. 4 & 5) and then northward through Etolin Straits between Nunivak Island and the delta margin (Wright and Sharma, 1973). More images are required, however, to determine whether it is typical for the highest concentrations of suspended sediment to move southward along the eastern coastline of Kuskokwim Bay and to find out where this major portion of the river sediment load may be deposited on the shelf (Figs. 2, 4, & 5; Table 1).

Distribution and thickness patterns of the late Holocene sandy silt from the Yukon River correlate with the location and turbidity of Yukon sediment plumes observed in ERTS imagery of the Bering Sea (Figs. 4, 5, & 7; Table 1). Thick sediment underlies both the northward and coastal margin plumes whereas thin sediment underlies the east central area of Norton Sound over which plumes have not been observed (Fig. 7). Because the thinnest deposits have accumulated in the central depression of Norton Sound, and the thickest deposits are associated with positive topography, it appears that sediment plume dispersal has been an important factor controlling depositional sites. The pattern of bottom sediment distribution suggests that the locations of sediment plumes shown in the available ERTS images are typical and that a significant part of the Yukon sediment plume moves in a counter-clockwise circulation gyre of Alaskan Coastal Water along the margin of Norton Sound (Fig. 1).

The capacity and duration of this circulation pattern in northern Bering Sea is crucial to the understanding of Yukon sediment budgets and the environmental impact of projected future development in this region. If most of the Yukon sediment followed the proposed dispersal paths since major flooding of northern Bering Sea and opening of all straits about 11,800 B.P. (McManus and others, in press), then deposits of Yukon sediment should be considerably thicker in regions of present deposits or they should be present throughout other areas of northern Bering Sea (Nelson and others, in preparation). There is an absence of Yukon sediment from St. Lawrence Island to Bering Straits and presence of only thin deposits over large regions of east central Norton Sound (Fig. 7). This lack of Yukon sediment in Bering Sea combined with the circulation pattern evident in ERTS images suggest that great quantities of Yukon sediment must eventually be carried northward from the Bering Sea by the Alaskan Coastal Water. The generally northward movement of much Yukon sediment into Chukchi Sea also is indicated by the presence of relatively thick deposits of Holocene silt over extensive areas of the eastern Chukchi Sea where there are no large river inputs (McManus and others, 1969).

Movement of the dense, turbid water masses through the northeastern Bering Sea has important implications for future mining of offshore gold placer deposits (Nelson, 1971; Nelson and Hopkins, 1972) and for projected harbor development associated with onshore mining

facilities in this region. Offshore placer mining may introduce large quantities of suspended sediment into the water, but this may be insignificant in view of the large amounts of Yukon derived sediment intermittently present in the water. The presence of high quantities of suspended sediment also must be taken into consideration so that future harbor design will avoid trapping such material.

#### REFERENCES CITED

- Coachman, L. K., and Aagaard, K., 1966, On the water exchange through Bering Strait: *Limnology and Oceanography*, v. 11, p. 44-59.
- Echols, R. J., and Fowler, G. A., 1973, Agglutinated Tintinnid loricae from some modern and late Pleistocene shelf sediments: *Micropaleontology*, v. 19, No. 4, p. 431-443.
- Fleming, R. H., and Heggarty, D., 1966, Oceanography of the southeastern Chukchi Sea, in Wilimovsky, N. J., Wolfe, J. M., eds., *Environment of Cape Thompson Region, Alaska*: U.S. Atomic Comm., p. 697-754.
- Goodman, J. R., Lincoln, J. H., Thompson, T. G., and Zeusler, F. A., 1942, Bering Sea, Bering Strait, Chukchi Sea during the summers of 1937, 1938: Univ. of Washington, pub. in *Oceanog.*, v. 3(4), p. 105-169.
- Hill, D. W., and Tedrow, J. C. F., 1961, Weathering and soil formation in the Arctic environment: *Am. Jour. Sci.*, v. 259, p. 84-101.
- Husby, D. M., 1969, Report of oceanographic cruise U.S.C.G.C. NORTHWIND, norther Bering Sea - Bering Strait - Chukchi Sea, July 1969: U.S. Coast Guard Oceanographic Report, No. 24, 75 p.
- \_\_\_\_\_, 1971, Oceanographic investigations in the northern Bering Sea and Bering Strait, June-July 1969: U.S. Coast Guard Oceanographic Report, No. 40, 50 p.
- Husby, D. N., and Hufford, G. L., 1971, Oceanographic investigation of the northern Bering Sea and Bering Strait, 8-21 June 1969: U.S. Coast Guard Oceanographic Report, No. 42, 55 p.
- Jordan, C. F., Freyer, G. E., and Hemmen, E. H., 1971, Size analysis of silt and clay by hydrophotometer: *Jour. of Sed. Pet.*, v. 41.
- Knebel, H. J., 1972, Holocene sedimentary framework on the east-central Bering Sea continental shelf: Ph.D. Dissertation, Univ. Washington, 186 p.
- Knebel, H. J., and Creager, J. S., 1973, Sedimentary environments of the east-central Bering Sea continental shelf: *Marine Geology*, v. 15, p. 25-47.

- Lamar, W. L., 1966, Chemical character and sedimentation of the waters, in Wilimovsky, N. J., Wolfe, J. W., eds., Environment of Cape Thompson Region, Alaska: U.S. Atomic Energy Comm., p. 133-148.
- Lisitsyn, A. P., 1966, Recent sedimentation in the Bering Sea: Akad. Nauk, U.S.S.R., Moscow, (English Transl., 1969, Isreal Program for Scientific Translations), Natl. Sci. Found. - U.S. Commerce Dept., Clearinghouse for Federal Scientific and Technical Information, Springfield, Virginia, 614 p.
- McManus, D. A., Kelley, J. C., and Creager, J. S., 1969, Continental shelf sedimentation in an Arctic environment; Geol. Soc. Am. Bull., v. 80, p. 1961-1984.
- McManus, D. A., and Smyth, C. S., 1970, Turbid bottom water on the continental shelf of northern Bering Sea; Jour. Sed. Pet., v. 40, p. 869-877.
- McManus, D. A., Venkatarathnam, K., Hopkins, D. M., and Nelson, C. H., in press, Yukon River sediment on the northernmost Bering Sea shelf: Jour. Sed. Pet., 18 p.
- \_\_\_\_\_, in preparation, Distribution of bottom sediments of the continental shelf, Northern Bering Sea: U.S. Geol. Survey Prof. Paper 759, 49 p.
- Neiman, A. A., 1961, Certain Regularities in the Quantative distribution of the benthos in the Bering Sea (in Russian); Okeanologia, v. 1, p. 294-304.
- Nelson, C. H., 1971, Northern Bering Sea, a model for depositional history of Arctic shelf placers: ecological impact of placer development, in Proceedings from the First International Conference on Port and Ocean Engineering under Arctic Conditions, v. 1., p. 246-254.
- Nelson, C. H., and Hopkins, D. M., 1972, Sedimentary processes and distribution of particulate gold in the northern Bering Sea: U.S. Geological Survey Prof. Paper 689, 27 p.
- Saur, J. F. T., Tully, J. P., and Lafond, E. C., 1954, Oceanographic cruise to the Bering and Chukchi Seas, Summer 1949, Part IV: Physical oceanographic studies: U.S. Navy Electronics Lab. Report No. 416, v. 1, 31 p.
- Winneberger, J. H., Austin, J. H., and Lkett, C. A., 1963, Membrane filter weight determinations: Jour. Water Pollution Control Federation, v. 35, p. 807-813.
- Wright, F. F., and Sharma, G. D., in press, Earth Resources Technology Satellite observations of high latitude estuarine circulation: Proceedings Second International Conference on Port and Ocean Engineering under Arctic Conditions: Univ. of Iceland, 13 p.

APPLICATION OF ERTS IMAGERY TO THE  
INTERPRETATION OF THE GEOLOGIC FRAMEWORK OF THE  
NORTHWESTERN OLYMPIC PENINSULA, WASHINGTON AND  
THE SOUTH SIDE OF VANCOUVER ISLAND, BRITISH COLUMBIA

by

Parke D. Snavely, Jr. and Norman S. MacLeod

Detailed geologic mapping in the northwesternmost part of the Olympic Peninsula and reconnaissance studies along the southern part of Vancouver Island (figs. 1 and 2) have established the stratigraphic and tectonic framework of the Tertiary sedimentary and volcanic rocks. Aerial photography, flown by Washington State in 1971 at a scale of 1:12,500, is a valuable aid to geologic studies in the northwestern Olympic Peninsula as the topographic expression of much of the terrane is geologically controlled. A late Pleistocene continental glacier overrode this region and scoured areas underlain by soft sedimentary rocks leaving more resistant rock units in bold relief.

Despite the high quality of the large scale aerial photography, however, it does not provide the small scale synoptic view of a large region which is available on ERTS imagery. Also this satellite imagery provides a geologic overview of major geologic features, such as faults and rock units, that is important to regional geologic synthesis in regions that have been mapped only in a reconnaissance.

The ground resolution of the ERTS Imagery obtained in October 11, 1972 (no. 1030-18425, band 7) is such as to preclude interpretation of small scale structures and stratigraphic details in Tertiary strata. The resolution of equant features on the imagery is about 200 m, but islands 100 m across can be detected because of their high contrast. Linear features 50 m in width, such as sequences of sandstone beds, are readily apparent on the imagery. Without previous knowledge of the geology of this region, however, it would be difficult in some cases to relate features on the ERTS imagery to geology.

U-2 black and white photography flown at 60,000 feet on July 11, 1973 has been compared with ERTS imagery data to evaluate the relative merits of these two tools for geologic interpretation of forested areas such as that present in the northwesternmost part of the Olympic Peninsula. The U-2 photography has much greater resolution as individual stratigraphic units much less than 50 m in width can be traced in some detail in logged off areas. However, in areas covered by thick timber, large scale geologic features are more readily apparent on the ERTS imagery as the relief is more accentuated and a more synoptic view is provided.

The principal geologic features that can be discerned on the ERTS imagery in the northwestern part of the Olympic Peninsula and on southern Vancouver Island are shown on the map in Figure 2 and are discussed

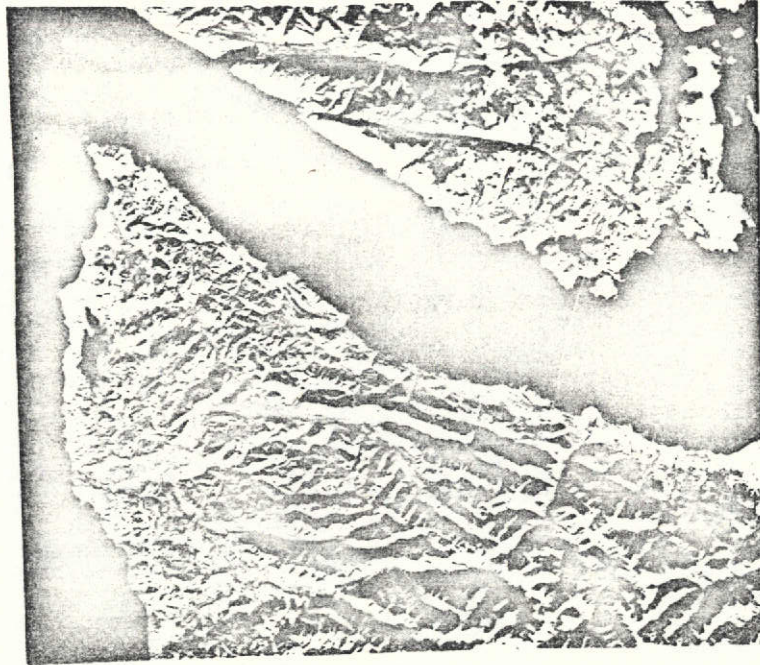


Figure 1. ERTS imagery of the northwestern part of the Olympic Peninsula and the southwestern part of Vancouver Island. Imagery obtained on October 11, 1972 (no. 1080-18425, band 7).

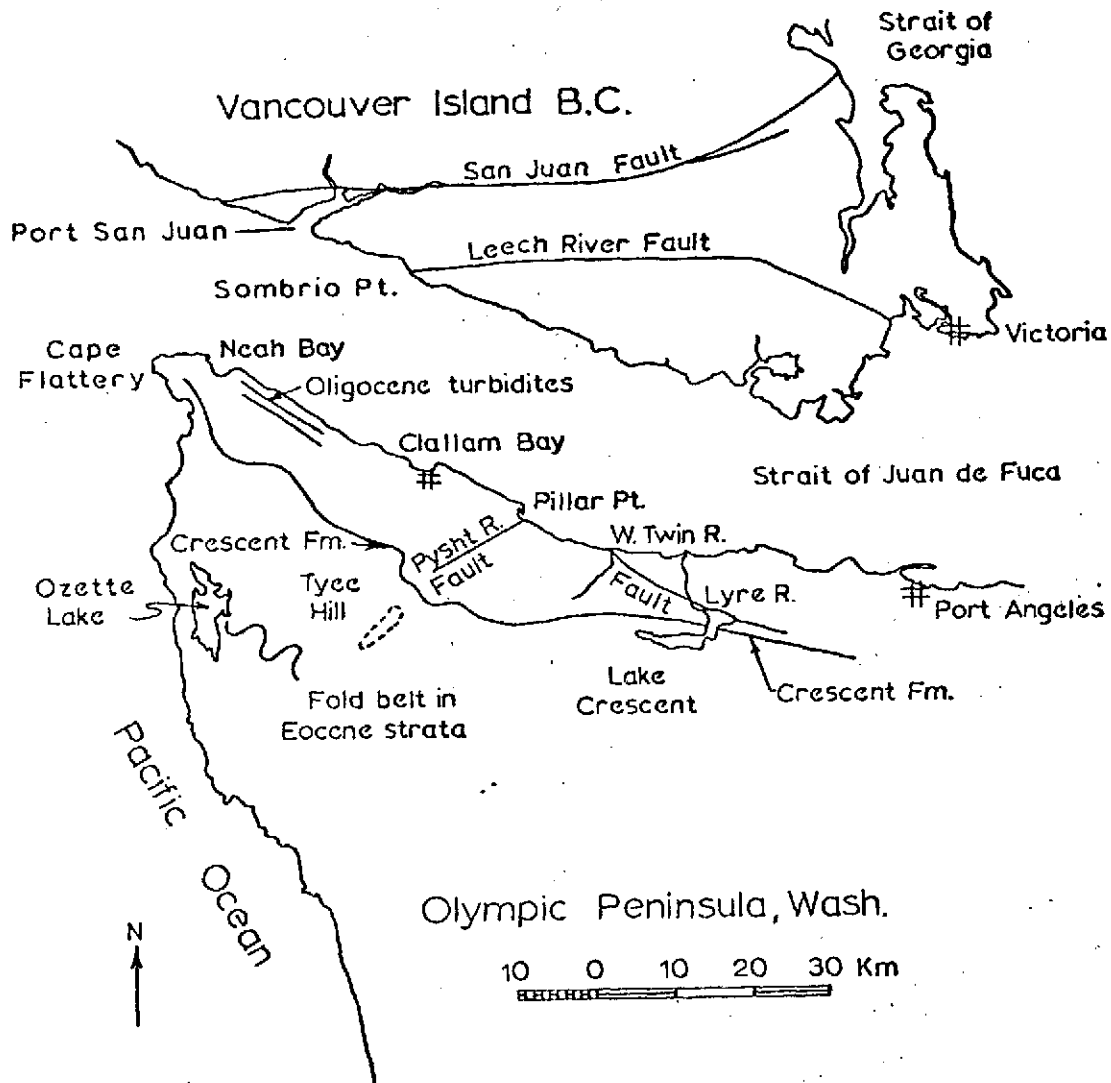


Figure 2. Principle geologic features that can be discerned on ERTS imagery of the northwestern Olympic Peninsula and southern Vancouver Island. Image was obtained on October 11, 1972 (no. 1080-18425, band 7).

below.

A north-dipping thick (7,000 m) homoclinal sequence of interbedded sandstone and siltstone of Eocene and Oligocene age exposed along the northwestern Olympic Peninsula is readily apparent on ERTS imagery because of its banded outcrop pattern. Packets of turbidite sandstone, 50-100 m thick, within Oligocene siltstone between Clallam Bay and Neah Bay are particularly well shown. Small faults that cut these sandstone units can be seen on the U-2 photography, but cannot be detected on the ERTS imagery. However, broad folds in this banded sequence and large faults that cut it can be detected on both.

The Pysht River Fault (Gower, 1960) that extends southwest from Pillar Point on the Strait of Juan de Fuca is readily apparent on the imagery. However, a marked lineation on the imagery extends southward beyond the mapped trace of the fault suggesting that it extends 6 km farther to the southeast. A large syncline in sandstone and siltstone east of the fault and a broad northeast-plunging syncline west of the fault show prominently on the image. North of Lake Crescent a marked northwest-trending lineation extends from near the head of the Lyre River on Lake Crescent to the coast near the mouth of the West Twin River. Although a fault was not mapped in this area by Brown and others (1960), a review of their geologic map indicates that a fault along the lineation on the image would explain numerous structural anomalies in this poorly exposed area.

The Tertiary sedimentary sequence overlies lower to middle Eocene submarine basalt which forms a high rugged ridge that is well defined on the image. Along the south side these volcanic rocks are thrust over a structurally complex assemblage of broken and folded mega-blocks of turbidite sandstone, siltstone, conglomerate, and mélanges composed of these rocks and basalt. Field studies have shown that many of the large "floating" blocks of sedimentary rocks measure 2-6 km in length and are complexly folded. Although the fold patterns in these blocks cannot be seen on either the 1:12,500 or U-2 black and white photography because of the dense forest cover and the modification of the relief by glacial outwash, a general pattern of folding can be detected on the ERTS image. One such folded block composed of interbedded sandstone and siltstone can be intermittently traced on the imagery along a sinuous path from Lake Ozette to a point near Tyee Hill. Field studies in this area are not yet sufficiently detailed to determine if the structural pattern suggested by the imagery is real. However, the imagery does provide a valuable guide to where new field studies should be undertaken to unravel the complex structure in this broken assemblage of rocks.

The most striking geologic features shown on the imagery are two large faults along the south side of Vancouver Island. The Leech River Fault that forms the boundary between Eocene basalts on the south and pre-Tertiary phyllites on the north is clearly defined from Sombrio Point on the Strait of Juan de Fuca, eastward to near the city of Victoria. About 10 km north of the Leech River Fault another major structure, the San Juan Fault, is

**ORIGINAL PAGE IS  
OF POOR QUALITY**

clearly defined and extends from the strait just west of Port San Juan across the entire southeastern tip of Vancouver Island to the Strait of Georgia. Numerous large scale west-trending lineations are readily apparent in the central part of Vancouver Island and some lie along faults mapped by Muller (1971).

ERTS imagery of the northern part of the Olympic Peninsula and the southern part of Vancouver is a valuable reconnaissance tool as it provides an overview of major geologic features. Large faults which juxtapose pre-Tertiary rocks of different lithologies on Vancouver Island are readily apparent but faults of equal magnitude that cut the Tertiary sedimentary rocks on the Olympic Peninsula cannot be discerned. Several faults with small displacements that cut obliquely across the bedded Tertiary sequence are clearly shown on the imagery. Thick bedded stratigraphic sequences along the north side of the Olympic Peninsula can be traced along their strike and around several large folds, but stratigraphic details in the more massive units cannot be seen. The value of ERTS imagery in this study area, and perhaps elsewhere, is inversely proportional to ones knowledge of the geologic framework as derived from surface mapping.

#### References Cited

- Brown, R. D., Jr., Gower, H. D., and Snavely, P. D., Jr., 1960, Geology of the Port Angeles-Lake Crescent area, Clallam County, Washington: U.S. Geol. Survey Oil and Gas Inv. Map OM-203.
- Gower, H. D., 1960, Geology of the Pysht Quadrangle, Washington: U.S. Geol. Survey Geologic Quad. Map GQ-129.
- Muller, J. E., 1971, Reconnaissance geologic map of Vancouver Island, British Columbia: Geol. Survey of Canada Open-file Map.

ORIGINAL PAGE IS  
OF POOR QUALITY

## SEASONAL DISTRIBUTION OF THE COLUMBIA RIVER EFFLUENT

by

Paul R. Carlson and T. John Conomos

### Introduction

The object of this chapter is to evaluate, using ERTS imagery, the seasonal distribution and dispersal of suspended particulate matter of the Columbia River effluent at sea. The green and red multispectral scanner bands (MSS-4, 0.5-0.6  $\mu\text{m}$  and MSS-5, 0.6-0.7  $\mu\text{m}$ ) of ERTS imagery can be used to delineate turbid river water where it flows into the coastal ocean (Carlson and others, 1973; Ruggles, 1973; Wright and others, 1973). Interpretation of flow direction of the nearshore near-surface water can be made from the dispersal patterns of the turbid water (Fig. 1; Carlson and Harden, 1973; Klemas and others, 1973). The repetitive, synoptic coverage afforded by ERTS provides a tool to obtain supplemental seasonal data of the coastal circulation patterns. Information evaluated in such studies may be applied, in some cases, to predict the behavior of particulate waste discharged into the coastal ocean.

The ground truth discussed herein is taken mostly from previous work (Conomos, 1968; Conomos and others, 1972a, b). ERTS imagery, sparse because of cloudy skies, was used to delineate the gross seasonal shifts in the effluent. ERTS was launched July 1972 and could have provided about 30 scenes of the Columbia River effluent, but in fact we have obtained only 4 useable scenes. The principal reasons for this paucity of useable images are the perpetual overcast skies in this region, and the location of the overpasses. The Columbia River mouth should have been visible on two consecutive days of each 18 day sequence, but normally we received only the image taken during the first day which did not cover more than about a 20 km wide strip of the ocean adjacent to the river mouth. The second pass would have shown a larger part of the ocean, but for some reason this image often was not obtained. The most likely explanation is that the satellite sensors were turned off prematurely by at least one frame.

### - Hydrographic Setting

#### The Columbia River

The Columbia River drains 670,000  $\text{km}^2$  of the northeastern United States and British Columbia (Fig. 2), and has an annual mean discharge of approximately 7,200  $\text{m}^3/\text{sec}$  (Roden, 1967). This greatly dominates the annual mean discharge (1,600  $\text{m}^3/\text{sec}$ ) of the numerous small coastal rivers of Washington and Oregon, which discharge directly into the sea.

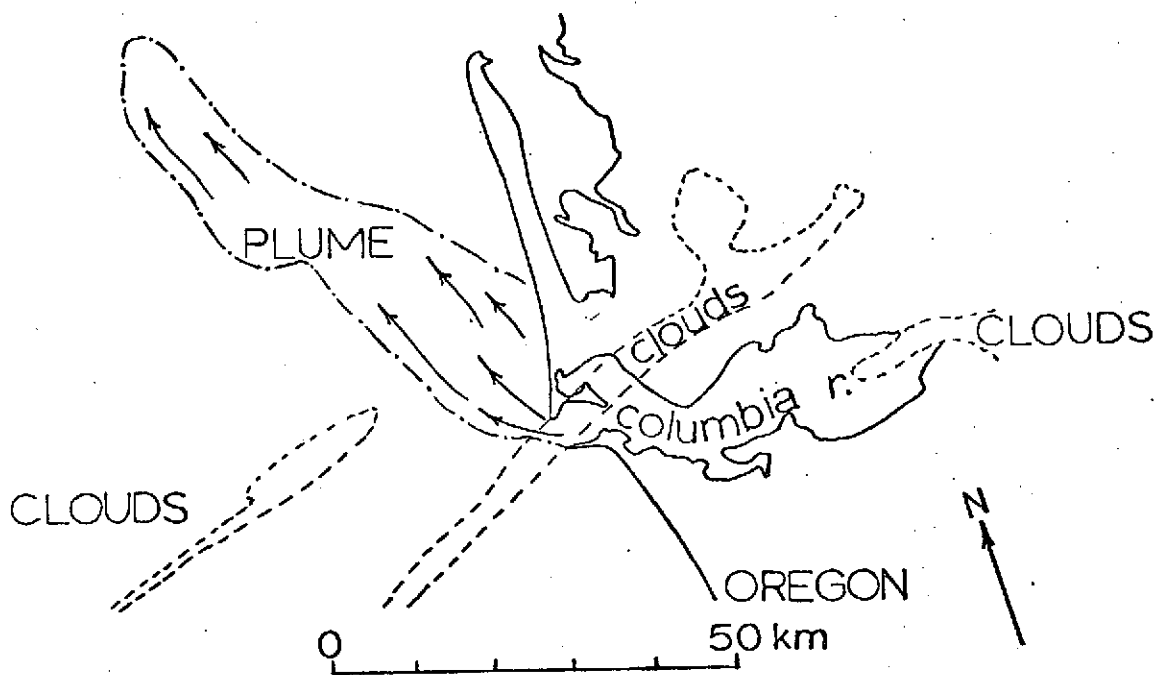
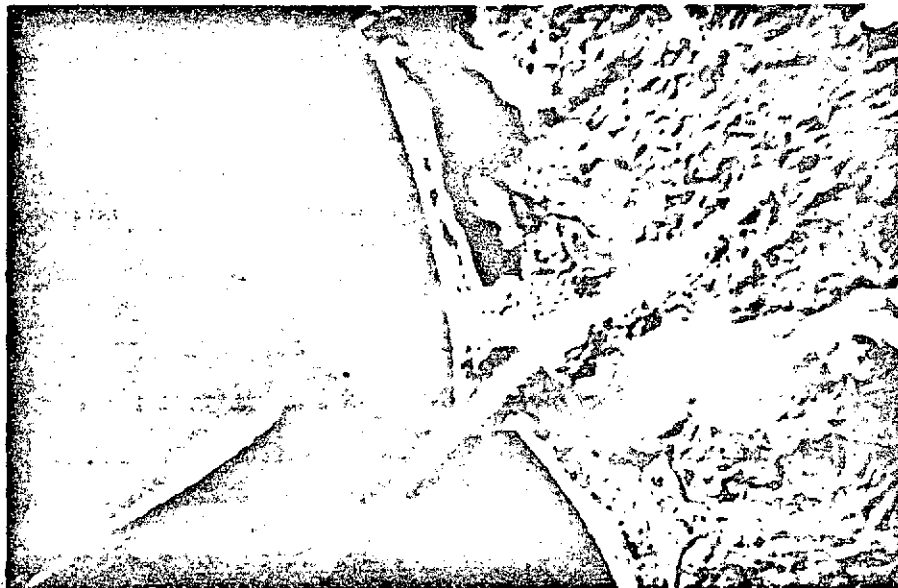


Figure 1. Upper-ERTS green-band image of Columbia River plume, Feb. 14, 1973. Lower-interpretative sketch of surface current flow based on deflection of plume.

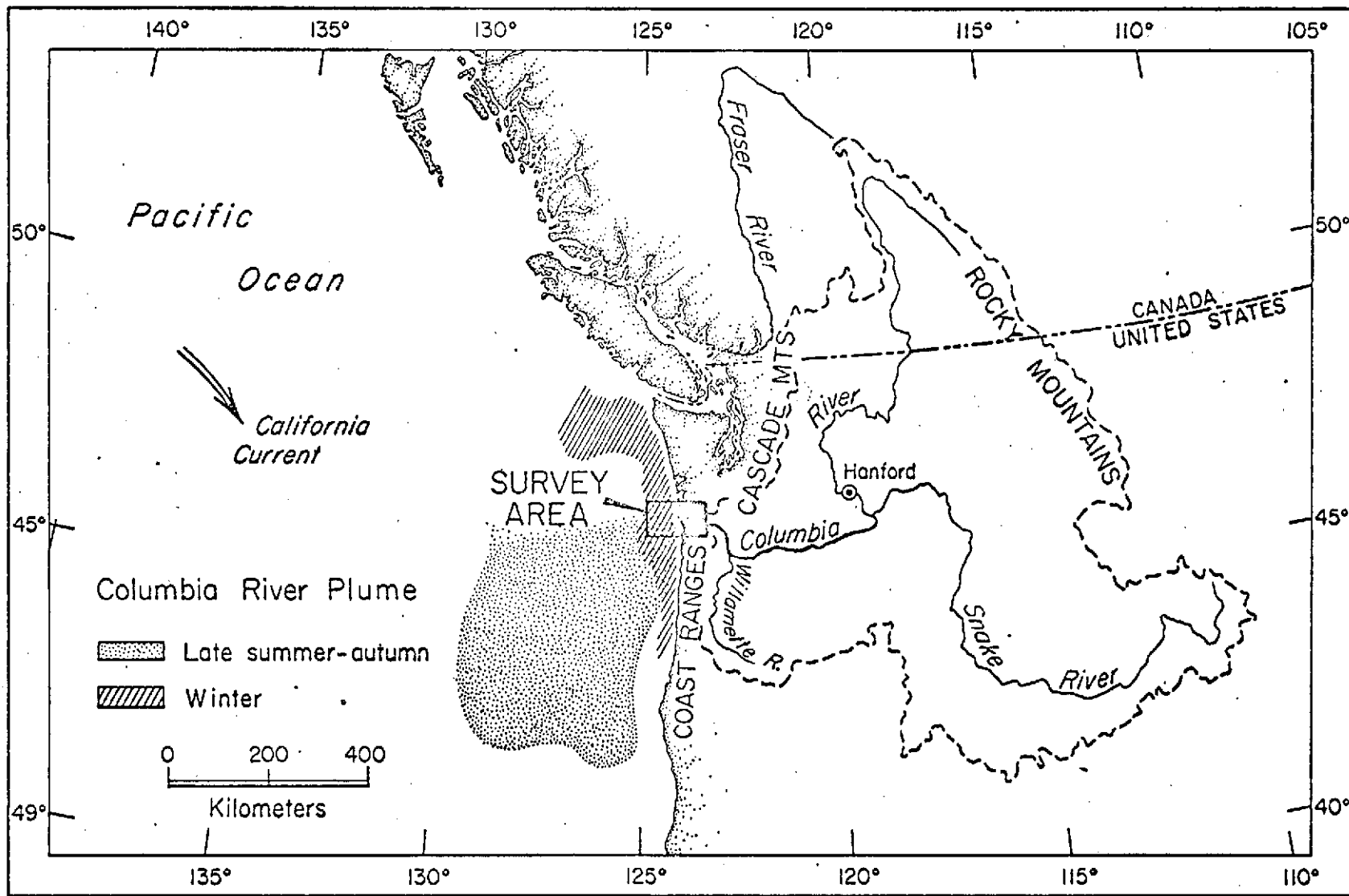


Figure 2. Regional index chart (Modified after Conomos, 1968).

There are usually two periods of maximum discharge per year in the Columbia River (Fig. 3). Normally, prolonged maximum flow occurs in mid-May to mid-June, and results from melting of snow which has accumulated during winter in the mountains and in the interior. Maxima associated with heavy rains or snow melts may occur at any time from November to March. Early autumn is a low-flow period for the Columbia and all the coastal rivers.

Heavy rain increases the winter runoff of the coastal rivers; their combined discharge, exclusive of the Columbia, accounts for about 40 percent of the total river discharge between the Strait of Juan de Fuca and San Francisco Bay, while the Columbia contributes 60 percent (Barnes and others, 1972). During late spring and summer, when the Columbia runoff is at its maximum, these coastal rivers account for less than 10 percent of the total discharge along the Washington-Oregon coast, and during early autumn they only account for about 5 percent of the total discharge; the contribution of the Columbia is 90 percent and 95 percent for late spring-summer and early autumn, respectively.

Although the annual average Columbia River discharge is 40 percent that of the Mississippi, its suspended sediment load ( $6.4 \times 10^9$  kg/yr) is less than 2 percent; the average suspended solid concentration (40 mg/l) is less than 3 percent of that of the Mississippi (Conomos, 1968).

The freshwater discharged by the river lowers the salinities of surface ocean water and forms an identifiable pool of low-salinity water ( $S \leq 32.5$  ‰) contiguous to the Columbia River mouth (Barnes and others, 1972; Conomos and others, 1972a). This pool extends offshore southwest of the river mouth in summer, and north along the coast in winter (Figs. 2, 4) in response to the prevailing winds (Fig. 3) and surface currents. A plume-like low-salinity pool is well developed and easily delineated during summer because then the Columbia River discharge is so much larger than that from nearby coastal rivers. The high discharge and the high concentrations of suspended matter which enter the ocean at this time provide a visibly detectable plume of turbid water (Pearcy and Mueller, 1969). However, during the summer of 1973, when ERTS had the potential of a synoptic overview of the plume of low-salinity turbid water, Columbia River discharge was the lowest it had been for the past 15 years (Nicholas Kallio, U.S. Geological Survey, oral communication, 1974, and therefore, the areal extent of the turbid water plume was greatly reduced. In 1972, however, shortly after launch of ERTS-1 imagery was received which showed spatial distribution of the turbid water and the deflection southward of this Columbia River effluent (Fig. 5a). A second image was obtained in January, 1973 (Fig. 5b) which showed the river effluent deflected northward.

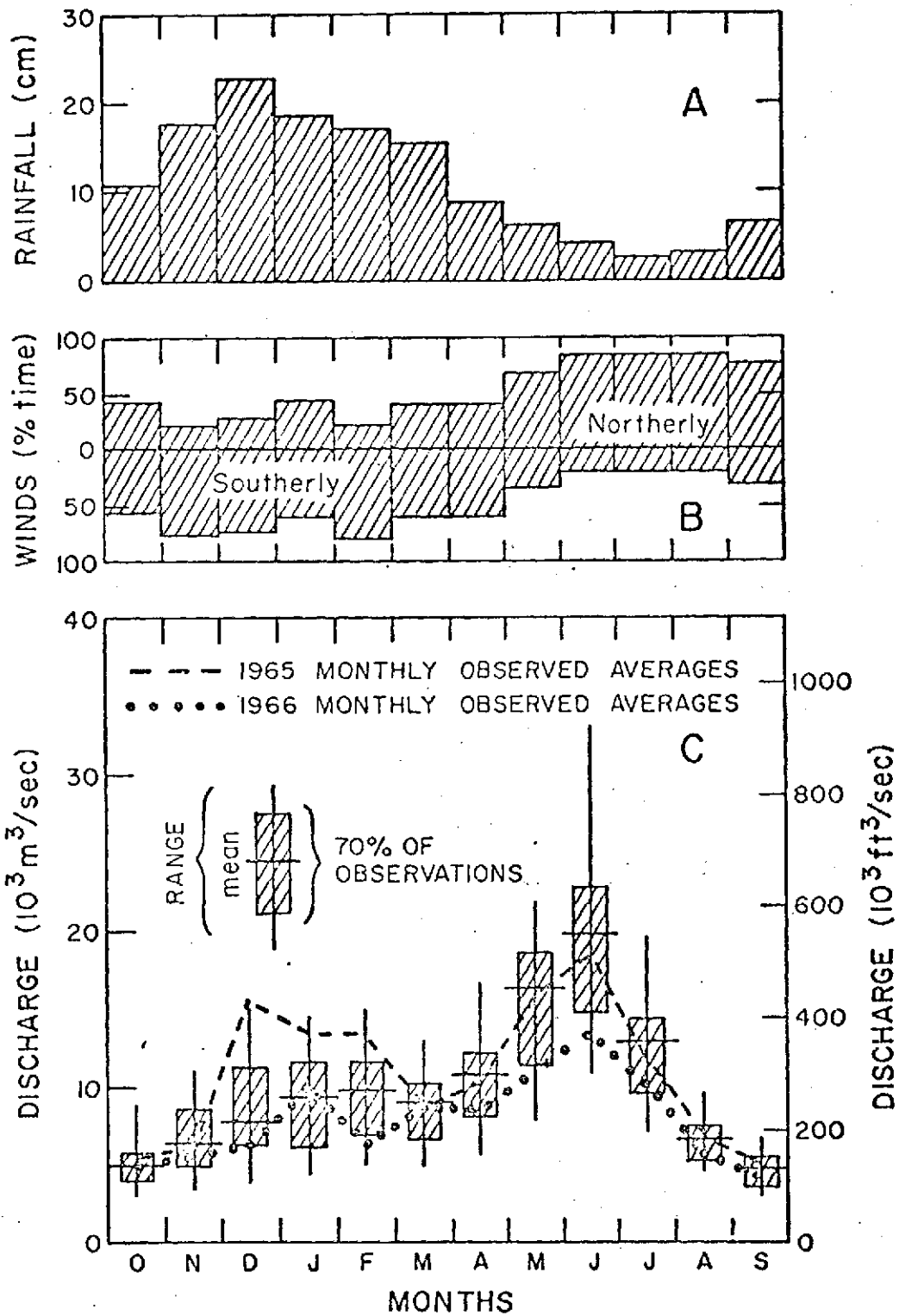


Figure 3. Average meteorologic and river discharge cycles. The 1965 (Orem, 1968) and 1966 (H. M. Orem, 1967, written communication) river discharge data are added to 1958-1962 monthly discharge averages (Modified after Conomos, 1968).

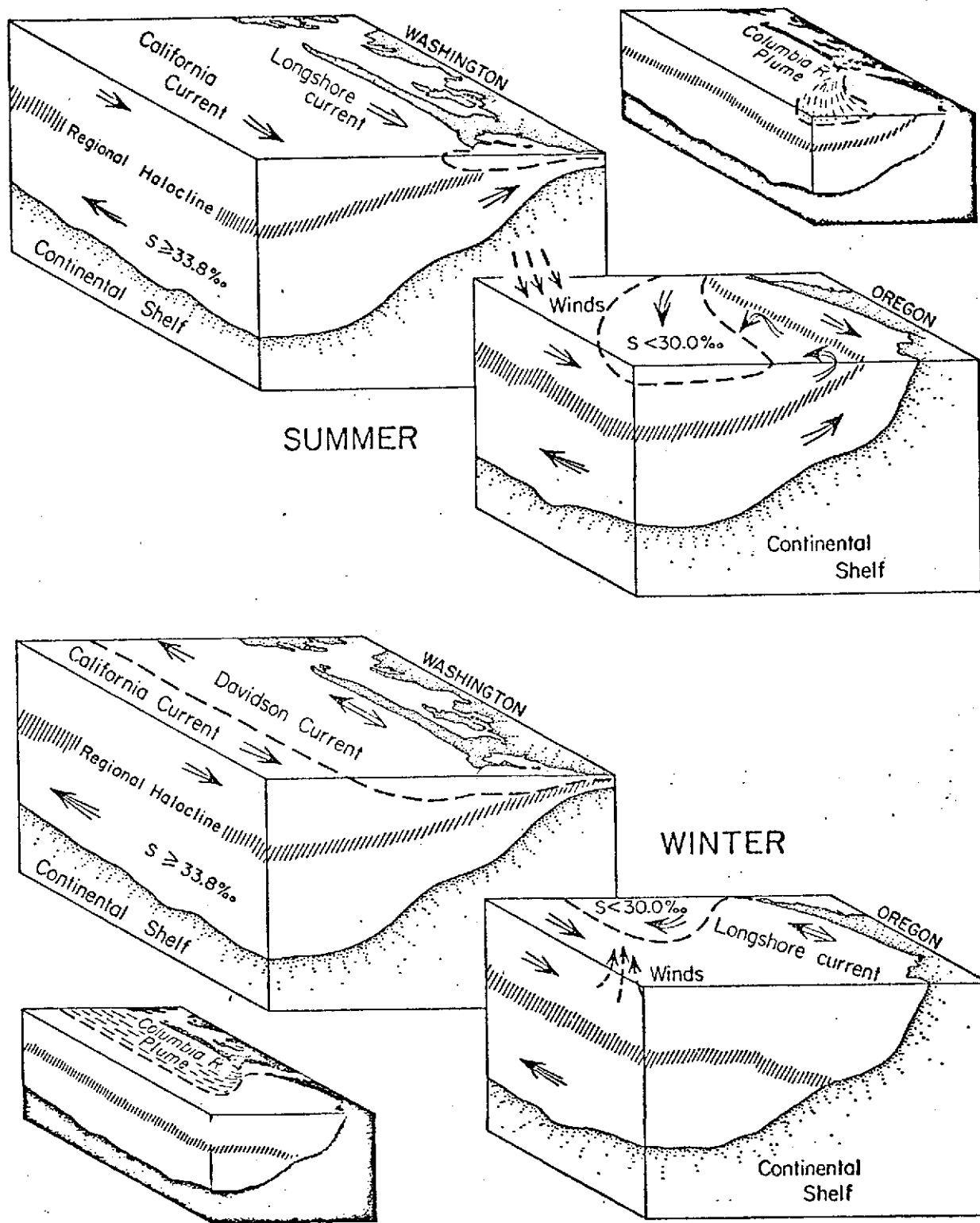
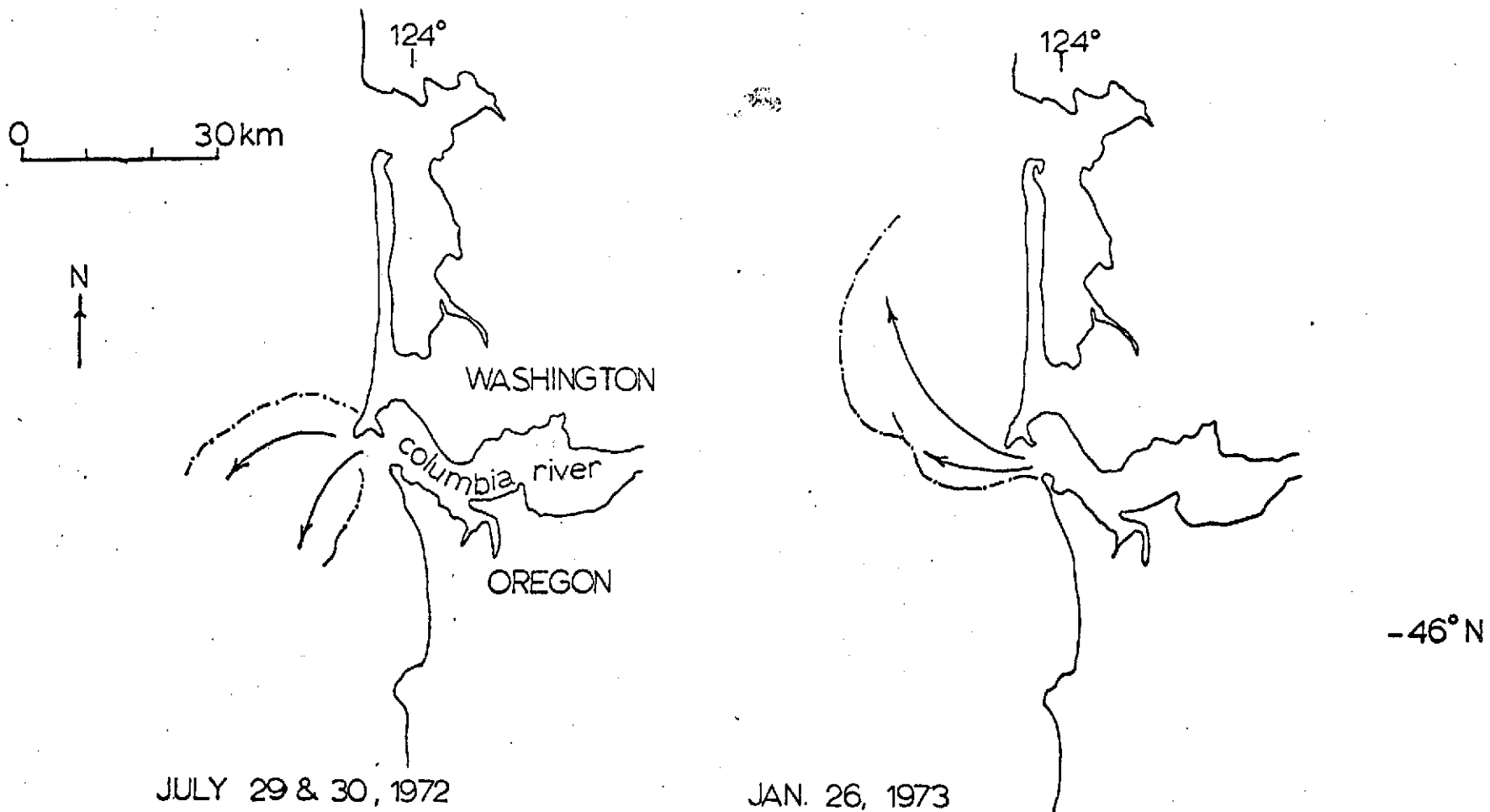


Figure 4. Summer and winter oceanographic conditions (Modified after Conomos, 1968).

ORIGINAL PAGE IS  
OF POOR QUALITY



**Figure 5.** Seasonal variations in position of the Columbia River plume as interpreted from ERTS green-band (0.5-0.6  $\mu\text{m}$ ) imagery, a) July 29-30, 1972 (no. 1006-18315 and 1007-18374) and b) January 26, 1973 (no. 1187-18383). Dashed lines indicate plume boundary and arrows show flow directions of the near surface water.

## The Northeast Pacific Ocean

The coastal northeast Pacific Ocean is characterized by relatively weak (5 to 30 cm/sec) and seasonally variable surface currents (Barnes et al, 1972). These include the southward-setting California Current, and the nearshore Davidson Current, a coastal current which sets northward in winter (Figs. 1, 5b) and reverses direction to the south in summer (Fig. 5a), becoming incorporated into the permanent California Current (Fig. 4).

### Nature of Suspended Particulate Matter

Suspended matter found in the river is primarily lithogenous, consisting of discrete mineral grains and lithic fragments (Table 1). About 35 km seaward of the river mouth (beyond the effluent; Figs. 1, 5), however, biogenous matter constitutes the bulk of the suspended matter found in the surface waters (Table 1).

Within 35 km of the river mouth, the type of biogenous and lithogenous matter present in a water parcel changes; these changes are dependent upon the spatial and temporal position of the parcel. Riverborne lithogenous matter extends into these areas in the low-salinity effluent water (Figs. 1, 5). The type and quantity of biogenous matter combined in a water parcel is largely dependent on the spatial position of the water parcel (Conomos, 1968).

In the river, the suspended matter concentrations (Table 2) and the (lithogenous) particle diameters are proportional to the river discharge. The concentrations ranged from 8 to 40 mg/l; corresponding to monthly mean river discharges of 4 to 14 x 10<sup>3</sup>m<sup>3</sup>/sec, respectively (Conomos, 1968).

In the ocean, the median concentrations and ranges decreased with distance from the river mouth (Table 2). Within 35 km of the river mouth, a region dominated by the turbid plume of river water (Figs. 1, 5), typical summer concentrations range from 2.5 to 4 mg/l; between 35 and 55 km, typical concentrations of 0.6 to 2 mg/l are measured.

There are distinct temporal changes in the transition and oceanic areas. Within 35 km of the river mouth, the variations are tidally dependent, with the highest concentrations associated with the low-salinity water, the turbid water of the river effluent (e.g. Figs. 1, 5). Seaward, variations are longer term, with late summer concentrations generally higher than early-summer concentrations (Table 2).

### Conclusions

Although no "water truth" was obtained offshore of the Columbia River when useable satellite images were obtained, comparison of river effluent patterns visible on ERTS images with previous measurements suggest that ERTS imagery is a useful tool to provide synoptic coverage. There is enough contrast between low-salinity river effluent and ambient ocean water to allow the effluent to be readily visible and thus mappable.

Table 1. Typical values of bulk composition and particle diameters<sup>a/</sup>

Area	Biogenous Matter			Lithogenous Matter Particle Diameters	
	Fraction of total (% by volume)	Phytoplankton (% marine)	Detritus/Living	Maximum	Modal
				( $\mu$ )	( $\mu$ )
River	5 - 15	0	<1	100 - 200	4 - 40
<35 km seaward of river	5 - 95	10 - 100	~1	40 - 70	4 - 50
>35 km seaward of river	70 - 95	95	>1	<4	<4

<sup>a/</sup> modified after Conomos, 1968.

ORIGINAL PAGE IS  
OF POOR QUALITY

Table 2. Typical suspended particulate matter concentrations as functions of river discharge and geographical area<sup>a/</sup>

	River Discharge (10 <sup>3</sup> m <sup>3</sup> /sec)	Suspended Particle Concentration (mg/l)		
		river	35 km from river	35 km from river <sup>b/</sup>
11-20 June 1965	14	40	4	0.6
14-26 September 1965	4	---	3	2
15-20 June 1966	10.5	15	2.5	1
13-23 August 1966	4	8	4	1.5

<sup>a/</sup> data from Conomos, 1968

<sup>b/</sup> >35 km, but <55 km from river mouth

The imagery could provide needed continuity between sampling points and could very likely provide the information necessary to explain the many apparent anomalies obtained in a single or even multiple vessel survey of such a rapidly changing environment.

#### References

- Barnes, C. A., Duxbury, A. C., and Morse, B. A., 1972, Circulation and selected properties of the Columbia River Effluent at sea, in Pruter, A. T., and Alverson, D. L., (eds.), *The Columbia River Estuary and adjacent ocean waters: Bioenvironmental studies: Univ. Washington Press, Seattle, p. 41-80.*
- Carlson, P. R., Conomos, T. J., Janda, R. J., and Peterson, D. H., 1973, Principal sources and dispersal patterns of suspended particulate matter in nearshore surface waters of the northeast Pacific Ocean and the Hawaiian Islands: ERTS Type II Progress Report, Natl. Tech. Info. Service E73-10487, 9 p.
- Carlson, P. R., and Harden, D. R., 1973, Principal sources and dispersal patterns of suspended particulate matter in nearshore surface waters of the northeast Pacific Ocean and seasonal variation in snow cover in the Sierra Nevada: ERTS Type I Progress Rept., Natl. Tech. Info. Service E73-11099/WR, 14 p.
- Conomos, T. J., 1968, Processes affecting suspended particulate matter in the Columbia River-Effluent system, Summer, 1965, 1966: Ph.D. thesis, Univ. Washington, 140 p.
- Conomos, T. J., Gross, M. G., Barnes, C. A., and Richards, F. A., 1972a, River-ocean nutrient relations in summer, in Pruter, A. T., and Alverson, D. L., (eds.), *The Columbia River Estuary and adjacent ocean waters: Bioenvironmental studies: Univ. Washington Press, p. 151-175.*
- Conomos, T. J., and Gross, M. G., 1972b, River-ocean suspended particulate matter relations in summer, in Pruter, A. T., and Alverson, D. L., (eds.), *The Columbia River Estuary and adjacent ocean waters: Bioenvironmental studies: Univ. Washington Press, Seattle, p. 176-202.*
- Klemas, V., Borchardt, J. F., and Treasure, W. M., 1973, Suspended sediment observations from ERTS-1: *Remote Sensing of Environ.*, v. 2, p. 205-221.
- Orem, H. M., 1968, Discharge in the lower Columbia River basin, 1928-1965: U.S. Geol. Surv. Circ. 550, 24 p.

- Pearcy, W. G., and Mueller, J. L., 1969, Upwelling, Columbia River Plume and Albacore Tuna: Sixth Intern. Symp. Remote Sensing Environ. Proc., Univ. Mich., Ann Arbor, p. 1101-1113.
- Roden, G. I., 1967, On river discharge into the northeastern Pacific Ocean and the Bering Sea: J. Geophys. Res., v. 72, p. 5613-5629.
- Ruggles, F. H., 1973, Plume development in Long Island Sound observed by remote sensing (ERTS-1), in Symposium on significant results obtained from the Earth Resources Technology Satellite-1: Goddard, Maryland, v. 1, p. 1299-1303.
- Wright, F. F., Sharma, G. D., and Burbank, D. C., 1973, ERTS-1 observations of sea surface circulation and sediment transport, Cook Inlet, Alaska, in Symposium on significant results obtained from the Earth Resources Technology Satellite-1: Goddard, Maryland, v. 1, p. 1315-1322.

DISTRIBUTION, ABUNDANCE, AND COMPOSITION OF SUSPENDED PARTICLES  
IN THE SAN FRANCISCO BAY SYSTEM, APRIL AND JULY 1973

by

P. R. Carlson, T. J. Conomos, H. J. Knebel, D. H. Peterson,  
E. P. Scrivani, R. E. Smith, W. C. Todd, S. M. Wienke

INTRODUCTION

This research evaluates the distribution, abundance, and composition of suspended particles in an estuarine environment. The information gained allows us to predict the behavior of man made and naturally occurring suspended particles. The San Francisco Bay system was chosen as the study area because much oceanographic data (i.e., water properties and movement, biota and sediments) had been collected in this system.

The following aspects of suspended matter were studied:

- (1) Determination of the concentrations of suspended particles in near-surface waters with emphasis on the temporal and spatial distribution as related to water properties and structure.
- (2) Determination of the bulk clay mineral composition of the lithogenous fraction of the near-surface suspended particles.
- (3) Determination of the species composition and cell numbers of phytoplankton in near-surface waters.

Spring and summer were chosen for the study, as then, the effects of high winter river discharge are diminishing and phytoplankton production is increasing towards the summer maximum. Although observations were planned in conjunction with ERTS overflights, cloudy skies frequently disrupted plans; imagery often provided clear coverage of only a portion of the bay system.

Previous Work

Past investigations concerned with the San Francisco Bay region presently are being compiled by the U.S. Geological Survey. The seasonal oceanographic framework of the adjacent ocean was briefly described by Conomos and others (1970a).

Investigations of the nontidal surface and near-bottom were made by Conomos and others (1970b, 1971). Investigations of physical processes occurring within the survey area include those of McCulloch and others (1970) who described south bay flushing as related to river discharge, and Peterson and others (1974a) who described the null zone in north bay.

Carlson and McCulloch (1974) described variations in circulation of surface waters based on aerial observations.

Descriptions of the water chemistry in north bay include those of Conomos and Peterson (1974) and Peterson and others (1974b). These studies of water chemistry have been complemented by studies concerned with the production of phytoplankton as related to hydrography (Scrivani, 1974).

Interest in the abundance, composition, and distribution of suspended particles in the oceans has increased in the last three decades because of the importance of this matter as a potential source of food for marine organisms. Investigations of suspended matter include world-wide surveys typified by those of Jerlov (1953) and Lisitsin (1962) and regional surveys of Manheim and others (1970, 1972).

Investigations of inorganic fraction have traditionally emphasized sedimentary processes. Suspended sediment concentrations of many major rivers have been monitored (for example, Dole and Stabler, 1909). Studies of estuarine sedimentary processes were summarized by Postma (1967), Schubel (1968), and Meade (1972). Studies of the distributions of particulate matter in major river effluents at sea include the Mississippi (Scruton and Moore, 1953), the Orinoco (van Andel and Postma, 1954), and the Columbia (Conomos and Gross, 1972). Carlson and Harden (this volume) have described some variations in the San Francisco Bay effluent as it is dispersed in the adjacent Pacific Ocean. Studies of mineral composition of particles suspended in the open ocean include those of Ishii and Ishikawa (1964), Jacobs and Ewing (1965), and Manheim and others (1972).

### Regional Setting

#### Climate

The climate is characterized by mild wet winters and cool foggy summers. Precipitation is highly seasonal with 90 percent of the annual precipitation usually occurring from November through April (Rantz, 1971). Prevailing summer winds are from the northwest and west; the winter winds, generated by storms, are from the southeast to south.

#### Hydrology

More than 90 percent of the mean annual river discharge ( $840 \text{ m}^3/\text{sec}$ ) entering the bay system is contributed to north bay by the combined inflows of the Sacramento and San Joaquin rivers (Fig. 1; McCulloch and others, 1970); about 5 percent is contributed directly into south bay by the small local streams. This mean annual discharge,  $4 \text{ m}^3/\text{sec}$ , is less than that of the wastewater flows,  $10 \text{ m}^3/\text{sec}$  (220 million gallons/day), contributed directly into south bay by the heavily populated surrounding communities (Hines, 1973). High river runoff occurs during the winter months and reflects the high precipitation in the drainage basin.

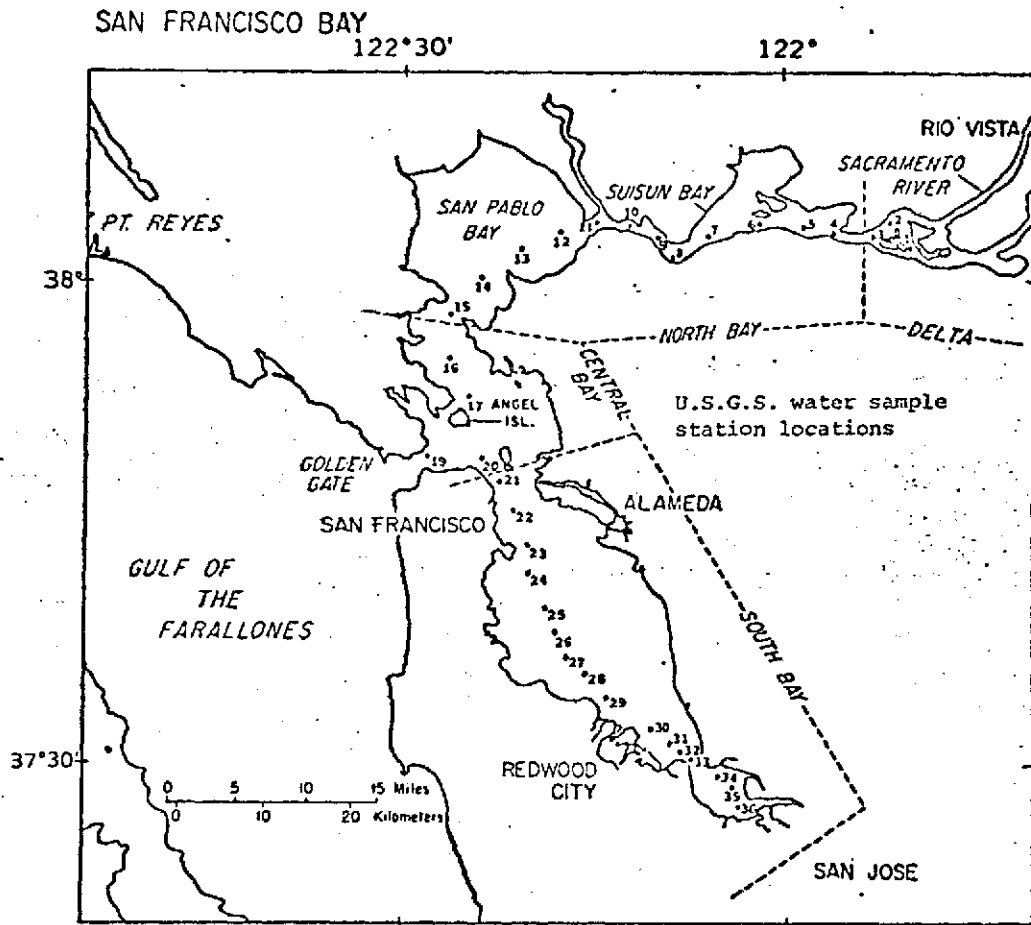


Figure 1. The San Francisco system and environments. North, south, and central bay designations are often used. Numbers indicated reoccupied hydrographic stations.

## Hydrography

The diurnal tidal range varies from 1.7 meters at Golden Gate to 2.7 meters at the south end of the bay system (U.S. Coast and Geodetic Survey, 1973). Waves generated in response to high winds and the long fetch within the south bay play a significant role in sediment transport. The observed frequency of wave heights of 0.5 to 1 meter is at least 50 percent (Conomos, 1963).

The water turbidity, expressed as Secchi disc depths, typically ranges from less than 0.25 m in the shallow areas to over 3 m in the channels nearest Golden Gate. The high turbidity is caused primarily by wave and current resuspension of fine-grained sediment in the shallow areas. In north bay, river-borne suspended particles are a dominant factor in increasing the turbidity. In south bay, secondary sources of turbidity are the streams and sewage effluents, and low-salinity high turbidity river water transported southward from north bay (McCulloch and others, 1970; Carlson and McCulloch, 1974).

Dilution of Pacific Ocean water by Sacramento-San Joaquin river discharge decreases the salinity and increases the turbidity in north bay. In south bay, the small streams and wastewater flows have only local effects in decreasing the salinity (McCulloch and others, 1970). Water salinity varies greatly both spatially and seasonally. At Golden Gate, for example, winter salinities typically range from 18 to 26 ‰ and reflect the high river inflows, while summer salinities are somewhat higher, ranging from 29 to 32 ‰. Salinity stratification is present during winter (vertical differences of up to 10 ‰) in most portions of the bay system. In the south bay during summer, however, little low-salinity water is present and the water column is well mixed by tidal currents and wind generated waves.

Water temperatures vary seasonally and are generally controlled by ocean and river water temperatures and insolation effects. In the channels, typical winter temperatures are 7 to 9 °C; summer temperatures often exceed 20 °C.

## Circulation

Circulation is controlled by tidal and nontidal water movements. Tidal currents, often in excess of 100 cm/sec, mix and move water, which in turn transports and resuspends bottom sediments. Nontidal circulation, generated by water density differences and wind is generally less than 10 cm/sec (Conomos and others, 1971). For describing this nontidal circulation, the bay system can be divided into (1) a north bay--central bay--Gulf of the Farallones region that demonstrates a permanent circulation cell typical of a partially mixed estuary, and (2) a south bay region that has seasonally reversing but sluggish near-bottom and surface currents (McCulloch and others, 1970; Conomos and others, 1971).

Perennial estuarine circulation in north and central bay and the adjacent ocean is maintained by Sacramento-San Joaquin River runoff. This runoff, mixed with ocean water, forms a turbid low-salinity low-density upper layer which moves seaward (Fig. 2). Ocean water at depth moves toward the river to replace ocean water which has been entrained or mixed upward into the surface outflow.

In contrast to north and central bay, south bay does not exhibit normal estuarine circulation, but instead experiences seasonally reversing surface and near-bottom nontidal currents. The role of nontidal circulation in transporting suspended sediment in south bay is unknown.

## METHODS AND MATERIALS

### Field Methods

Samples were collected and observations made during April and July 1973 cruises of the R/V Polaris to coincide approximately with ERTS overflights. The observations were made within either a one- (July) or two-day (April) period at 36 stations in the midchannel of the bay system between the fresh-water boundary and the southern end of south bay (Fig. 1).

Analyses were made with a continuous-flow system in which the water was pumped from 2 m to the ship through a towable salinity-temperature-depth pumping system (Beers and others, 1967). Simultaneous continuous determinations of turbidity were made (Schemel, this volume).

Discrete water samples were drawn for studies of phytoplankton cell counts, particle counts, particle mass determinations, and x-ray diffractometric analysis. For gravimetric and x-ray diffractometric determinations of the suspended particles, between 250 and 750 ml of water were filtered through silver membrane filters with a 0.45  $\mu$  pore diameter. The filters were subjected subsequently to gravimetric, microscopic, and x-ray diffractometric analyses. Procedures for collection and presentation of phytoplankton are similar to those of Vollenweider (1969).

### Analytical Methods

Salinity was determined by conductivity measurements (Brown and Hamon, 1961). The turbidity was measured by transmissometric techniques (Jerlov, 1968).

To minimize contamination and sample loss, the salt was not rinsed from the filters. The concentration of suspended particulate matter was calculated from the weight differences between the tare weight of the filter and the filter with air-dried suspensate, divided by the



Figure 2. Plume of turbid, low salinity water in the Gulf of the Farrallones. Note variations in turbidity of surface water throughout bay system. ERTS image, band 5 (0.6-0.7  $\mu\text{m}$ ), no. 1255-18183, April 4, 1973.

ORIGINAL PAGE IS  
OF POOR QUALITY

volume of water filtered.

These filters were then cut in half; one half was subjected to X-ray diffractometric analysis, and the other half was examined by scanning electron microscopy (SEM). For the X-ray diffractometric analyses of the crystalline constituents of the suspensate, a Norelco<sup>R</sup> X-ray diffractometer was used with nickel-filtered copper K $\alpha$  radiation and a Geiger detector. For each sample, four X-ray diffraction spectra were obtained: air dried, glycolated, and heated at 400° C and 550° C according to the method of Hathaway (1956).

For SEM analysis, approximately 0.25 cm<sup>2</sup> of the silver filter with suspensate was glued on a cylindrical specimen stub. The specimen was then coated under vacuum with vapor generated from a 60-40 percent gold-palladium wire. The sample was then viewed on a cathode ray oscilloscope at 700 and 5000x magnification. Desired images were photographed for future study.

For determination of particle numbers and volumes, water samples were immediately analyzed with a Coulter<sup>R</sup> particle counter (Sheldon and Parson, 1967). The sample was mixed by shaking and swirling; 150-200 ml were poured into the instrument beaker and stirred continuously during measurements. Each analysis was conducted twice through a 200- $\mu$  aperture tube, so that the counts on a 2-ml volume were measured and also until a desired number of particles had been counted. Particle-free salt solution was added if necessary to insure that either there was sufficient electrolyte present for maintenance of the electric field, or that the sample concentration was low enough to minimize sample counting errors caused by coincidence factors (Sheldon and Parsons, 1967); any errors introduced by coincidence factors were not corrected. A ragweed pollen standard was frequently used for instrument calibration.

Procedures for phytoplankton species identification and cell counts are similar to those of Strickland (1966) and Lund and others (1958).

## RESULTS

### Water Characteristics

#### Salinity and Temperatures

The temperatures of the near-surface (2 m) waters were controlled by successive admixtures of warmer river water and cooler ocean water (Fig. 3). There was significant warming of estuarine waters between April and July; river temperatures rose 6°C from 16 to 22°C, whereas the ocean temperatures rose 3°C from 12 to 15°C.

The salinities of both ocean and bay waters increased from April to July; at any given station salinities increased from 3 to 5 ‰. Salt water (>1 ‰) intruded several kilometers landward in the estuary (Fig. 3) from April to July.

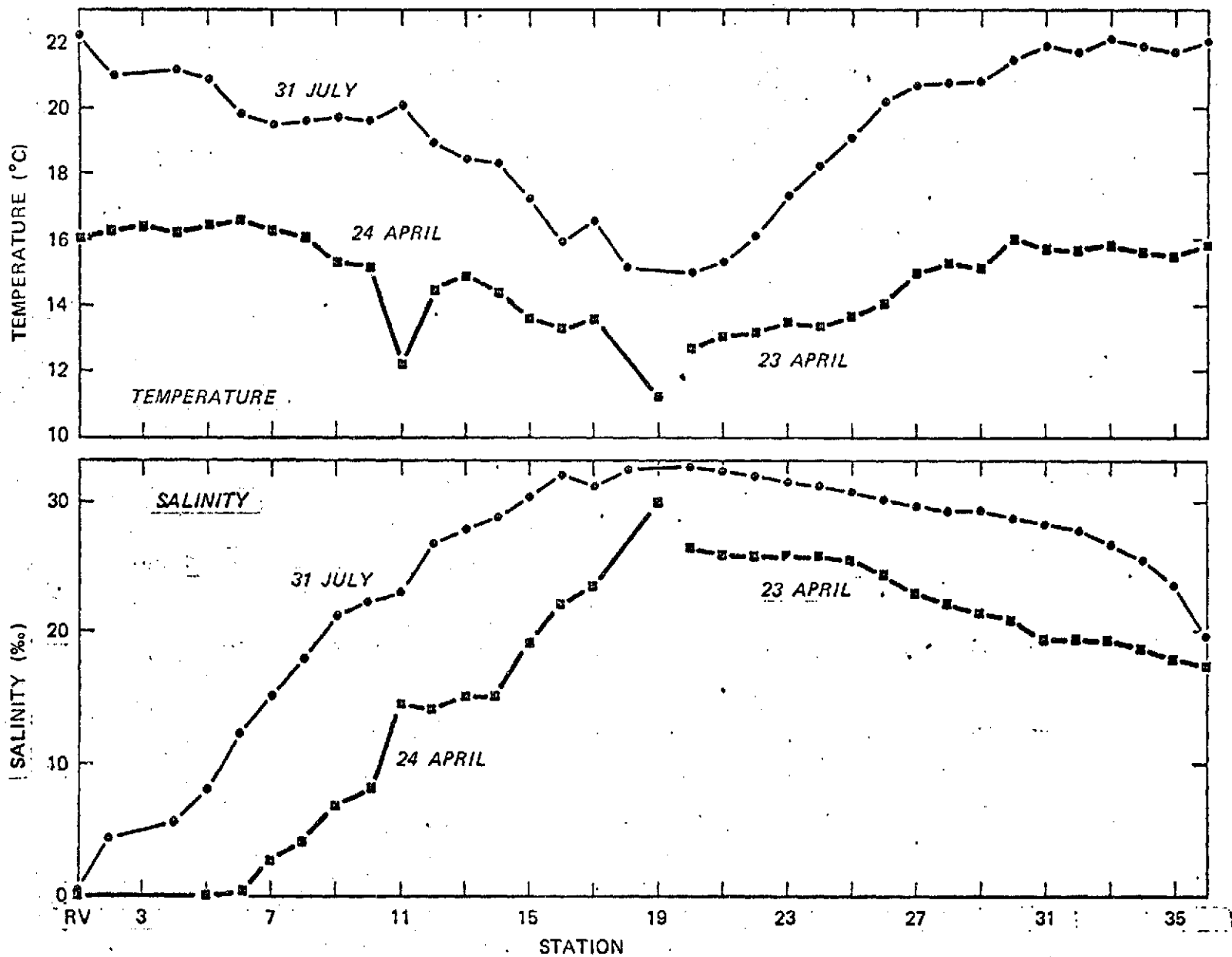


Figure 3. Longitudinal distribution of salinity and temperature at 2 m measured during April and July sampling cruises, from Rio Vista (RV) to Golden Gate (Sta. 19) in North Bay and Sta. 21 to Sta. 36 in South Bay (see fig. 1 for station locations).

## Turbidity

The water turbidity, as measured by a transmissometer, showed a generally similar distribution for both April and July (Fig. 4). The most turbid water was found in north bay between stations 2 and 12 (Fig. 5) and at the southern end of south bay (stations 31 to 36; Fig. 2). It should be noted that this north bay water at 2m depth (stations 2 to 12) is more turbid than that contributed by the river, and that the zone of highest water turbidity shifted landward in July. The highest turbidity area was located between stations 7 to 11 during April and stations 2 to 7 during July. The least turbid water was found in central bay (stations 14 to 23). The bay water at 2 m was generally more turbid during April than July.

## Suspended Particle Characteristics

### Nature of particles

There are two different types of suspended particles:

(1) lithogenous: inorganic and generally crystalline; ultimately derived from the erosive weathering of rocks and transported to the bay system by fluvial processes;

(2) biogenous: particles formed by organisms; organic in nature, they may be either living (phytoplankton and zooplankton) or nonliving (organic detritus) (Parsons, 1963). This biogenous matter can be riverborne (contributed directly by the river) or ambient (formed in the oceanic and estuarine areas).

Riverborne suspended particles, are primarily lithogenous, consisting of discrete mineral grains and lithic fragments (Fig. 6, 8). The remaining fraction includes both living and detrital biogenous matter. The living portion is principally phytoplankton in the form of diatoms (Scrivani, 1974). The organic detritus is mainly plant fibers (Figs. 6, 7, 8, 9).

Near Golden Gate biogenous matter constitutes the bulk of the suspended particles (Figs. 7, 9) and consists of small standing stocks of phytoplankton, with diatoms predominating (Scrivani, 1974). The organic detritus is mainly fecal pellets, wood fibers, and fragmented plant cells.

The type of biogenous and lithogenous particles present in a water parcel change depending on the spatial and temporal position of the parcel. Riverborne lithogenous matter extended further seaward in the low-salinity water during April than during July (Fig. 10).

### Particle concentrations

Particle concentrations were greatest in north bay, having maximum values of 140 mg/l (Fig. 11); the lowest concentrations (10 mg/l) were at Golden

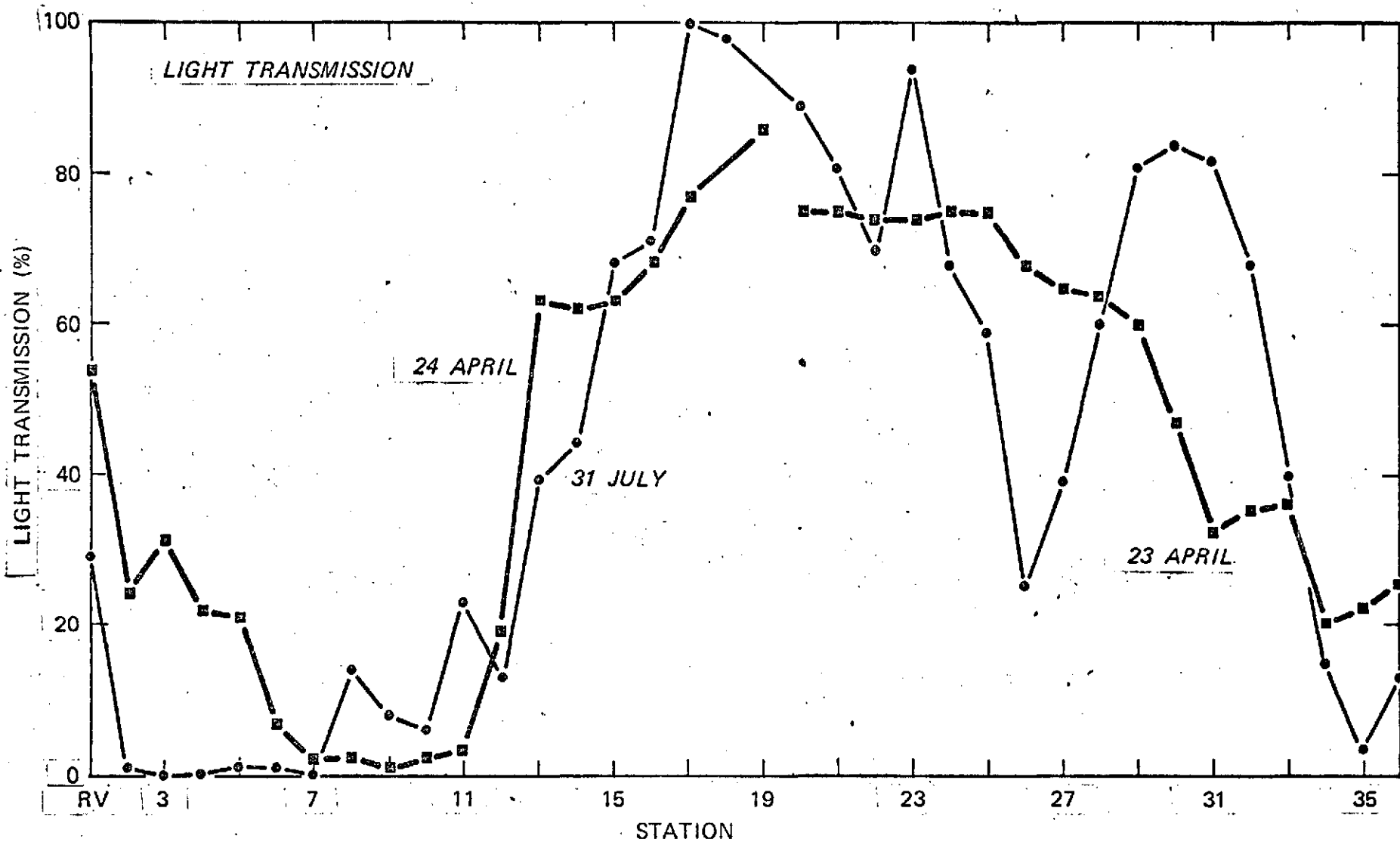
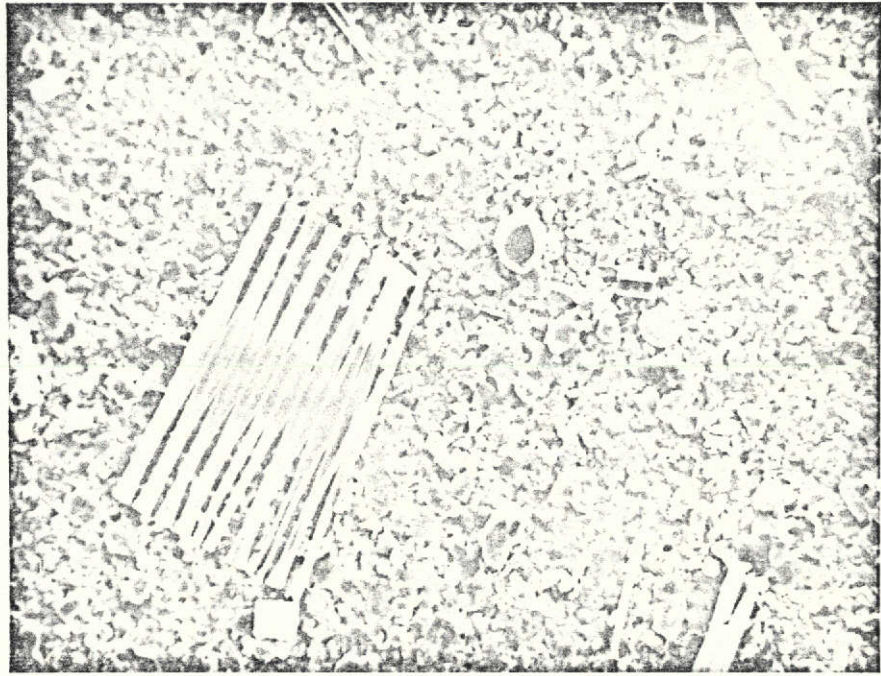


Figure 4. Longitudinal distribution of light transmissivity at 2 m measured during April and July sampling cruises, from Rio Vista (RV) to Golden Gate (Sta. 19) in North Bay and Sta. 21 to Sta. 36 in South Bay (see fig. 1 for station locations).



Figure 5. Turbid water in the eastern half of Carquinez Strait and the western half of Suisun Bay. Infrared photograph (690-760 nm) from U-2 aircraft at altitude of  $\sim 21,000$  m, April 3, 1973, (flight no. 73-051; accession no. 1057-0159).

A.



B.

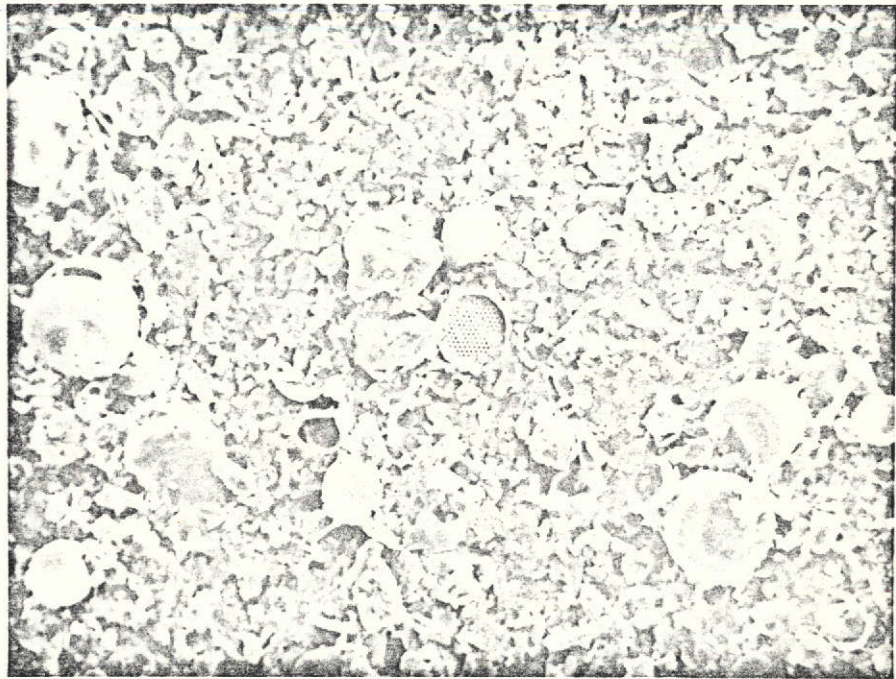
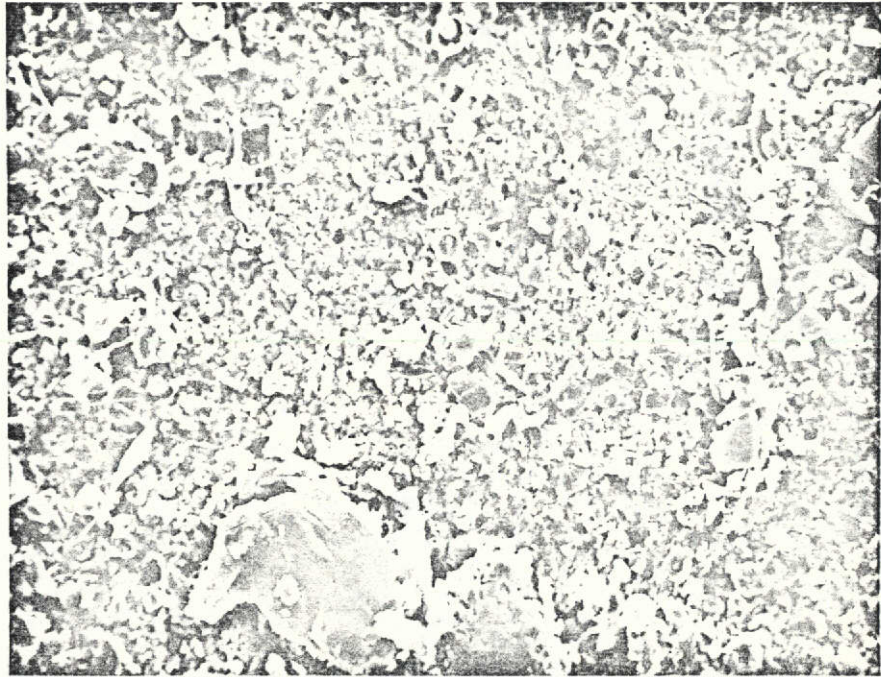


Figure 6. Typical suspended matter (2-m depth) viewed with a scanning electron microscope at 700x magnification. A: Station RV 24 April 1973 identifiable organisms include Fragilaria (lower left), Melosira (upper right), Asterionella (upper center), and Cyclotella (right center). B: Station 6, 24 April 1973; identifiable organisms include Stephanodiscus (left center), Coscinodiscus (center), and Cyclotella (lower right).

A.



B.

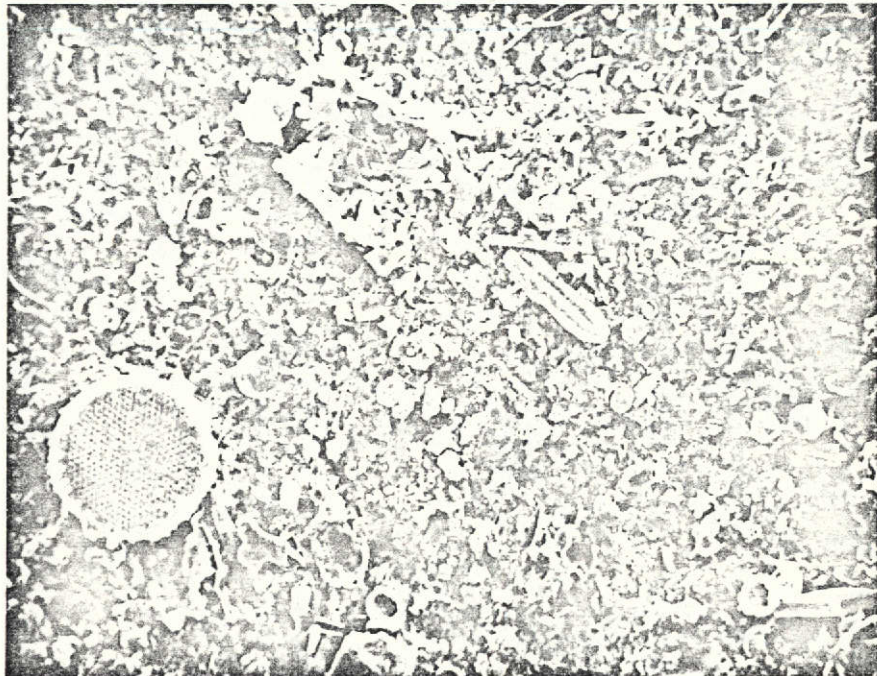


Figure 7. Typical suspended matter (2-m depth) viewed with a scanning electron microscope at 700x magnification. A: Station 19, 24 April 1973; identifiable organisms include Cylindrotheca (left center) and a fragment of Coscinodiscus (lower center). B: Station 36, 23 April 1973; identifiable organisms include Stephanodiscus (left center) and Diploneis (center).

A.

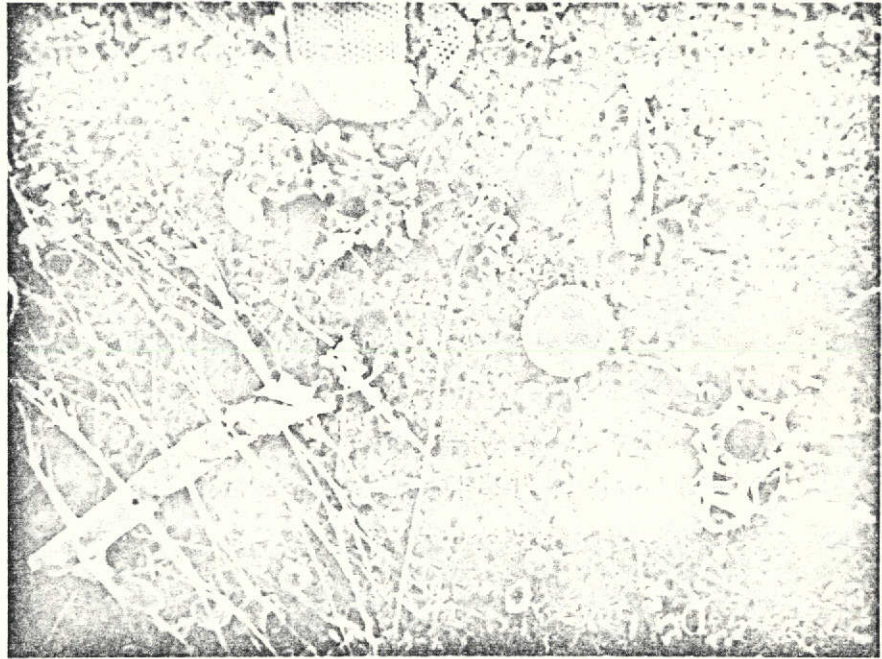


B.



Figure 8. Typical suspended matter (2-m depth) viewed with a scanning electron microscope at 700x magnification. A: Station 3, 31 July 1973; identifiable organisms include Thalassiosira (center and upper right). B: Station 6, 31 July 1973; identifiable organisms include pennate diatom (upper center), a fragment of Skeletonema (right center), Thalassiosira (lower center) and Chaetoceros (lower left).

A.



B.

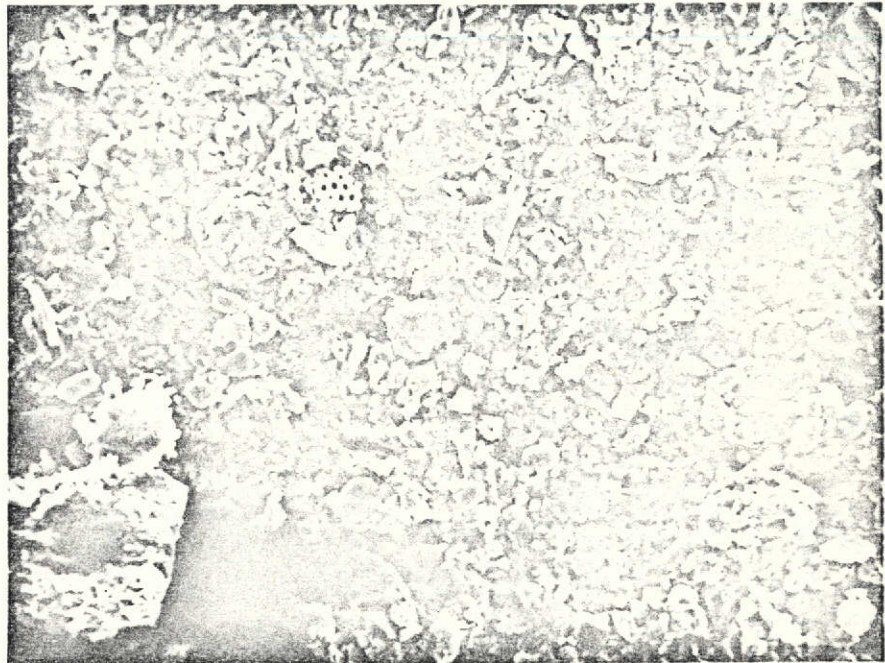


Figure 9. Typical suspended matter (2-m depth) viewed with a scanning electron microscope at 700x magnification. A: Station 19, 31 July 1973; identifiable organisms include Coscinodiscus (upper center), Thalassiosira (center), Silicoflagellate skeleton (lower right), and Chaetoceros (lower left). B. Station 36, 31 July 1973.

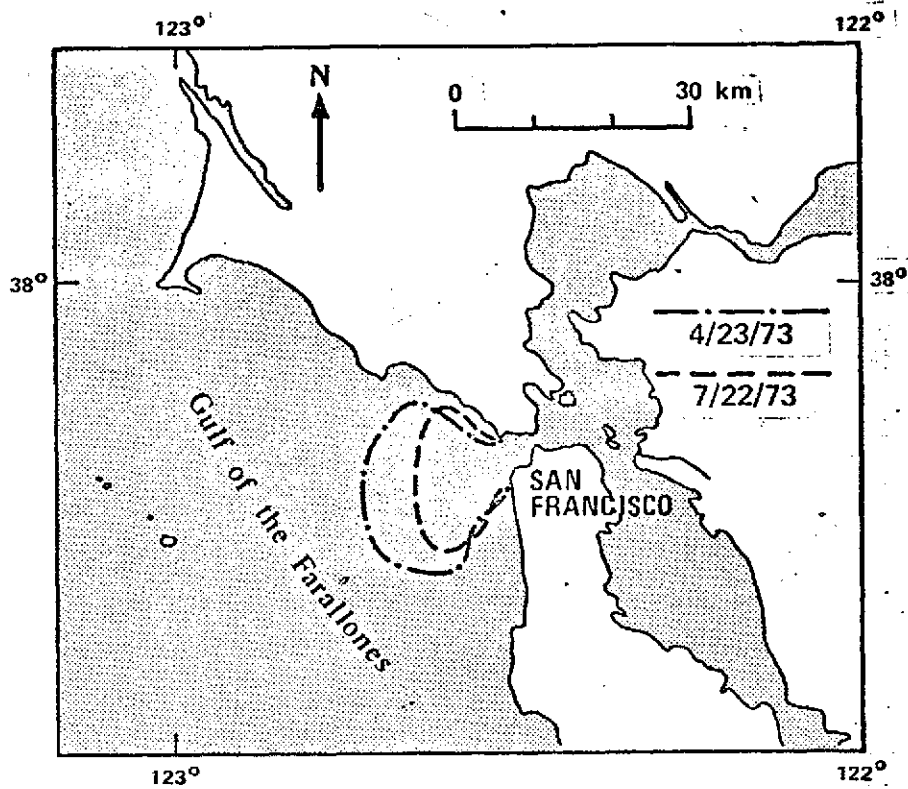


Figure 10. Suspended sediment plume boundaries in the Gulf of the Farallones for spring (dash-dot) and summer (dash) discharge conditions. Traced from ERTS imagery MSS-4 band of April 23, 1973 (no. E-1274-18241) and July 22, 1973 (no. E-1364-18231).

ORIGINAL PAGE IS  
OF POOR QUALITY

66

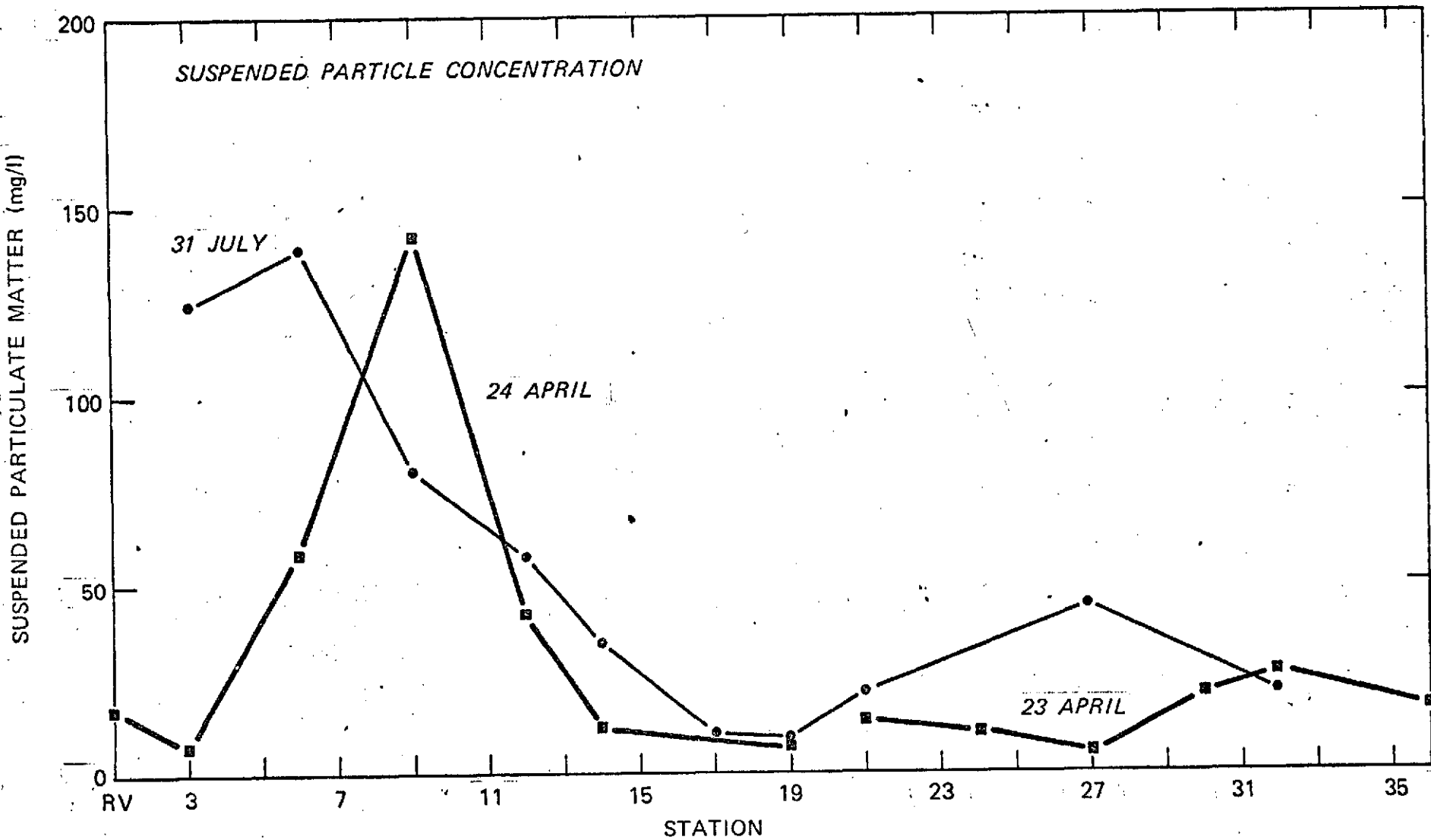


Figure 11. Longitudinal distribution of suspended particles at 2 m, expressed in mg/l, determined during April and July sampling cruises (Sta. RV-19 in North Bay and Sta. 21-36 in South Bay).

Gate (station 19). South bay was characterized by water of intermediate concentrations, ranging from 10 to 40 mg/l. The concentration maximums in north bay coincide both temporally and spatially with the turbidity maximums (Figs. 4, 11).

Particle concentrations, as measured with a Coulter counter, ranged from 40,000 to 90,000 particles/ml in April (Fig. 12) and from 13,000 to 50,000 particles/ml in July (Fig. 13). During April the highest numbers were found in north bay and coincided with the turbidity (Fig. 4) and suspended particle (Fig. 11) maximums; during July, this maximum was not as well defined. The south bay concentrations during April and July were similar.

#### Phytoplankton cell numbers

Cell numbers ranged from 1300 to 1400 cells/ml during April (Fig. 12) and from 1100 to 1500 cells/ml during July (Fig. 13). Highest numbers were found at stations 7 and 9 during April and July, respectively.

#### Particle sizes

The range of particle diameters, measured by Coulter<sup>R</sup> counter, is about 2 to 100  $\mu$ . During April, the mode of this size distribution varied spatially (Fig. 14): in river water, the mode was  $\leq 4 \mu$ , whereas in the area of the turbidity maximum, a well-defined mode occurred between 8 and 20  $\mu$ ; at Golden Gate, oceanic waters were characterized by particles of two discrete modal diameters, 8 and 64  $\mu$ ; in south bay, the modal diameter was 8  $\mu$ . During July (Fig. 15), the particles in the turbidity maximum showed similar distributions to those seen in April, with modal diameters of about 16  $\mu$ ; similarly, the Golden Gate station showed a bimodal distribution, and the south bay station showed a particle modal diameter of about 8  $\mu$ .

Phytoplankton cell sizes ranged from 10 to 70  $\mu$  and were dependent on the species measured.

#### Clay mineral composition

The detection limits of x-ray diffractometric techniques are dictated by the amount of lithogenous matter on the filters. Detectible quantities were found in water samples in north bay and at the southern end of south bay; near Golden Gate, detectible quantities have only been collected during higher river discharge when relatively turbid low-salinity water is present.

Semiquantitative determinations of sample composition were made from the diffractometric spectra. The method by which the proportions of clay mineral groups were determined is as follows: (1) the increase in the area of the 10 Å peak of the sample when heated to 400° C compared to the area of the 10 Å peak of the glycolated sample was assigned to

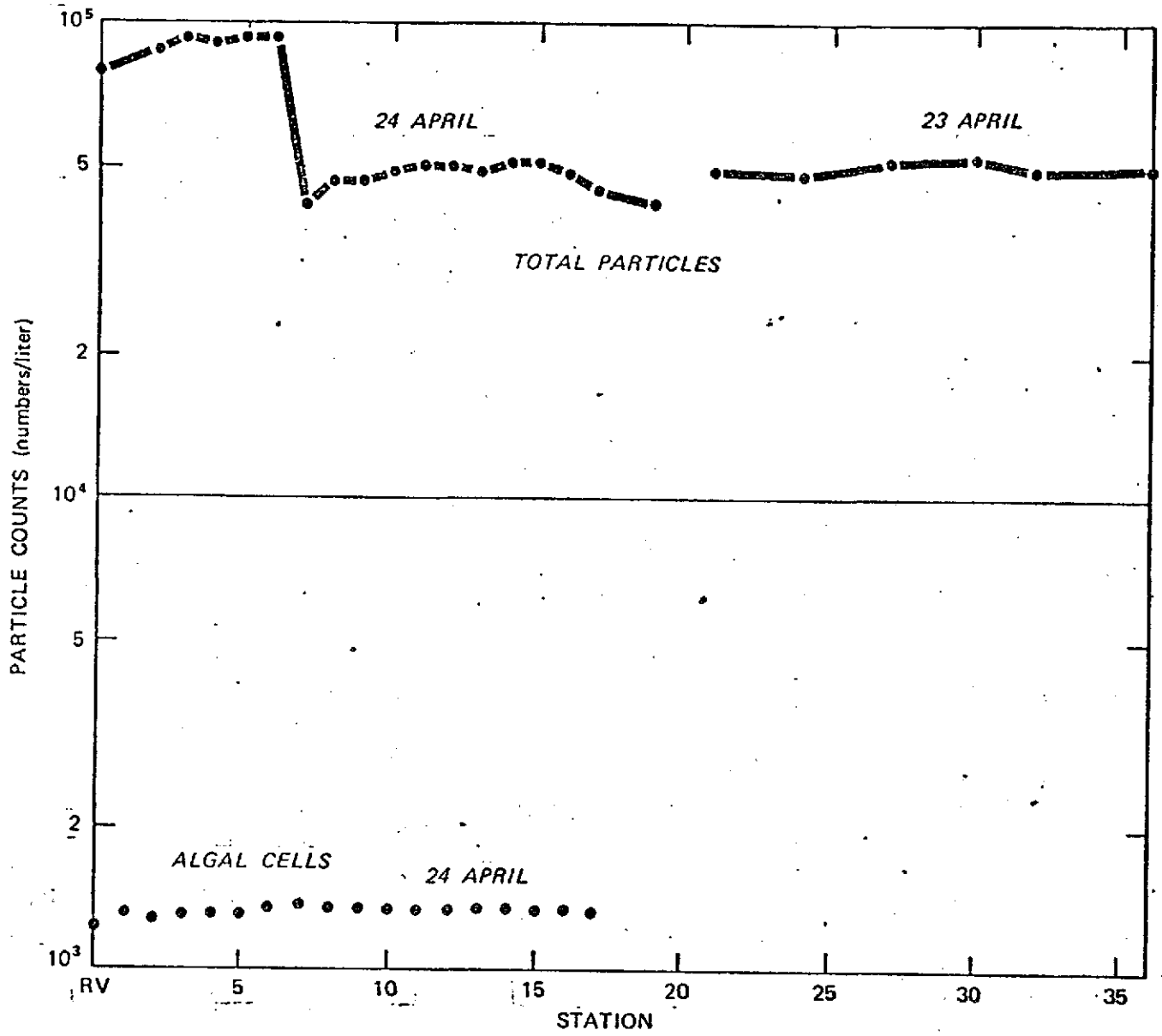


Figure 12. Longitudinal distribution of suspended particles at 2m, measured during April sampling cruise. Total particle numbers determined by Coulter<sup>R</sup> counter; algal cell numbers determined by optical counting techniques. (See fig. 1 for station locations).

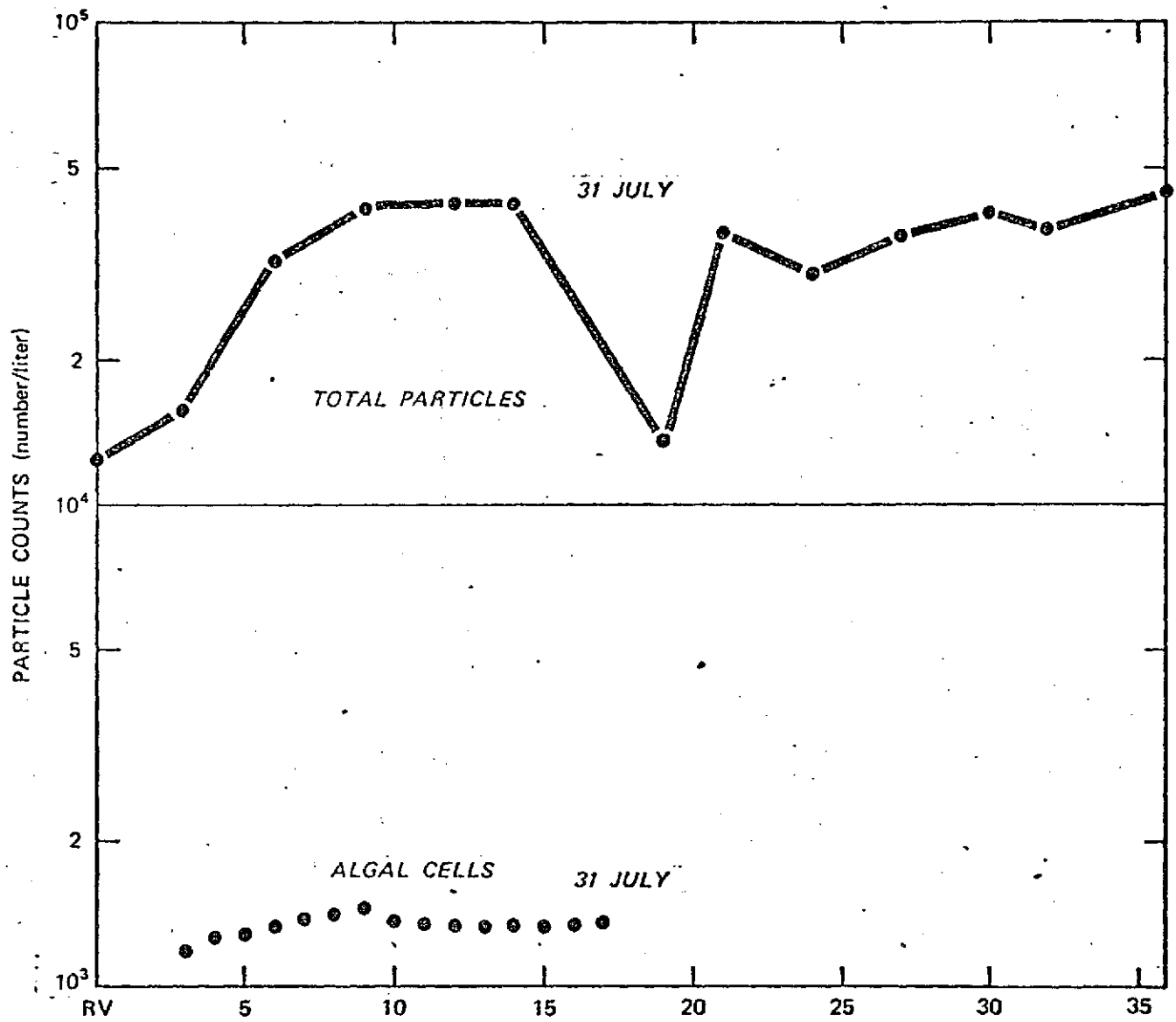


Figure 13. Longitudinal distribution of suspended particles at 2 m, measured during July sampling cruise. Total particle numbers determined by Coulter<sup>R</sup> counter; algal cell numbers determined by optical counting techniques. (See fig. 1 for station locations).

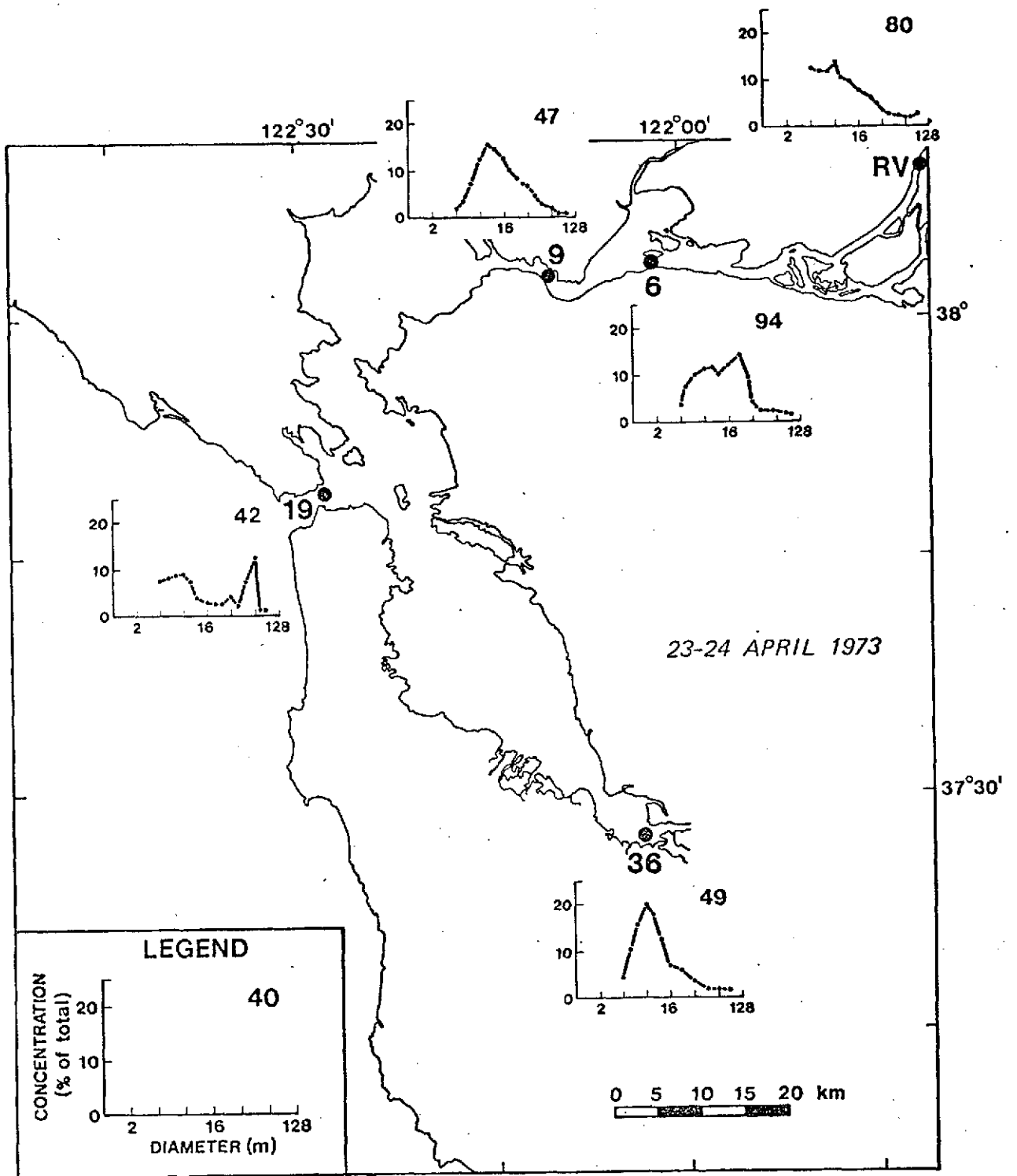


Figure 14. Suspended particle concentrations and diameters measured at selected stations during April sampling cruise. Sampling depth, 2 m; data determined by Coulter<sup>R</sup> counter. Large numbers at upper right of graphs (e.g. 40 in legend) are counts of particles  $\times 10^3/\text{ml}$ .

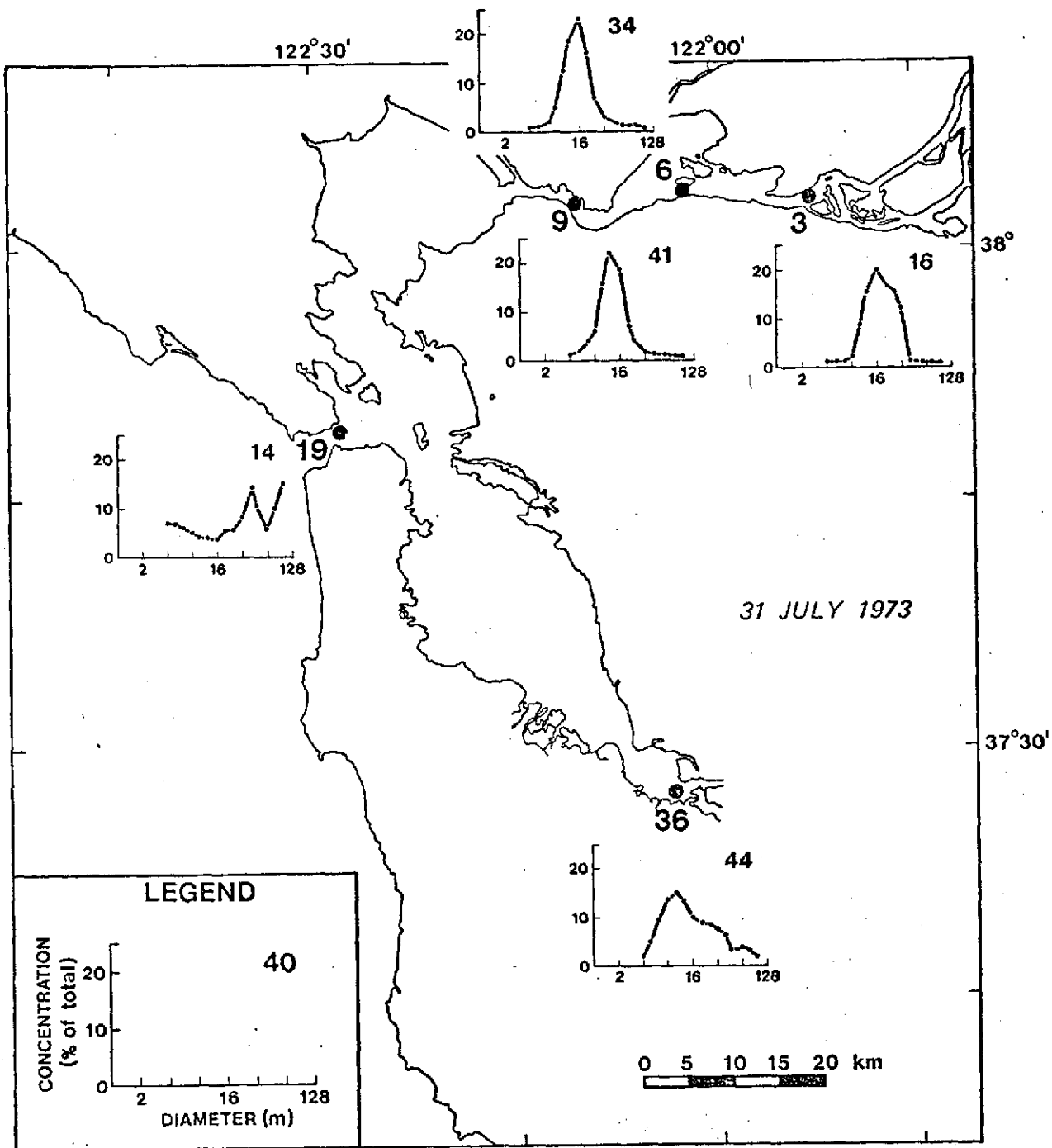


Figure 15. Suspended particle concentrations and diameters measured at selected stations during July sampling cruise. Sampling depth, 2 m; data determined by Coulter<sup>R</sup> counter. Large numbers at upper right of graphs (e.g. 40 in legend) are counts of particles  $\times 10^3/\text{ml}$ .

montmorillonite plus mixed-layer montmorillonite-illite (M+MI); (2) the 10 Å peak area of the glycolated sample was assigned to illite (I); and (3) half the area of the 7 Å peak of the glycolated sample was assigned to chlorite plus kaolinite (C + K) (J. C. Hathaway, 1974, oral comm.). The results were then expressed in relative percent. The "percentages" of the clay minerals thus computed are useful only for delineating areal trends and may or may not correspond with the absolute amounts of clay minerals within San Francisco Bay. Other methods of estimating the relative abundance of clay mineral groups are currently being employed and may be used subsequently to outline the temporal and spatial variability of clay minerals within San Francisco Bay. Thus, the data presented in this report must be regarded as preliminary.

The relative abundances of I, C+K, and M+MI are indicated in Figures 16 and 17. During April, no distinct longitudinal trends were evident (Fig. 16). There was, however, a suggestion that I dominates over M+MI in the northernmost portion of north bay, whereas M+MI dominates over I in the southernmost portion of south bay; in the central portion of the bay system, random admixtures of I and M+MI are present. During July, station 36 showed the same distribution as was observed in April (Fig. 17). In north bay, however, a distinct longitudinal trend was observed: I progressively increased and M+MI decreased in relative abundance from stations 9 to 19 (Golden Gate).

## DISCUSSION

### General Sedimentologic Features

The sedimentological patterns and processes of north bay are controlled by the high annual river flow from the delta: large volumes of sediment are contributed by this river flow, and the river flow in turn generates and maintains a turbidity maximum (Conomos and Peterson, 1974). In north bay estuarine circulation is generated by the discharge of the Sacramento and San Joaquin Rivers which varies generally from the winter high of 700-1400 m<sup>3</sup>/sec to the summer low of 100-500 m<sup>3</sup>/sec. Even at low flow, the discharge is sufficient to maintain an estuarine cell in the northern reach of the estuary (Conomos et al., 1971). Estuarine circulation is characterized by a null zone (zone where landward-flowing bottom density currents and seaward-flowing bottom river currents have equal and opposite effects on the non-tidal flow. The null zone migrates longitudinally in response to seasonal changes in river inflow. This null zone is also the location of the turbidity maximum (Conomos and Peterson, 1974).

By contrast, south bay receives small volumes of riverborne sediment; the sedimentological patterns and processes are largely controlled by recycling of bottom sediments into the water column by tidal currents and wind-induced waves (Conomos, 1963). Hence, the distribution of suspended particles seems random, and no turbidity maximum is present.

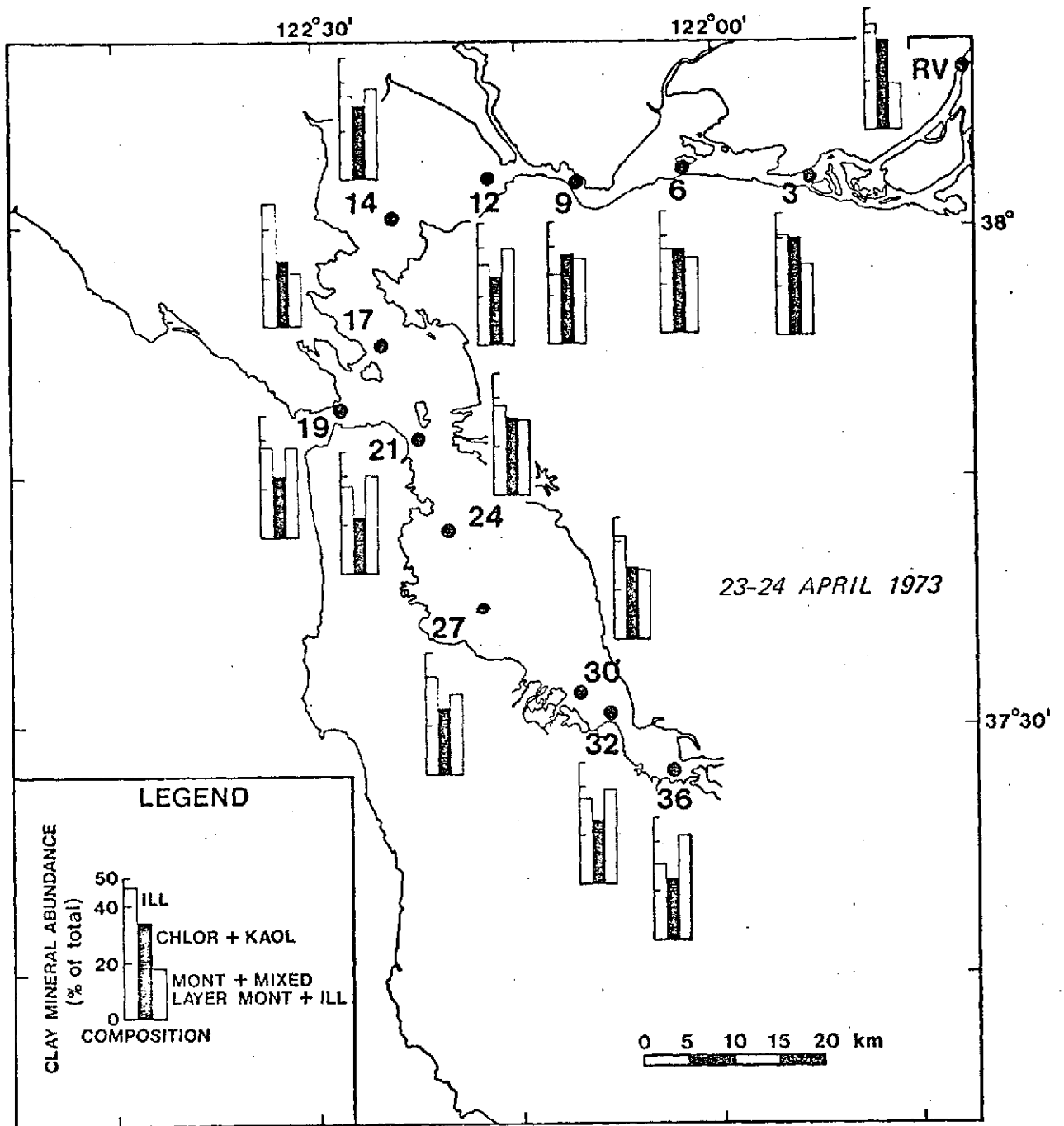


Figure 16. Longitudinal distribution of clay minerals collected during April sampling cruise. Sampling depths, 2 m; data determined by x-ray diffractometric techniques.

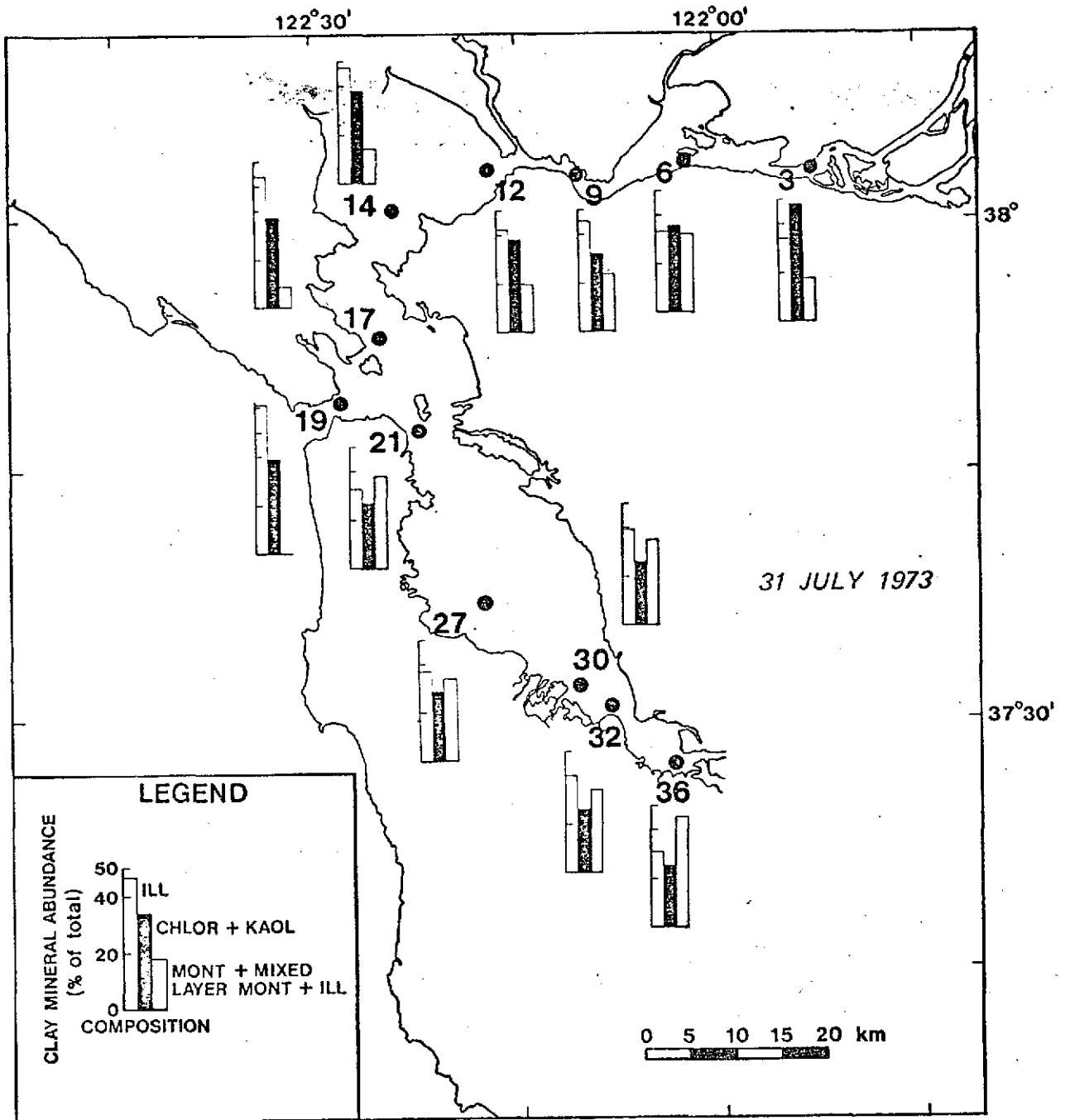


Figure 17. Longitudinal distribution of clay minerals collected during July sampling cruise. Sampling depth, 2 m; data determined by x-ray diffractometric techniques.

The abundance and composition of the suspended particles in the turbidity maximum changes seasonally. With the decline of winter high river inflow the concentration of riverborne suspended particles decreases. During this period, the phytoplankton concentration in the turbidity maximum often increases five-fold, and the suspended-particle concentration diminishes by about 50 percent (typically 200 to 100 mg/L). By late summer, phytoplankton (diatoms constituting a major portion of the biomass) and zooplankton constitute a significant fraction of the suspended particles at the turbidity maximum, increasing from a typical winter concentration of 3 percent by weight to a summer concentration of about 30 percent (Conomos and Peterson, 1974).

Advective transport that introduces particulate matter into a trap formed by the convergence of the landward-flowing density current and the seaward-flowing near-bottom river current at the null zone explains the accumulation and maintenance of the lithogenous as well as the biogenous components of the turbidity maximum (see, for example, Glangeaud, 1938; Postma, 1967; Meade, 1969; Schubel, 1969; Conomos and Peterson, 1974).

The gross features seen in the transmissometer (Fig. 4), gravimetric (Fig. 11) and particle and phytoplankton cell count (Figs. 12, 13) data define this turbidity maximum. In addition, the longitudinal migration of the null zone and its attendant turbidity maximum caused by differences in river inflow are indicated by this data. More detailed discussions of the processes and rates pertaining to the distribution, abundance, and movement of both lithogenous and biogenous particles follow.

## Processes and Rates

### Lithogenous Particles

The higher suspended particle concentration in the river in April compared to July (Figs. 12, 13) may be explained by the relative availability of lithogenous particles to be transported, or to the increased capacity of the stream (Leopold et al., 1964, p. 182). During low discharge, the suspended lithogenous particles reaching the mainstream Sacramento and San Joaquin Rivers may be deposited in the river beds. During relatively large winter discharges these particles may be resuspended and transported downstream. The capacity, or the total load a river may carry, is increased by a concomitant increase of total volume of flow, or discharge, and generally increased particle concentrations.

In the bay system, however, the high tidal current velocities dominate over the hydraulic current velocities. These tidal currents are strong and cause sufficient turbulence to resuspend considerable amounts of particulate matter into the surface layers of the estuary in cloud-like bodies, a condition commonly seen in south bay and the shallow portions of north bay (Fig. 18). This resuspension as a function of

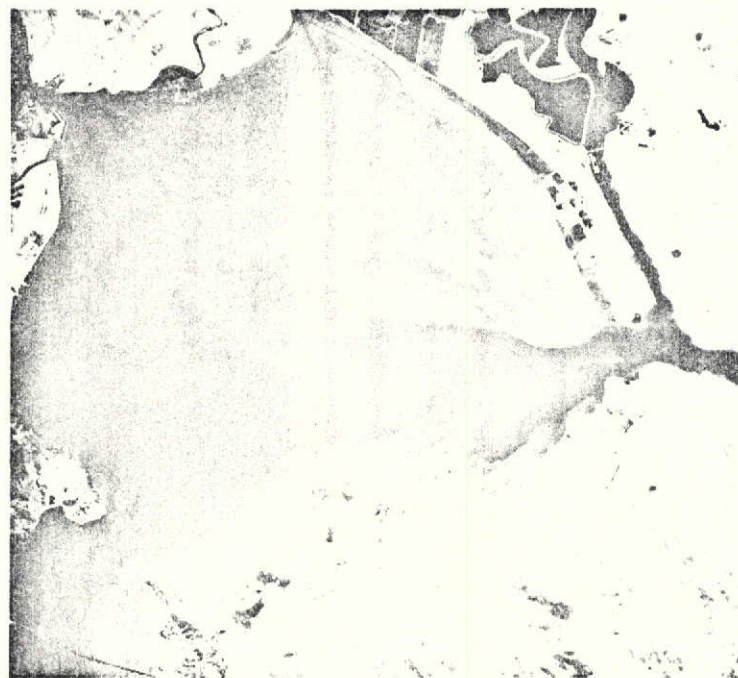


Figure 18. Water circulation patterns in the San Francisco Bay system: (left) ERTS image band 5 (0.6-0.7  $\mu\text{m}$ ), no. 1021-18172, August 13, 1972; (right) infrared photograph (690-760 nm) of San Pablo Bay showing resuspended sediment over the shallow portions of the bay, taken from U-2 aircraft at  $\sim$ 21,000 m, April 3, 1972 (flight no. 73-051; accession no. 1057-0157).

tidal variation (time), has been clearly observed at time series stations occupied at selected areas during summer and winter sampling periods (Peterson and others, 1974a).

Although the spatial and temporal changes in lithogenous particle diameters (Figs. 14, 15) are difficult to evaluate because the data represent admixtures of both (larger diameter) phytoplankton cells and detritus, certain features can be explained. Firstly, flocculation of lithogenous particles can explain the abrupt change in particle size distribution seen in between stations RV and 3 during April (Fig. 14); particles  $\pm 4 \mu$  at station RV ( $0^{\circ}/\text{oo}$  salinity; Fig. 3) became agglomerated, forming larger diameter (8-16  $\mu$ ) particles in the presence of salt in the water (station 6 near surface salinity =  $0.5^{\circ}/\text{oo}$ ). Phytoplankton, found in large numbers in this area, however, commonly have diameters of about 16  $\mu$ , and numerically may help enhance this size fraction. Secondly, the large ( $>64 \mu$ ) diameter mode found at Golden Gate during both April and July is due to large oceanic phytoplankters. Thirdly, the concentration of suspended particles decreases seaward, because of progressive lateral mixing with less turbid water (Figs. 14, 15). This third factor does not completely explain the concentration decrease, as the small ( $\leq 4 \mu$ ) modal diameter particles decrease from the river to Golden Gate. Coarser particles apparently settle out of a given water parcel relatively faster because of a progressive decrease in water turbulence and vertical mixing. This decrease is a function of distance seaward from the river and of time elapsed since delivery at the river mouths.

The average horizontal movement of surface water within north bay is on the order of 5 to 10 km/day (Conomos et al., 1971). The corresponding vertical water movements are about 1 m/day. As these upward water movements are approximately equivalent to settling rates for lithogenous matter  $\sim 4 \mu$  in diameter (Conomos and Gross, 1972), any lithogenous particles which have settling rates equal to or less than these values could remain in suspension until they are transported to areas where vertical water movements are smaller.

The size differentiation with time and distance towards the ocean, arising from differing settling rates and transport behavior, is perhaps reflected in the progressive changes in clay mineral composition seen during July (Fig. 17). The progressive diminution of M+MI and the enhancement of I seaward is similar to the observations of the Columbia River effluent reported by Conomos (1968). The reason for this progressive change is unknown. These components should have approximately equal settling rates as shown by observation (Whitehouse et al., 1959) and by theory based on grain diameter, morphology, and specific gravity (Conomos, 1968).

#### Biogenous particles

The concentrations of algal cells are low relative to the lithogenous fraction (Figs. 12, 13). Processes determining the concentration of the biogenous fraction include primary productivity, which increases the

amount of living biogenous matter present, and grazing and settling, which decrease the amount present.

The surface layers of the adjacent ocean (Gulf of the Farallones) and the area of the turbidity maximum are important sources of biogenous matter. Data from Peterson and others (1974b) and Scrivani (1974), consistent with previous data (Bain and McCarty, 1965), indicate that both the rate of primary production and the concentration of chlorophyll a in the waters are high; light rather than nutrients limits phytoplankton production during most of the year.

Major processes decreasing the concentrations of biogenous particles are grazing by zooplankton and removal by settling. Grazing, although important in affecting the size and quantity of organic particles, has not been extensively investigated. Diatoms (Smyda and Boleyn, 1965, 1966a, b) and organic matter (Hobson, 1967) have been reported to settle at a rate of about 1 m/day, rates of the same order as the rates of vertical water movements while horizontal movements are  $10^4$  times greater. It may be concluded that removal by settling of planktonic diatoms and organic matter from the low-salinity waters in north bay would be minimized by the vertical water movements. These particles could be held near the water surface at least until they were carried out of north bay, a situation similar to that in the Columbia River effluent (Conomos, 1968).

Furthermore, it is probable that any organic particles may be returned to the area of turbidity maximum by the nearbottom density current which flows landward. In south bay, where vertical mixing by winds and tidal currents often extends to the bottom, most of the phytoplankton (comprised mainly of benthic forms) are eroded from the substrate and recycled vertically through the water column.

#### SUMMARY AND CONCLUSIONS

Lithogenous particles, kept in suspension in the river, are transported downstream to the estuarine area at varying rates which are dependent on the river discharge level. The finer-grained suspended particles may be retained in the seaward-flowing lower-salinity layer, with the coarser-grained matter settling out. Both successive dilution and particle settling decrease the concentration of suspended particles from river to ocean. In south bay, wave and current resuspension largely determine the spatial and temporal distribution of fine-grained lithogenous particles. These particles may be held near the surface in areas where their settling velocity is of the same magnitude as the vertical water velocities. The suspended particles thus retained near the surface are transported out of north bay by horizontal advection as well as horizontal diffusion.

The paths of the biogenous particles largely depend on the water movements, and the material behaves much like the finest-grained lithogenous matter. The concentration increases are caused mainly by

phytoplankton growth, whereas the decreases are due primarily to successive dilution with water of lower biogenous matter concentrations.

#### REFERENCES

- Bain, R. C., and McCarty, J. C., 1965, Nutrient productivity studies in San Francisco Bay: U.S. Public Health Service, Central Pacific Basins Water Pollution Control Proj. Tech. Rept. 65-1.
- Beers, J. R., Stewart, G. L., and Strickland, J. D. H., 1967, A pumping system for sampling small plankton: Jour. Fish. Res. Bd. Can., v. 24, p. 1811-1818.
- Brown, George, ed., 1961, The x-ray identification and crystal structures of clay minerals: Mineral Soc. London, London, 544 p.
- Brown, N. L., and Hamon, B. V., 1961, An inductive salinometer: Deep-Sea Research, v. 8, p. 65-75.
- Carlson, P. R., and Harden, D. R., 1974, ERTS observations of surface currents along the Pacific Coast of the United States, in Principle sources and dispersal patterns of suspended particulate matter in nearshore surface waters of the northeast Pacific Ocean and the Hawaiian Islands, Carlson, P. R., Conomos, T. J., Janda, R. J., and Peterson, D. H., eds: ERTS-1 Final Report, Natl. Tech. Info. Service, p.
- Carlson, P. R., and McCulloch, D. S., 1974, Aerial observations of suspended-sediment plumes in San Francisco Bay and the adjacent Pacific Ocean: U.S. Geol. Survey Jour. Research, v. 2, p. 519-526.
- Conomos, T. J., 1963, Geologic aspects of the recent sediments of South San Francisco Bay: San Jose State University, San Jose, California, M. S. thesis, 118 p.
- Conomos, T. J., 1968, Processes affecting suspended particulate matter in the Columbia River--Effluent System, summer 1965, 1966: University of Washington, Seattle, Ph.D. thesis, 141 p.
- Conomos, T. J., Broenkow, W. W., Peterson, D. H., and Carlson, P. R., 1970a, Seasonal variations in hydrographic properties of the ocean adjacent to San Francisco, California [abs.]: Geol. Soc. America, v. 2, no. 2, p. 83.
- Conomos, T. J., Peterson, D. H., Carlson, P. T., and McCulloch, D. S., 1970b, Movement of seabed drifters in the San Francisco Bay Estuary and the adjacent Pacific Ocean: A preliminary report: U.S. Geol. Survey Circ. 637B, p. B1-B8.

- Conomos, T. J., and Gross, M. G., 1972, River-ocean suspended particulate matter relations in summer, in Pruter, A. T., and Alverson, D. L., eds., Columbia River Estuary and Adjacent Ocean Waters: Bioenvironmental Studies, Univ. of Washington Press, Seattle, Chapt. 8, p. 176-202.
- Conomos, T. J., McCulloch, D. S., Peterson, D. H., and Carlson, P. R., 1971, Drift of surface and near-bottom waters of the San Francisco Bay system: March 1970 through April 1971: U.S. Geol. Survey open-file map.
- Conomos, T. J., and Peterson, D. H., 1974, Biological and chemical aspects of the San Francisco Bay turbidity maximum: Symposium International Relations Sedimentaires et Estuaires et Plateaux Continentaux, Institut de Geologie du Bassin d'Aquitaine.
- Dole, R. B., and Stabler, H., 1909, Denudation, in Papers on the conservation of water resources: U.S. Geol. Survey Water-Supply Paper No. 234, p. 76-93.
- Glangeaud, L., 1938, Transport et sédimentation dans l'estuaire et a l'embouchure de la Gironde. Caractères pétrographiques des formations fluviatiles, saumâtres, littorales, et néritiques: Geol. Soc. France Bull., v. 8, p. 599-630.
- Hathaway, J. D., 1956, Procedure for clay mineral analyses used in the sedimentary petrology laboratory of the U.S. Geological Survey: Clay Mineral Bull., v. 3, p. 8-13.
- Hines, W. G., 1973, A review of wastewater problems and wastewater management planning in the San Francisco Bay region, California: U.S. Geol. Survey open-file report, 46 p.
- Hobson, L. A., 1967, The seasonal and vertical distribution of suspended particulate matter in an area of the northeast Pacific Ocean: Limnology and Oceanography, v. 12, p. 642-649.
- Ishii, J., and Ishikawa, T., 1964, Detection of mineral components of suspended matter in sea water by x-ray diffractometers, in Studies on oceanography: Univ. of Washington Press, Seattle, p. 288-295.
- Jacobs, M. G., and Ewing, Maurice, 1965, Mineralogy of particulate matter suspended in sea water: Science, v. 149, p. 313-314.
- Jerlov, N. G., 1953, Particle distribution in the ocean: Swed. Deep-Sea Expedition Report 3, p. 73-97.
- \_\_\_\_\_, 1968, Optical oceanography: Elsevier Publishing Co., New York, 194 p.

- Leopold, L. B., Wolman, M. G., and Miller, J. P., 1964, Fluvial processes in geomorphology: W. H. Freeman and Co., San Francisco, 522 p.
- Lisitsin, A. P., 1962, Distribution and composition of suspended materials in seas and oceans, in Recent sediments of the seas and oceans: U.S.S.R. Acad. Sci., Comm. on Sediments, Div. Geol. Geogr. Sci., Moscow (in Russian), p. 175-231. Translation by Sophie S. Rodolpho.
- Lund, J. W. D., Kipling, C., and Le Cren, E. D., 1958, The inverted microscope method of estimating algal numbers and the statistical basis of estimating counting: *Hydrobiologia*, v. 11, p. 143-170.
- Manheim, F. T., Hathaway, J. C., and Uchupi, Elazar, 1972, Suspended matter in surface waters of the northern Gulf of Mexico: *Limnology and Oceanography*, v. 17, p. 17-27.
- Manheim, F. T., Meade, R. H., and Bond, G. C., 1970, Suspended matter in surface waters of the Atlantic Continental Margin from Cape Cod to the Florida Keys: *Science*, v. 167, p. 371-376.
- McCulloch, D. S., Peterson, D. H., Carlson, P. R., and Conomos, T. J., 1970, Some effects of fresh water inflow on the flushing of South San Francisco Bay: A preliminary report: U.S. Geol. Survey Circ. 637A, p. A1-A27.
- Meade, R. H., 1969, Landward transport of bottom sediments in estuaries of the Atlantic coastal plain: *Jour. Sed. Petrology*, v. 39, p. 222-234.
- \_\_\_\_\_, 1972, Transport and deposition of sediments in estuaries, in Nelson, B. W., ed., *Estuaries: Geol. Soc. of America Memoir 133*, p. 91-120.
- Parson, T. R., 1963, Suspended organic matter in sea water, in Sears, M., ed., *Progress in Oceanography, Vol. I: Pergamon Press, London*, p. 205-232.
- Peterson, D. H., Conomos, T. J., Broenkow, W. W., and Doherty, P. C., 1974a, Location of the nontidal current null zone in Northern San Francisco Bay: *Estuarine and Coastal Mar. Sci. (In press)*.
- Peterson, D. H., Conomos, T. J., Broenkow, W. W., and Scrivani, E. P., 1974b, Processes controlling the dissolved silica distribution in San Francisco Bay: *Proc. of the Second International Estuarine Research Conf., Estuarine Research Federation (In press)*.
- Postma, H., 1967, Sediment transport and sedimentation in the estuarine environment, in Lauff, G. H., ed., *Estuaries: Am. Assoc. Adv. Sci. Pub. No. 83*, p. 158-179.

- Rantz, S. E., 1971, Precipitation depth-duration-frequency relations for the San Francisco Bay region, California, and isohyetal map of San Francisco Bay region, California, showing mean annual precipitations: U.S. Geol. Survey open-file report, 5 p., 1 map, 1:500,000.
- Schemel, L. E., 1974, A performance evaluation of the Turner Designs model 10 fluorometer/nephelometer for turbidity studies in natural waters, in Principle sources and dispersal patterns of suspended particulate matter in nearshore surface waters of the northeast Pacific Ocean and the Hawaiian Islands, Carlson, P. R., Conomos, T. J., Janda, R. J., and Peterson, D. H., eds.: ERTS-1 Final Report, Natl. Tech. Info. Service, p.
- Schubel, J. R., 1968, Turbidity maximum of northern Chesapeake Bay: Science, v. 161, p. 1013-1015.
- \_\_\_\_\_, 1969, Distribution and transportation of suspended sediment in the upper Chesapeake Bay: Johns Hopkins Univ. Chesapeake Bay Inst. Tech. Rept. No. 60, 29 p.
- Scrivani, E. P., 1974, An investigation of the phytoplankton and primary productivity of San Francisco Bay: California Univ., Berkeley, Ph.D. thesis, 174 p.
- Scruton, P. C., and Moore, D. G., 1953, Distribution of surface turbidity off the Mississippi Delta: Am. Assoc. Petroleum Geologists Bull., v. 37(5), p. 1067-1074.
- Sheldon, R. W., and Parsons, T. R., 1967, A practical manual on the use of the Coulter counter in marine research: Coulter Electronic Sales Co. of Canada, Toronto, 66 p.
- Smayda, T. J., and Boleyn, B. J., 1965, Experimental observations on the flotation of marine diatoms: I. Thalassiosira cf. nana, Thalassiosira rotula and Nitzschia seriata: Limnology and Oceanography, v. 10, p. 499-509.
- \_\_\_\_\_, 1966a, Experimental observations on the flotation of marine diatoms: II. Skeletonema costatum and Rhizosolenia setigera. Limnology and Oceanography, v. 11, p. 18-34.
- \_\_\_\_\_, 1966b, Experimental observations on the flotation of marine diatoms: III. Bacteriastrum hyalinum and Chaetoceros lauderi: Limnology and Oceanography, v. 11, p. 34-43.
- Strickland, J. D. H., 1966, Measuring the production of marine phytoplankton: Fisheries Research Board Canada Bull. No. 122, 172 p.
- United States Coast and Geodetic Survey, 1973, Tide Table, West Coast, North and South America: U.S. Printing Office, Washington, D.C.

van Andel, Tj. H., and Postma, H., 1954, Recent sediments of the Gulf of Paria. Reports of the Orinoco Shelf Expedition: I. Verh. Kon. Ned. Akad. Wetensch., v. 20, 245 p.

Vollenweider, R. A., 1969, A manual on methods for measuring primary production in aquatic environments: International Biological Program Handbook No. 12, Blackwell, Oxford.

Whitehouse, U. G., Jeffrey, L. M., and Debbrecht, J. D., 1959, Differential settling tendencies of clay minerals in saline waters, in Ingerson, E., ed., Clays and Clay Minerals. Seventh Natl. Conf. Clays Clay Mineral., Proc., Pergamon Press, London, p. 1-79.

A FIELD EVALUATION OF A NEPHELOMETER  
FOR THE DETECTION OF TURBIDITY VARIATIONS  
IN SAN FRANCISCO BAY AND THE GULF OF THE FARALLONES

by

Laurence E. Schemel

Aerial photographs and satellite imagery of San Francisco bay estuary and adjacent Pacific Ocean commonly resolve surficial turbidity variations (Fig. 1; Carlson and McCulloch, 1974). These variations may be studied from a surface vessel by continuously pumping surface waters along a transect and measuring the turbidity of the sample stream. This report demonstrates the range and sensitivity characteristics of a fluorometer equipped with a flow-sample nephelometry cell in turbid water sampled in San Francisco bay and clear water sampled in the Gulf of the Farrallones.

Turbidity, a non-specific optical property of natural waters, is conveniently evaluated by transmissometers, which measure the degree of extinction of a light beam, and nephelometers, which measure the level of scattered light at one or more angles to the incident beam (Jerlov, 1968). The transmission measurement relates by a logarithmic function to the volume attenuation coefficient, which is the sum of the scattering and absorption caused by both particles and light absorbing constituents (Tyler and Preisendorfer, 1962). The scatterance at one angle, as measured with a nephelometer (commonly at 90 degrees), is in practice not easily related to the total scattering coefficient in natural waters (Morrison, 1970), and is usually referenced to a turbidity standard when evaluating relative turbidity and changes in turbidity (Hochgesang, 1964).

Nephelometers respond linearly to changes in particle concentration in clearer waters and exhibit high sensitivity (Turner, 1973). Turbid waters commonly found in estuaries severely limit light penetration to short distances, and may only be measured effectively by transmissometers with short optical paths and nephelometers. Nephelometers are not directly dependent upon optical path length for sensitivity, making possible a sensing cell design with considerably less internal volume than that required for transmissometers in flow-sample systems. This allows better resolution of short-duration turbidity variations.

#### Instrumentation and Methods

A continuous water sampling and analysis system was used to obtain water quality and turbidity records (Table 1). In situ salinity and temperature, water sampling depth, nephelometer turbidity, chlorophyll a fluorescence, and percent transmission data were recorded on an analog stripchart. The 1 decimeter transmissometer was calibrated to 100 percent in distilled water. Nephelometer turbidity and chlorophyll a fluorescence were recorded as percent of full scale at each sensitivity setting. Further

6-2

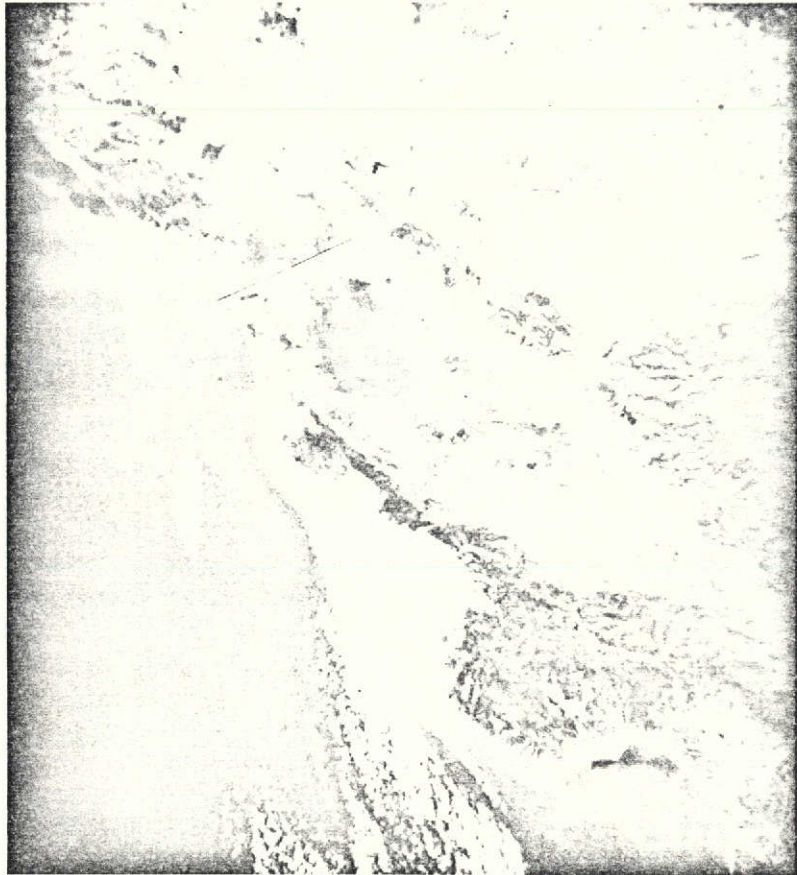


Figure 1. Turbid water plumes in San Francisco bay estuary and adjacent Pacific Ocean. ERTS image, band 4 (0.5-0.6  $\mu\text{m}$ ), no. 1327-18180, June 15, 1973.

Table 1. Continuous water sampling and analysis instrumentation.

<u>Instrument</u>	<u>Manufacturer</u>
Salinity-Temperature-Depth/ Pumping system, OSEAS	Interocean Systems, San Diego, Calif.
Fluorometer/Nephelometer, Model 10	Turner Designs, Palo Alto, Calif.
Fluorometer, Model 111	G. K. Turner Associates, Palo Alto, Calif.
Analog recorder, Model 260	Gould Inc., Cleveland, Ohio
Transmissometer, Model 411	Hydroproducts Inc., San Diego, Calif.

standardizations were not performed on these instruments as correlative changes were desired rather than absolute data.

### Results and Discussion

Relatively clear surface and subsurface waters were sampled on August 9, 1973, in the Gulf of the Farallones (Figs. 2, 3). A coastward surface water turbidity increase was detected by a nephelometer turbidity increase from 55 to 96 percent. The transmissometer response was a decrease from 96 to 92 percent. In this particular case, a longer path length (perhaps 1 meter) transmissometer would have been necessary to achieve sensitivity of the order that was exhibited by the nephelometer.

The correlation of the nephelometer and chlorophyll a fluorescence records during the vertical profile suggests that phytoplankton constituted a significant fraction of the measured turbidity. The ability of both the fluorometer and nephelometer to detect structure in the vertical distributions of turbidity and chlorophyll a is a function of both their sensitivities and temporal resolutions, the latter being a consequence of their low volume flow-sample cells.

On February 5, 1974, a surface sampling was performed from the San Rafael bridge to a station located off Point San Pablo and return (Figs. 2, 4). A distinct boundary of two adjacent surface water masses was detected each time it was crossed by large changes in salinity, transmission, and nephelometer turbidity. Although the sensitivities of the nephelometer and transmissometer were comparable, the transmissometer depicted a more diffuse boundary because its larger flow cell volume allowed considerable mixing.

Short duration turbidity and salinity variations, a consequence of the turbulent mixing of turbid low-salinity water with clear higher-salinity deeper water, were resolved by the nephelometer and salinometer in the more turbid water area. During this time, the transmissometer recorded zero or near-zero percent. Since light was not able to sufficiently penetrate the distance of its optical path, a shorter path length transmissometer would have been necessary to achieve adequate turbidity range, but with a probable loss of sensitivity. Four scale changes enabled the nephelometer to maintain optimum sensitivity over a wide range of turbidity during the entire transect.

### Conclusions

The nephelometer is capable of detecting turbidity variations in clear water with greater sensitivity than the 1 decimeter transmissometer used in this study. Turbidity variations in more turbid water may be measured largely as a consequence of the short optical path length in the low-volume nephelometry flow-sample cell. Short duration variations are resolved, allowing correlation of turbidity, in situ salinity, and chlorophyll a fluorescence records.

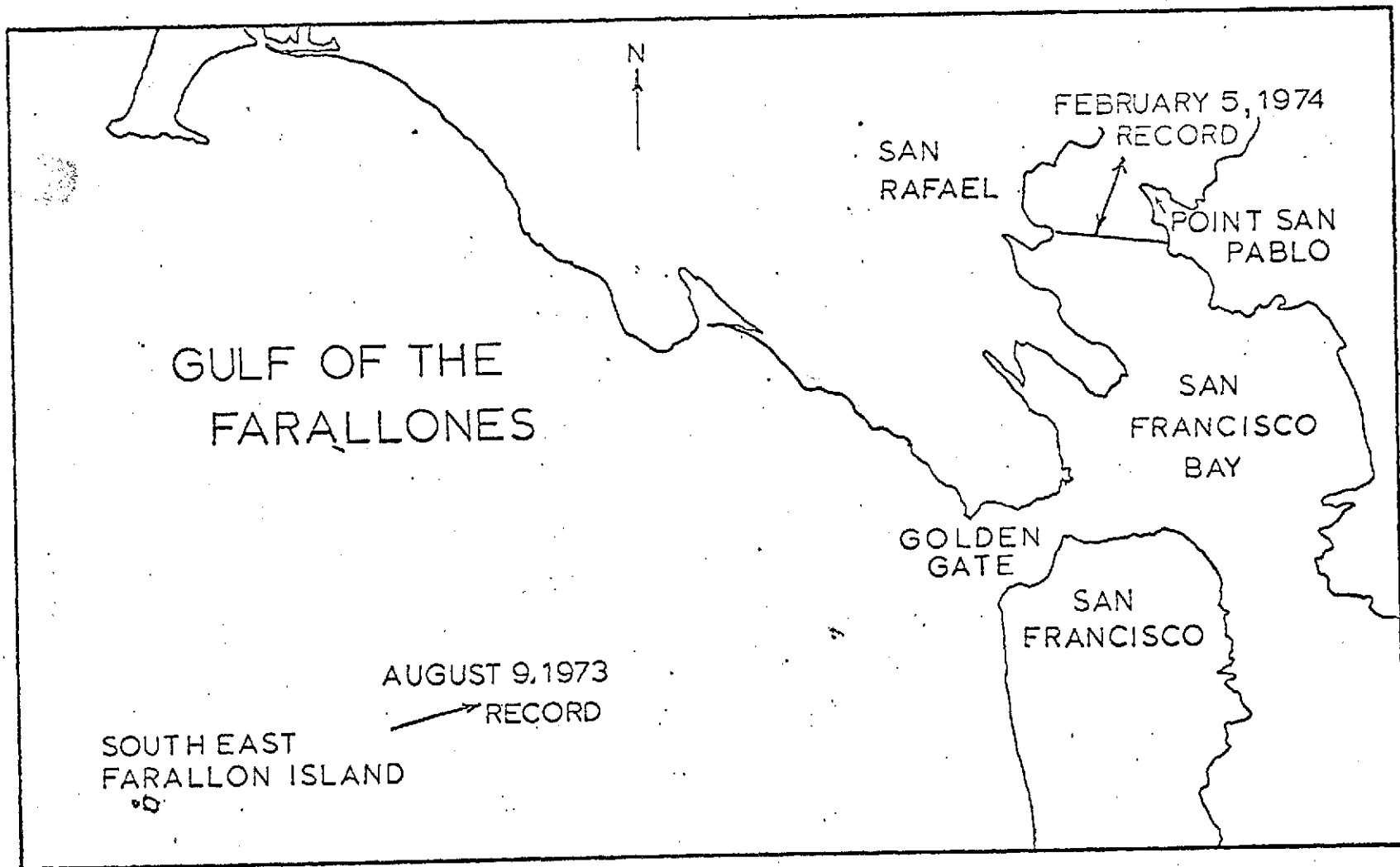


Figure 2. Locations of records obtained on August 9, 1973 and February 5, 1974.

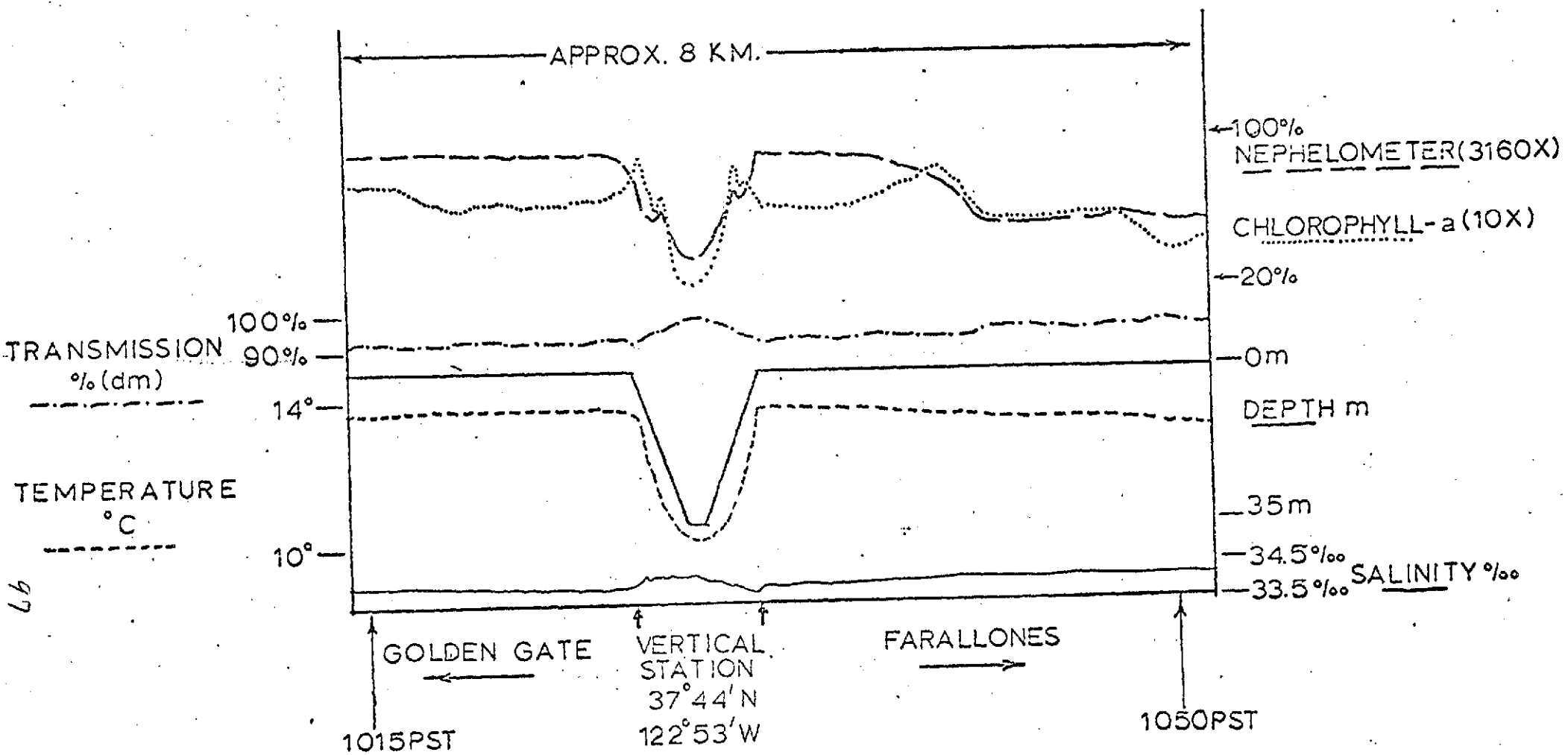


Figure 3. Salinity, temperature, chlorophyll a fluorescence, and turbidity of surface and sub-surface waters in the Gulf of the Farallones, August 9, 1973.

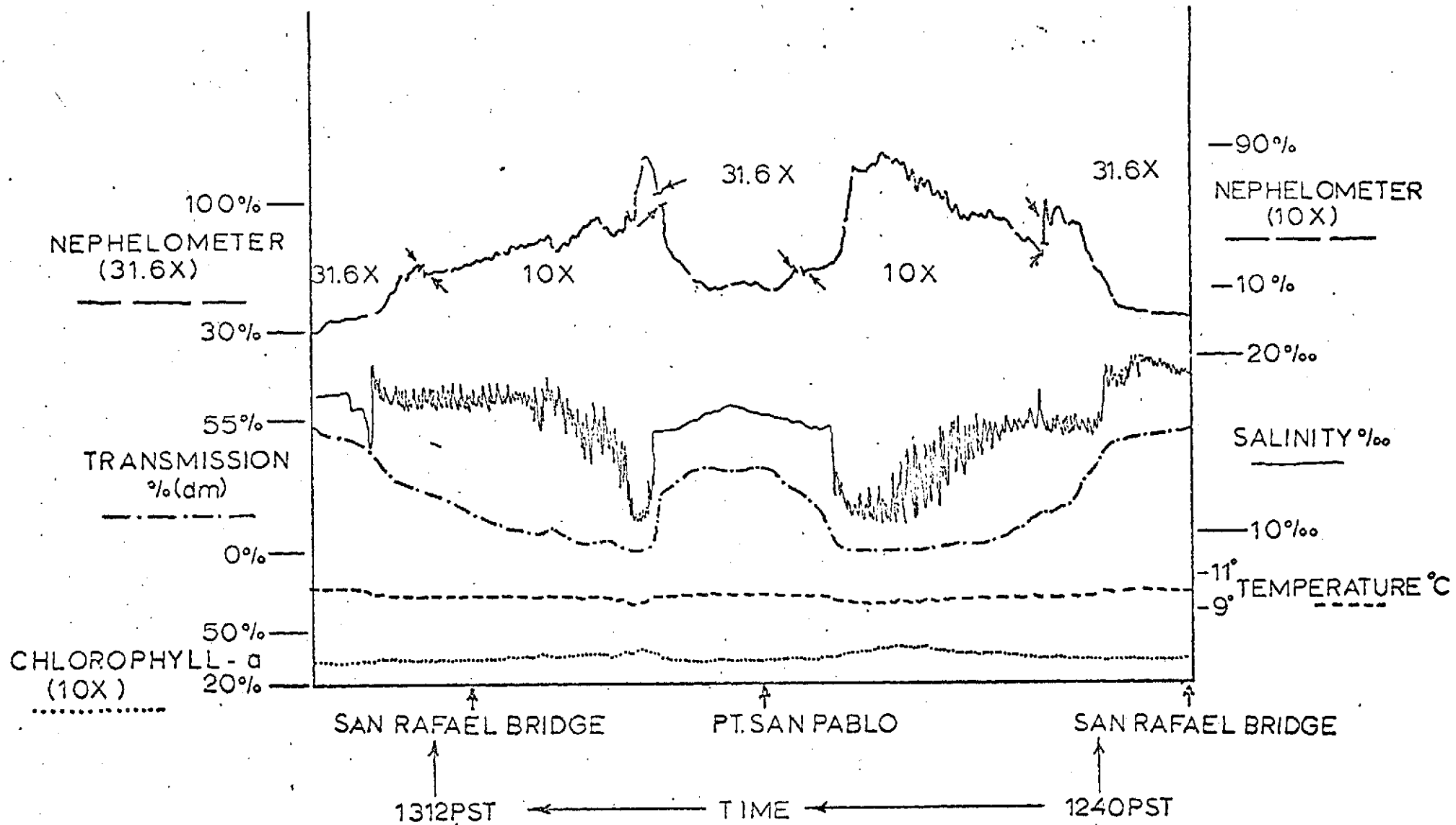


Figure 4. Salinity, temperature, chlorophyll a fluorescence, and turbidity of surface waters in San Francisco Bay, February 5, 1974.

## References

- Carlson, P. R., and McCulloch, D. S., 1974, Aerial observations of suspended sediment plumes in San Francisco bay and the adjacent Pacific Ocean: U.S. Geol. Survey Jour. of Research, v. 2, no. 5, p. 519-526.
- Hochgesang, F. P., 1964, Nephelometry and Turbidity, in Kolthoff, I. M. and Elving, P. J., eds., Treatist on Analytical Chemistry: Part 1, v. 5, John Wiley and Sons, New York, N.Y.
- Jerlov, N. G., 1968, Optical Oceanography: American Elsevier Publishing Co., Inc., New York, N.Y.
- Morrison, R. E., 1970, Experimental studies on the optical properties of seawater, Jour. Geophys. Research, v.75, no. 3, p. 612-628.
- Turner, G. K., 1973, Clarity, nephelometry, and turbidity: Fluorometric Facts Series, available from Turner Designs, Inc., Palo Alto, Ca.
- Tyler, J. E., and Preisendorfer, R. W., 1962, Transmission of energy within the sea, in Hill, M. N., ed., The Sea, v. 1: John Wiley and Sons, New York, N.Y.

ERTS OBSERVATIONS OF SURFACE  
CURRENTS ALONG THE PACIFIC COAST OF THE UNITED STATES

by

Paul R. Carlson and Deborah R. Harden

Introduction

Oceanographers have studied the current flow along the Pacific coast for many years, but their efforts have been directed largely at the problem of current dynamics of the offshore water. Three decades ago, Sverdrup and others (1942), reported that the California Current, the southerly extension of the West Wind Drift (Fig. 1), flowed south most of the year, but in the winter in response to a regional reversal in wind direction, there was a corresponding reversal in surface current flow (Davidson Current). Subsequent studies (Reid, Roden, and Wylie, 1958; Reid and Schwartzlose, 1963; Burt and Wyatt, 1964) have substantiated the seasonal reversal of near-surface currents along the west coast of North America. However, these studies have concentrated on the offshore waters and have used ocean-going vessels to deploy drift bottles. As a result, a synoptic picture was difficult to reconstruct, and information for the nearshore, near-surface zone has been scarce.

This report demonstrates the utility of satellite imagery and drift card data to add to the information of near-surface water movement in the very nearshore waters of the west coast, indicates seasonal reversals of these nearshore waters, and illustrates some techniques used to study the distribution and nature of the suspended matter in the nearshore water.

Techniques

In the study area, which includes central and northern California, Oregon, and Washington, ERTS imagery has recorded areas of differing water color up to 30 km offshore, but most of the turbid water visible on the satellite imagery is within 10 km of the shoreline. The green band (MSS-4, 0.5-0.6  $\mu\text{m}$ ) very clearly shows turbid water in the nearshore zone (Fig. 2). This turbid water is often present off major rivers as discrete sediment-laden plumes. Such plumes serve as tracers of near-surface currents, as they become elongated in the direction of flow (Fig. 2). With very turbid water, as in some estuaries or near the effluents of major rivers, details of the overlapping suspended sediment lobes become obscured on the green band. Under these conditions, the red band (MSS-5, 0.6-0.7  $\mu\text{m}$ ) shows greater detail (Fig. 3) because this wavelength does not penetrate the water column as deeply. Combined use of green and red bands provides optimum detail of the complex turbidity patterns in estuarine and coastal waters.

Observations were made in the Gulf of the Farallones concurrent with ERTS overflights. Measurements were made of the water turbidity and

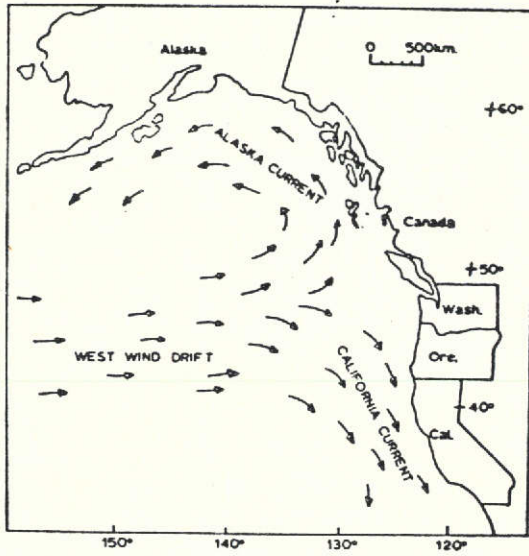


Figure 1. Surface currents of the northeast Pacific Ocean. Modified from Uda (1963); and Dodimead, Favorite, and Hirano (1963).

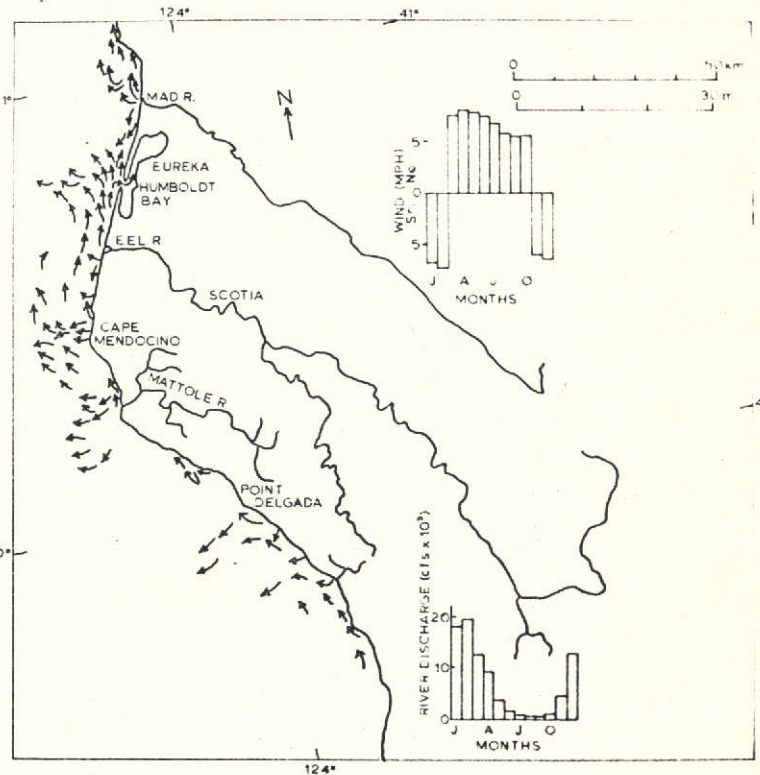


Figure 2. Plumes of turbid water and sketch of inferred current directions. ERTS multispectral scanner image, band 4 (0.5-0.6  $\mu$ m) no. 1167-18283 of northern California coast, January 6, 1973. The prevailing wind direction measured at Eureka for January is from the southeast (U.S. Dept. of Commerce, 1972). The suspended sediment concentration in the Eel River at Scotia was 122 mg/l on January 5, 1973, at 1610 hrs. (U.S. Geol. Survey, unpublished data, 1973). Image has been enhanced photographically using direct reversal high-contrast film (Allred, 1971).

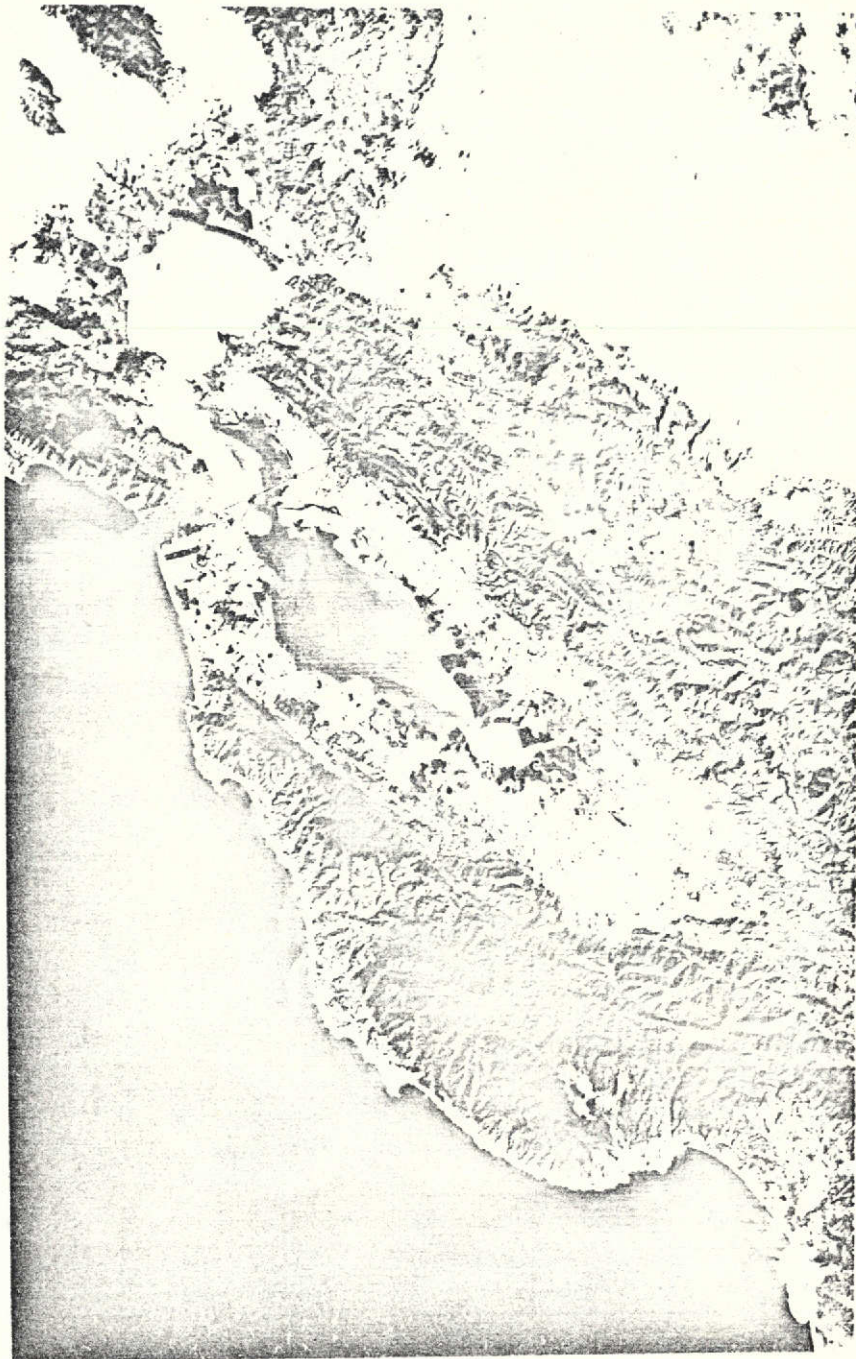


Figure 3. Turbid water of San Francisco Bay and adjacent Pacific Ocean. ERTS image band 5 (0.6-0.7  $\mu\text{m}$ ) no. 1183-18182, January 22, 1973. Note plume of turbid water in Gulf of Farallones (left edge) and San Francisco Bay (left of center). The source of this plume is the Sacramento-San Joaquin River system (under clouds, upper right). The source of the plume in Monterey Bay (lower right) is the Salinas River.

suspended particle characteristics using transmissometer and nephelometer (see Schemel, this volume), Secchi disc and Coulter counter. Concentration of suspended matter was obtained by filtering water samples through silver filters (pore diameters 0.45  $\mu$ ) and salinity was measured by an in situ salinometer. Computer analyses of digital tapes of images (Honey and Lyons, 1974), density slicing (Ross, 1973), and microdensitometer traces were made across selected images in order to compare image data with "water-truth."

Drift cards were deployed to verify the interpretations of surface current directions as deduced from ERTS imagery (Fig. 4). Furthermore, the drift cards provided information when the coastal zone was obscured by clouds during ERTS overpasses. The orange plastic cards have a weight in one corner and a styrofoam float in the opposite corner, which cause them to float almost totally submerged and thus be carried by the near-surface currents. The cards were air-dropped off the mouths of rivers and streams from central California to southern Oregon every two months during satellite overflights from June 1973 through February 1974. About 1,900 cards, in packets of 50, were dropped during each period, at distances of 1.6 and 8.1 km (1 and 5 miles) seaward of the river mouths. The inferred drift and minimum speed of the surface water as indicated by these cards, was determined by plotting the release times and locations and the recovery times and locations. Comparison of drift card vectors with interpretations of current directions deduced from ERTS imagery shows similar patterns (Fig. 5), and thus reinforces the reliability of the ERTS imagery as a tool for studying the movement of the surface currents.

#### Sources of Turbid Water

The principle sources of nearshore turbid water along the west coast, readily seen on ERTS imagery, are (1) the rivers draining the Coast Ranges (Fig. 6), (2) the Columbia River, which drains much of the Pacific Northwest (see Carlson and Conomos, this volume) and, the Sacramento-San Joaquin River system, which drains the west flank of the Sierra Nevada Mountains and flows into San Francisco Bay. Secondary sources of turbid water are coastal landslides, beach cliff and headland erosion, reworking of the bottom sediment by storm waves, plankton blooms, and waste water effluents. During times of high river discharge, the very turbid water being introduced to the nearshore zone, often masks the secondary sources of suspended matter on ERTS imagery (i.e., Eel River, Fig. 2). However, use of U-2 and other aerial photographs to supplement the satellite imagery provides the necessary resolution to detect secondary sources of suspended matter, such as pulp mill effluents (Fig. 7).

Although the waters of the Sacramento-San Joaquin drainage system enter a large estuary, much of the suspended load is carried through the system to the ocean (Fig. 3). The turbid, low salinity water bifurcates as it enters the central part of San Francisco Bay (Carlson and others, 1970); one lobe flows into the south bay and the second, larger lobe flows through the bay into the Pacific Ocean (Fig. 3 and 8). The ocean plumes of turbid

# OCEAN RESEARCH DROGUE

## U. S. GEOLOGICAL SURVEY

VITAL RESEARCH DATA REQUESTED  
PLEASE READ OPPOSITE SIDE AND FILL OUT  
RECOVERY DATA ON CARD BELOW.

AFTER COMPLETING THE REQUESTED DATA ON THE  
CARD PLEASE MAIL IT AT YOUR EARLIEST OPPOR-  
TUNITY.

NO POSTAGE IS NEEDED

<p>POSTAGE AND FEE PAID U.S. DEPARTMENT OF THE INTERIOR INT 413</p> <p>OFFICE OF MARINE GEOLOGY U. S. GEOLOGICAL SURVEY 345 Middlefield Road Menlo Park, California 94025</p> <p>Attention: Dr. Paul R. Carlson</p>	<p>NO POSTAGE NEEDED</p> <p>TO REMOVE CARD CUT ALONG BROKEN LINES AND FOLDED EDGE</p>	<p>DRIFT DROGUE</p> <p>RECOVERY DATA</p> <p>(TO BE FILLED IN BY FINDER)</p>	<p>NO. 12473</p>
		<p>LOCATION</p> <p>DATE</p> <p>MONTH</p> <p>DAY</p> <p>YEAR</p> <p>FINDER</p> <p>ADDRESS</p> <p>ZIP CODE</p>	<p>DATA</p> <p>INSTRUCTIONS</p> <p>DROGUE RECOVERY</p> <p>PLEASE GIVE NEAREST LAND- MARK, DISTANCE, SHORE, CHANNEL, ISLAND, HEAD- LAND BEARINGS, ETC., PLUS LATITUDE AND LONGITUDE IF AVAILABLE.</p> <p>DROGUE RECOVERY</p> <p>NAME OF</p> <p>CARD CAN BE WRITTEN ON WITH PENCIL OR BALL POINT PEN</p>

# OCEAN RESEARCH DROGUE

## U. S. GEOLOGICAL SURVEY

VITAL RESEARCH DATA REQUESTED  
PLEASE READ BELOW AND FILL OUT RECOVERY DATA  
CARD ON OPPOSITE SIDE.

TO THE FINDER:

THIS DRIFT DROGUE WAS RELEASED IN THE  
SAN FRANCISCO BAY SYSTEM OR OFF CALIFORNIA  
OR OREGON AS PART OF A DETAILED STUDY OF  
IN-SHORE AND COASTAL CURRENTS. A DETAILED  
SURVEY OF THE SEASONAL MOVEMENT OF THESE  
WATERS WILL HELP US BETTER UNDERSTAND THE  
EFFECTS OF RIVER DISCHARGE AND WIND ON THESE  
WATER MOVEMENTS. THIS UNDERSTANDING IS IM-  
PORTANT, AS WATER MOVEMENTS CONTROL SEDI-  
MENT DISTRIBUTION AS WELL AS MOVEMENT AND  
EVENTUAL DEPOSITION OF NATURAL AND MAN-  
MADE POLLUTANTS.

YOU CAN ADD TO OUR UNDERSTANDING OF  
WATER MOVEMENTS IN THE BAY SYSTEM AND  
COASTAL OCEAN BY RETURNING THE ADDRESSED  
CARD WITH THE REQUESTED INFORMATION ON LO-  
CATION AND DATE THE DRIFT DROGUE WAS FOUND.  
NO POSTAGE IS NECESSARY.

DR. PAUL R. CARLSON  
U. S. GEOLOGICAL SURVEY  
345 MIDDLEFIELD ROAD  
MENLO PARK, CALIFORNIA 94025

ORIGINAL PAGE IS  
OF POOR QUALITY

Figure 4. Example of drift card used to determine flow velocities of nearshore surface currents.

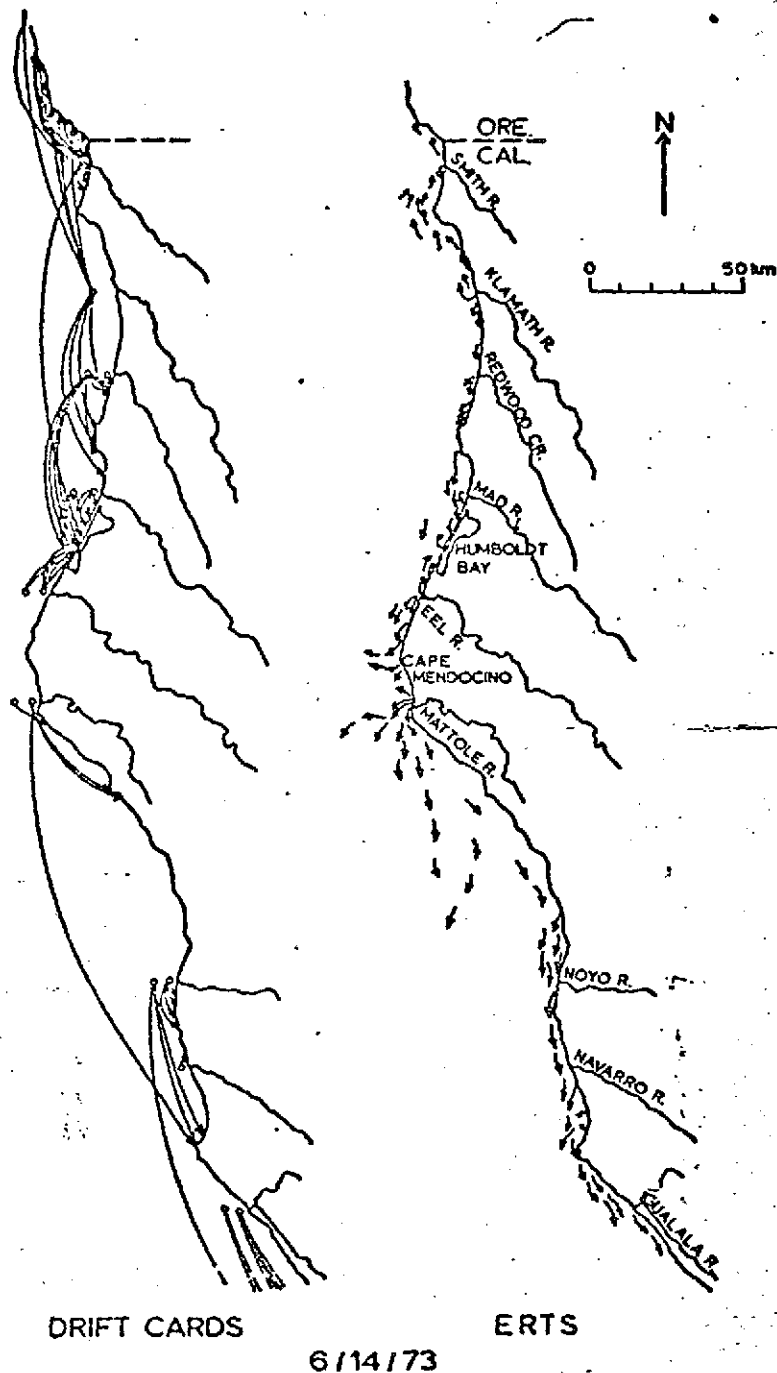


Figure 5. Near-surface nearshore current directions, mid-June 1973, along the northern California coast as indicated by drift cards and ERTS imagery. The long continuous arrows connect the point of origin (small circles off rivers) and point of recovery (arrowheads impinging on coastline) of drift cards dropped on June 14, 1973, and reported by August 14, 1973. Current directions as represented by arrows were interpreted from configurations of suspended sediment plumes present on ERTS imagery (band 4) of June 17, 1973 (no. 1329-18281, -18283, and -18290).

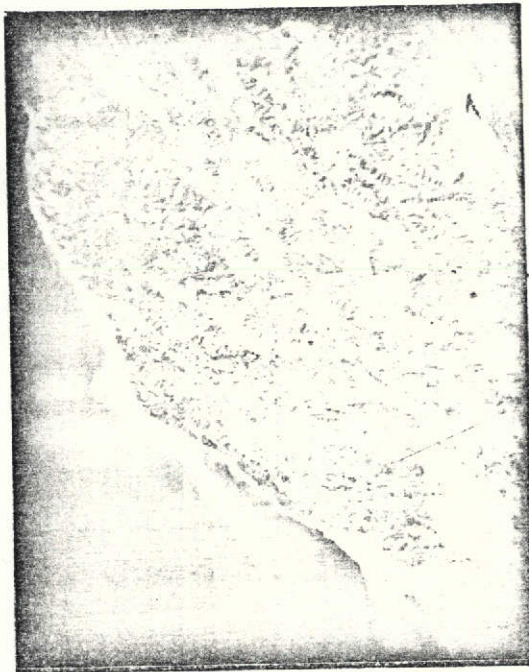


Figure 6. Plumes of turbid water from central California coastal rivers. Pt. Arena at center of coastline, Russian River plume in lower fourth of image. Note the distinct southerly flow. ERTS band 4, May 11, 1973 (no. 1292-18234).



Figure 7. Turbid water off Humboldt Bay. The largest part of the turbid water probably came from the Eel and Mad Rivers located south and north of the bay, however, the two light colored plumes just north of the bay entrance mark the effluents from two paper mills located along the peninsula. U-2 photograph taken January 4, 1973, from an altitude of 21,300 m (65,000 ft).

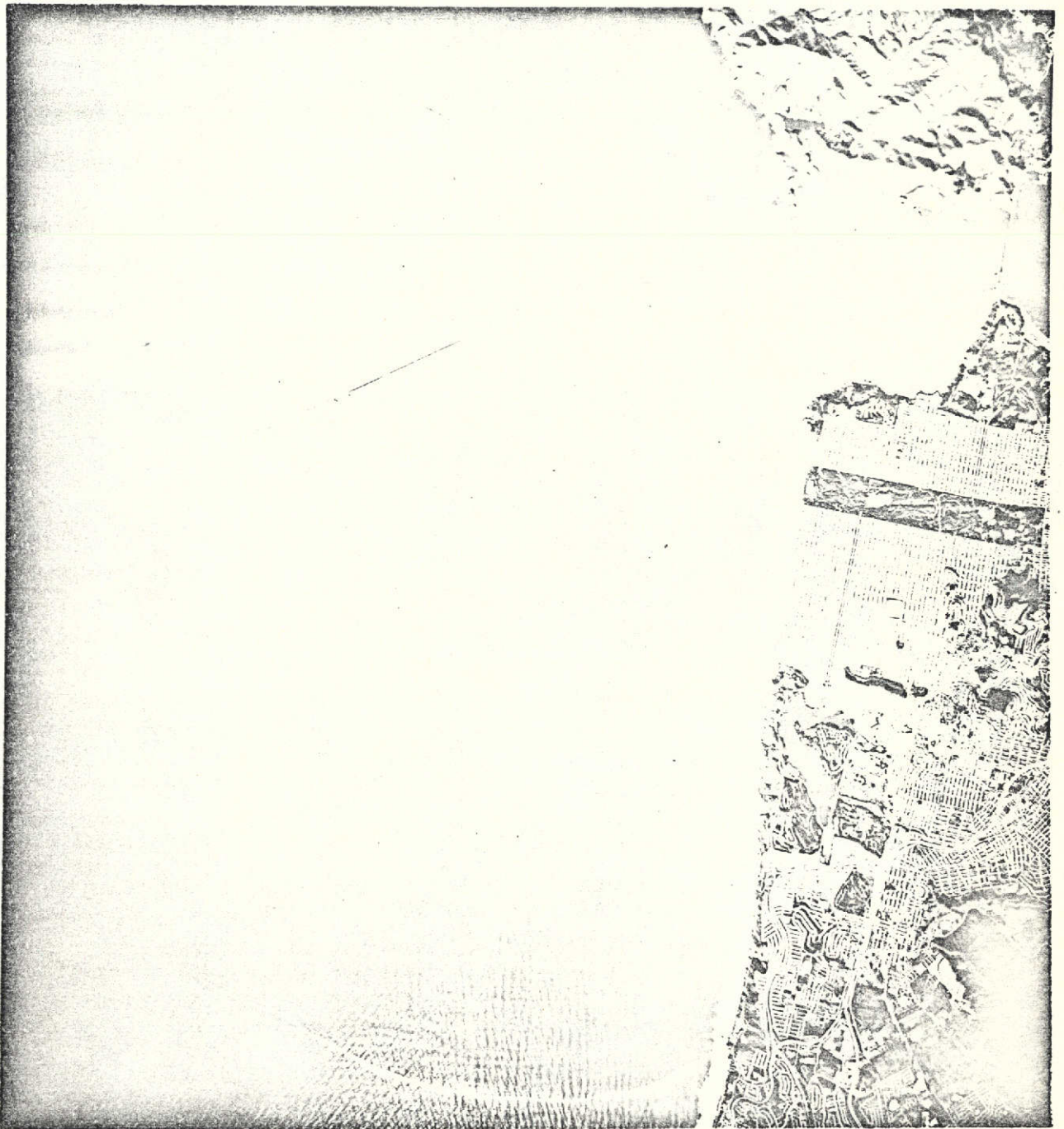


Figure 8. Plume of Turbid, low-salinity water discharged from San Francisco Bay (upper right) into the Gulf of the Farallones. U-2 photograph taken December 18, 1973 from an altitude of 21,300 m (65,000 ft). Marin Peninsula (upper edge) across Golden Gate Bridge from San Francisco (right center).

water have been observed for several years on high- and low-altitude photography (Fig. 8) and satellite imagery. There is a good correlation between surface area of the visible plume of turbid water and discharge from the Sacramento-San Joaquin River system (Carlson and McCulloch, 1974; Fig. 9).

Stations in the Gulf of the Farallones were occupied during ERTS overflights on January 23, May 30, and August 9, 1973 at which time measurements were made of physical characteristics of the water and suspended matter (Table 1 and Fig. 10). The concentration of suspended matter decreased oceanward during the winter cruise (Table 1). The coincident ERTS image and film density measurements (Fig. 11) indicate a similar trend with much more turbid water in the bay and a decrease in turbidity values through the plume into the Gulf. Comparison of the size and concentration of suspended matter from the winter sampling (1/23/73) with those of spring (5/30/73) and summer (8/9/73) (Table 1 and Fig. 10), shows considerable variation seasonally and from station to station. Factors influencing the variations in suspended matter in the Gulf of the Farallones are: (1) discharge and suspended sediment load from the Sacramento-San Joaquin River system; (2) wind and waves which affect longshore transport, resuspension of bottom sediments, and upwelling of nutrient-laden waters; and (3) phytoplankton blooms which have patchy and sporadic distributions. The larger median diameters and principle modes measured on those samples collected at the seaward end of the January and May sampling lines (Table 1 and Fig. 10) suggest the importance of the phytoplankton in those waters. The larger particles and smaller amounts of suspended matter measured on the August cruise (Table 1) also indicate the prevalence of phytoplankton (especially diatoms such as Asterionella, Chaetoceros, Coscinodiscus, and Skeletonema; E. P. Scrivani, U. Calif., Berkeley, oral commun., 1974.

ERTS imagery provides a synoptic view of a large section of the coastal zone, often recording more than one river effluent on a given image and thus providing a constant tonality and simultaneous comparison of plume configuration (Fig. 12). The image of the turbid water from the Gulf of the Farallones to Monterey Bay shows the complex nature of the plumes, and the accompanying sketch indicates the ranges in turbidity of the plumes and adjacent water. In San Francisco Bay, the Secchi disc visibility depths ranged from 0.5 to 1 m, whereas, in the Gulf of the Farallones and in Monterey Bay the values ranged from 2-3 m in the plume to 5-6 m in the less turbid water outside the main plume (Fig. 12). By way of comparison, Secchi disc visibility depths of 30 to 40 m have been measured in oceanic waters 85-100 km seaward of San Francisco (Frederick, 1970). At the time of the satellite pass (Fig. 12) the coastal currents seemed to be moving toward the south. An exception is off the Salinas River where the plume was deflected north, suggesting the presence of a counterclockwise gyre in Monterey Bay.

Portions of the same ERTS image were also studied using computer display of digital tape data (Honey and Lyons, 1974) and density slicing

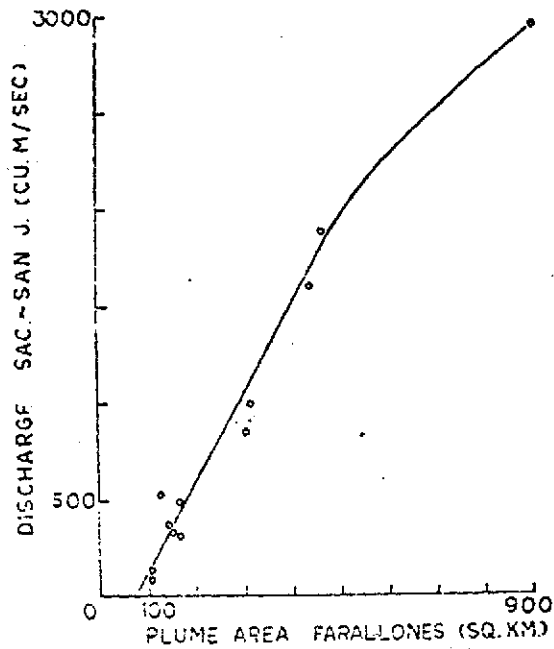


Figure 9. Sacramento-San Joaquin river discharge versus surface area of turbid water plume in Gulf of Farallones. Surface areas of plumes measured from aerial photographs and satellite images taken during the period November 1967 through May 1973. Discharge data from U.S. Bur. Reclamation (Norman Beck, oral commun., 1973) and U.S. Geol. Survey (Sally Walker, oral and written commun., 1973).

ORIGINAL PAGE IS  
OF POOR QUALITY

Table 1. Physical characteristics of water and suspended matter in the upper meter in the Gulf of the Farallones. Station locations are shown on Figure 10 except Farallon Islands and Swell stations which are located 25 and 12 km seaward of Light Buoy.

Station	S <sup>o</sup> /oo*	1/23/73			S <sup>o</sup> /oo	5/30/73			S <sup>o</sup> /oo	8/9/73			Secchi depth m
		Sus. Sed. mg/l	Med. diam. μ	Princ. mode μ		Sus. Sed. mg/l	Med. diam. μ	Princ. mode μ		Sus. Sed. mg/l	Med. diam. μ	Princ. mode μ	
Golden Gate Br.	15	14.3	11	9	29.4	14.8	18	8	32.4	6.4	12	7	4
Mile Rock	16	16.0	11	9	30.2	14.8	14	8	32.7	5.2	18	20	
Shoal	20.5	11.6	7	5.5	31.5	22.0	14	10	33.0	3.8	22	20	5
	21	10.4	9	7.5									
Light Buoy	22.8	7.2	18	20	32.5	5.4	13	5	34.0	7.4	23	20	6
Swell					33.8	4.8	18	13 & 36	34.0	5.4	23	21	
Farallon Islands									34.0	4.2	18	13	12

\*S<sup>o</sup>/oo = Salinity parts per thousand; Sus. sed. mg/l = suspended sediment milligrams per liter; Med. diam. μ = median diameter microns (of suspended particles); Principle mode μ = most prevalent particle size; Secchi depth m = Depth in meters at which 30 cm. diameter white disc disappears from sight.

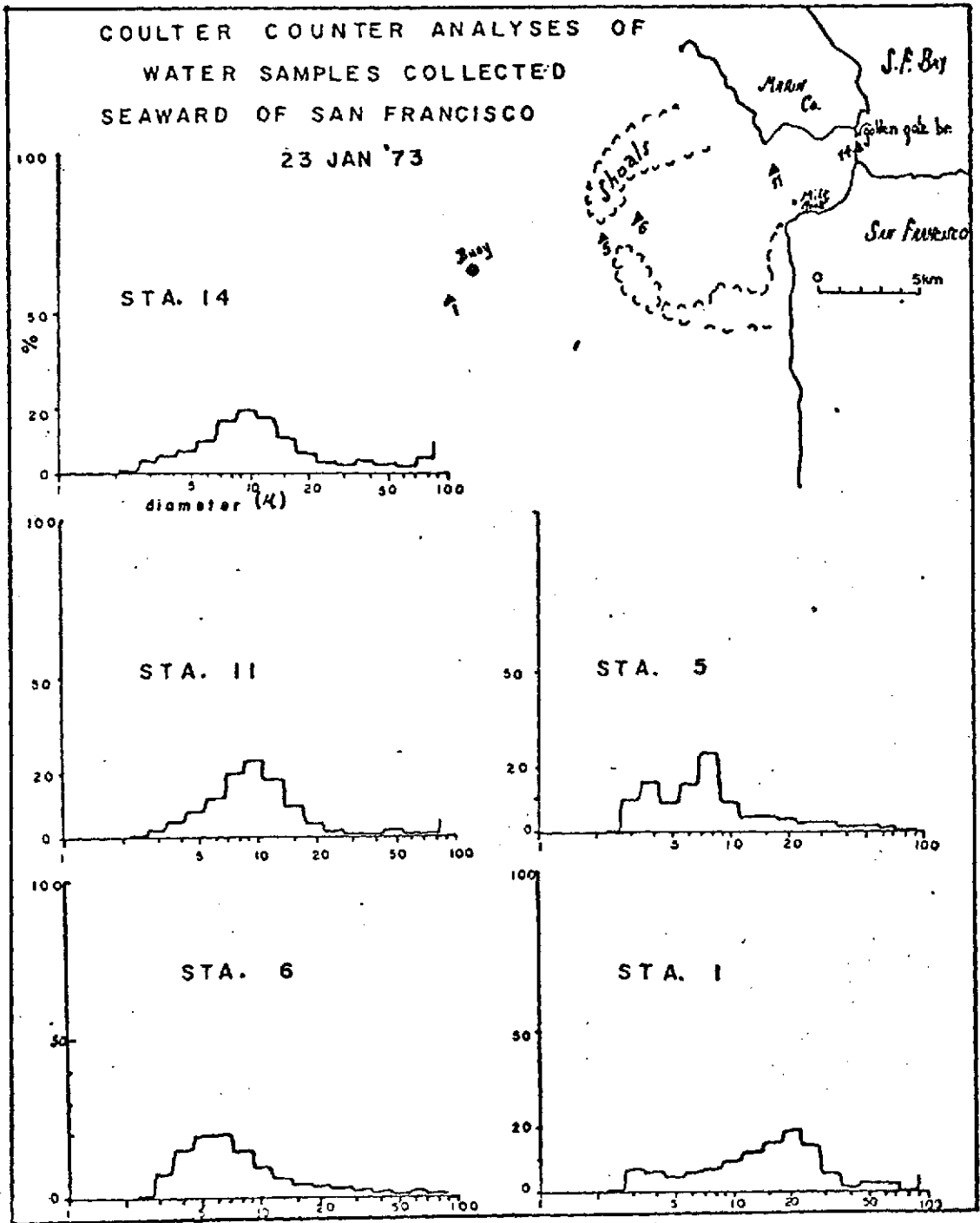


Figure 10. Particle size variations of suspended matter in Gulf of Farallones, January, May, and August 1973.



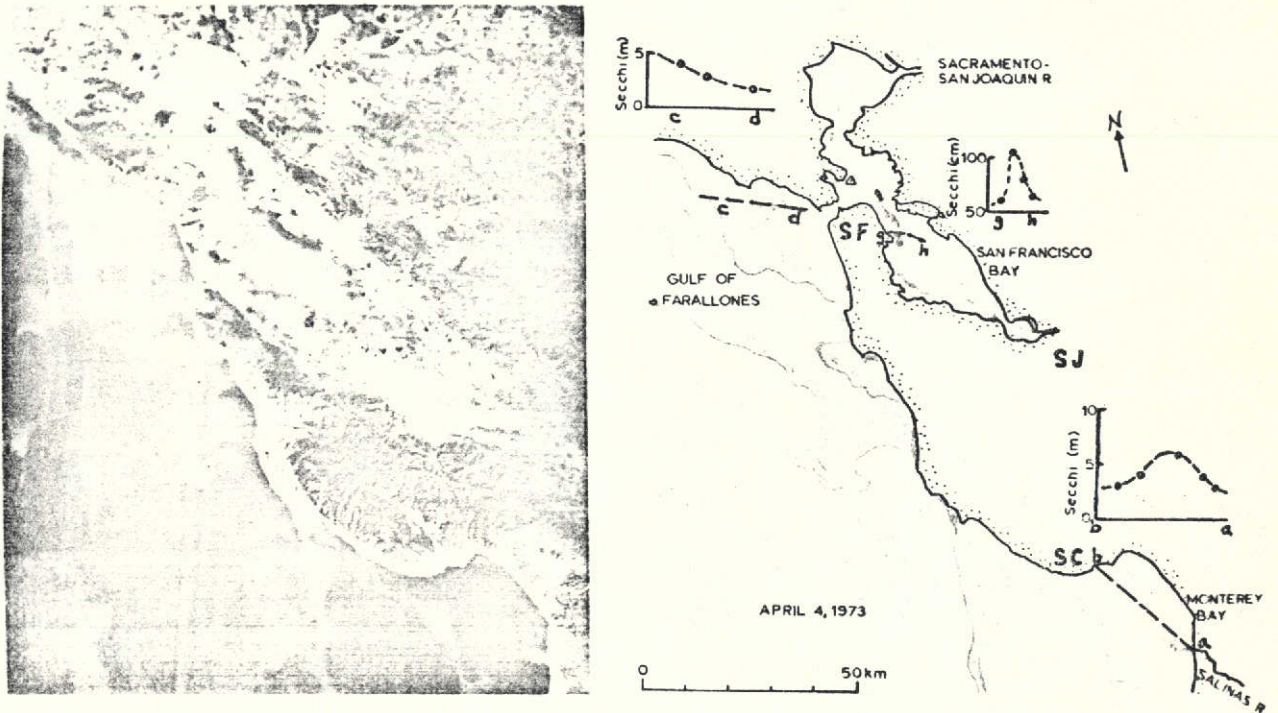


Figure 12. ERTS image and sketch of turbid water in San Francisco Bay, Monterey Bay, and the Gulf of the Farallones. The complex lines offshore separate tonal differences that signify different turbidities. The three graphs of Secchi disc visibility depth illustrate the ranges in turbidity shown by the ERTS image of April 4, 1973, (no. 1255-18183). The Secchi disc measurements were made April 4, 5, and 19, 1973, in San Francisco Bay, the Gulf of the Farallones, and Monterey Bay. Measurements in Monterey Bay by Moss Landing Marine Laboratory (Broenkow and Benz, 1973).

with the I<sup>2</sup>S Digicol (Ross, 1973). The ERTS digital tapes were utilized to provide a printout of the reflectance levels of a portion of the Gulf of the Farallones north of the Golden Gate Strait (Fig. 13). This printout shows the northern boundary of the plume (compare with Fig. 12) and also shows much more detail within the plume than could possibly be monitored at the instant of the image collection even if several vessels were used. However, if one generalizes on the digital printout, the gross features can be determined. The rapid changes in such a dynamic environment makes this computer technique of plume monitoring impractical, at least with present sampling procedures. The density slicing technique involved the use of ERTS transparencies and the I<sup>2</sup>S Digicol. Photographs and transparent overlays can be used with this system to record variations in density of the positive transparency which are manifestations of the variations in water turbidity. The density slicing results are shown in Figure 14. Comparison with Figure 12 shows how the Digicol highlights the plume area and how the densities change across the plume. Note that the higher values of percentage of light transmitted correspond to the more turbid water. The turbid water in the Gulf of the Farrallones on April 4, 1973 can be divided into three discrete units, (Fig. 14) which are outlined by the dashed lines and characterized by the measured values listed in Table 2.

Table 2. Characteristics of the turbid water in the Gulf of the Farallones.

	<u>% transmitted light (Digicol) (a)</u>	<u>Secchi disc visibility depth (m) (b)</u>	<u>Suspended sediment concentrations (mg/l) (b)</u>
main plume	45-55	≤2	25-30
intermediate	40-45	~3	20-25
outer	<40	~4	10-15

(a) From April 4, 1973 ERTS image and Digicol measurements (Fig. 14).

(b) Water truth collected April 5, 1973 along line C-D (Fig. 12), over 2-hour time period that bracketed time of image reception.

#### Seasonal Reversals of Coastal Currents

The seasonally changing flow directions of nearshore currents along the northern California coast can be traced from ERTS imagery (Fig. 15). In the fall of 1972 currents were flowing southward at the time of an ERTS overpass, but during the winter the flow was distinctly northward. By spring of 1973 the flow had reversed again. This same sequence of current reversals took place along the central California coast during the same seasons of 1972 and 1973 (Fig. 16) and along the Oregon and Washington coasts in the winter and spring of 1973 (Fig. 17). Continued



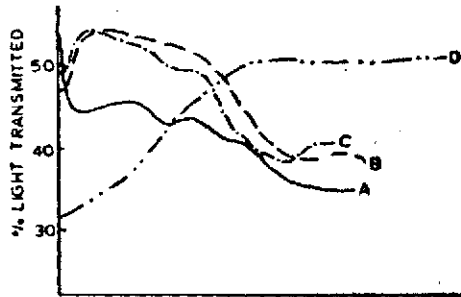
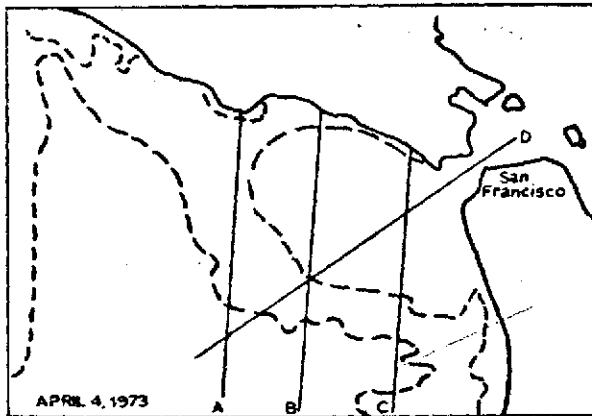


Figure 14. Variations in reflectance of various colors of water in the Gulf of the Farallones recorded as density variations from ERTS imagery of April 4, 1973, no. 1255-18183. Compare with Figures 11 and 12. Top right: Plume of turbid, low salinity water off San Francisco as portrayed on the I<sup>2</sup>S Digicol. Original color print of the video display was taken with Kodachrome X film. Bottom right: Black and White display of same image as top right. Jagged white line is an example of light transmitted through the ERTS transparency along the straight white line (line B on sketches). Top left: Location map of ERTS image (dashed lines represent water color boundaries) and lines of light transmittance profiles. Bottom left: Light transmittance profiles across the plume of turbid water in the Gulf of the Farallones.

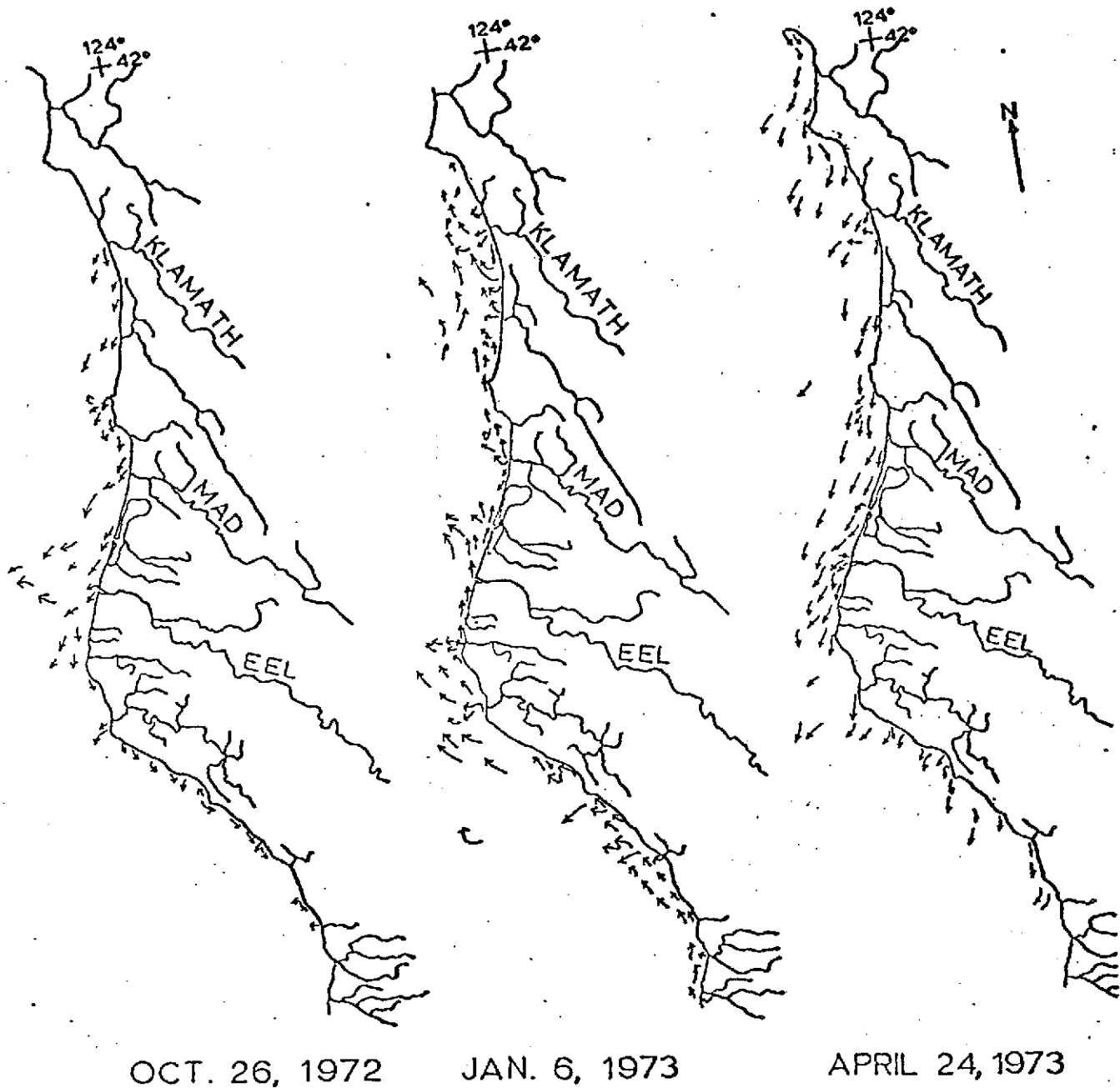


Figure 15. Seasonal reversal of nearshore currents along the northern California coast. Current directions interpreted from ERTS imagery, band 4, October 26, 1972, (no. 1095-18280 and 18283), January 6, 1973, (no. 1167-18280 and 18283), and April 24, 1973, (no. 1275-18284 and 18290).

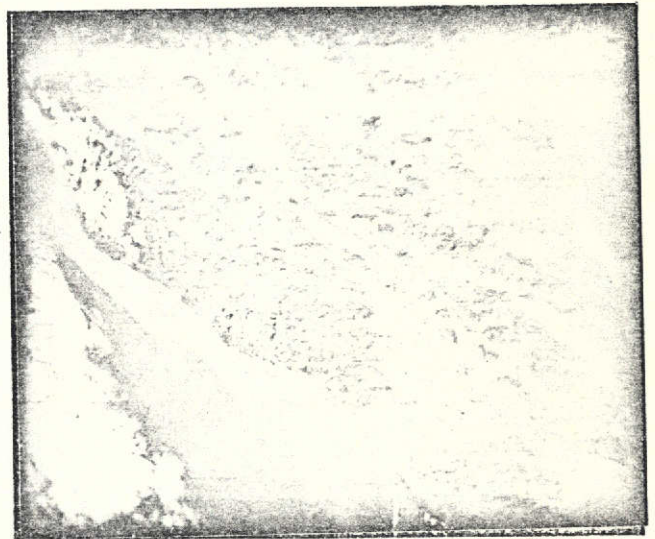
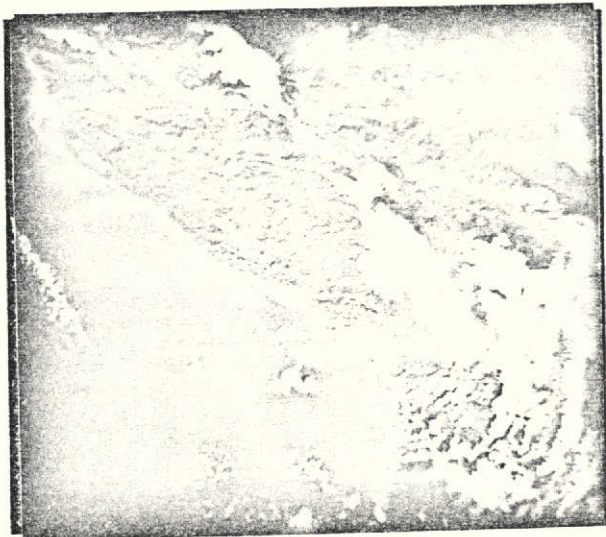


Figure 16. Current reversals along the central California coast. The left-hand image, taken November 11, 1972 (E-1112-18233), shows turbid-water plumes deflected northward, whereas the right-hand image, taken March 18, 1973 (no. 1238-18235), shows plumes deflected southward. Both images are of coastline between Pt. Arena, top left, and Pt. Reyes, near bottom right (ERTS band 4).

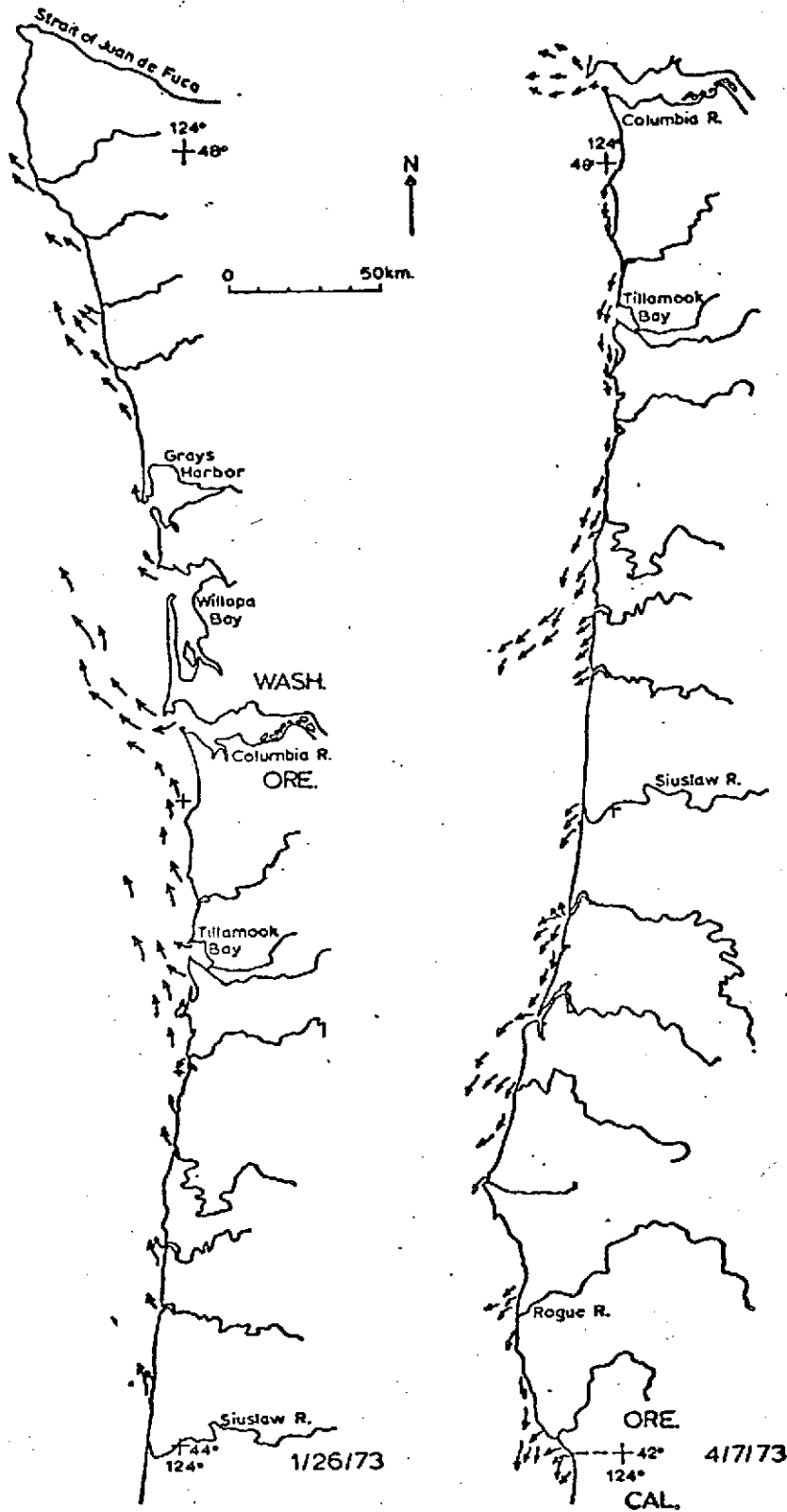


Figure 17. Reversal of nearshore currents along the coast of the Pacific Northwest. Current directions interpreted from ERTS imagery, band 4, January 26, 1973 (1187-18380; 1187-18383; 1187-18385) and April 7, 1973 (1258-18331; 1258-18334; 1258-18340; 1258-18343).

monitoring of the seasonal pattern of current flow was made possible through bimonthly drift card releases from June 1973 through February 1974 (Fig. 18). It was indeed fortunate that we began this supplemental program (Fig. 5) because clouds obscured the coastal zone during most of the ERTS passes from August through December 1973. Comparison of the flow patterns in October of 1972 and 1973 (Figs. 15 and 18) suggest that the northerly flowing Davidson Current surfaced earlier in 1973 than in 1972, an observation that would not have been possible with the use of ERTS imagery alone because of the prevalence of clouds in October 1973.

The drift card trends seem to show two quite different patterns of flow broken at Cape Mendocino. South of the cape, the flow was quite consistently one direction, except for counterclockwise gyres off San Francisco Bay and in Monterey Bay in August (Fig. 18B). North of Cape Mendocino, however, the flow direction indicated by the drift card returns was much more complex (Fig. 18A). The convergent patterns off Humboldt Bay may be related to tidal circulation of the bay system and may be influenced further by the discharge plumes of the adjacent Eel and Mad Rivers. Off the Smith and Klamath Rivers and Redwood Creek, divergent patterns can be seen in the June 1973 data. Divergency also occurred off Redwood Creek in October 1973 and off the Mad River in February 1974. The complex patterns indicating convergence and divergence probably are related to a combination of several factors including seasonal upwelling, coastal configuration, submarine morphology, and local effects of the wind.

In addition to current directions, the card returns provide minimum speeds for these nearshore currents. Speeds of 50 km/day (58 cm/sec) were attained by several cards that were released near the Russian River on June 14, 1973 and found 50 km south at Point Reyes beach one day later (Fig. 18). Other returns indicated speeds of less than 1 km/day. In order to obtain a general picture of the current speed, an average of the two fastest speeds in a given direction was calculated for each drop point. The mean values of the average speeds were then determined for each drift-card deployment date and are listed on Table 3. The dual flow directions listed for several of the dates resulted from the counterclockwise gyres in Monterey Bay and the Gulf of the Farallones (8/27/73), central coast) and the divergent and convergent conditions found off several of the northern coastal rivers (6/14/73, 8/27/73, and 2/6/74).

Although these current speeds will vary somewhat from year to year with local variations in wind velocities, the velocities are generally consistent with the regional wind patterns (Fig. 2 and Table 4). The surface currents apparently were weakest in late summer, a time of reduced windspeed. The most rapid flow along the central coast was southward in June, reaching speeds of over 40 km/day (46.3 cm/sec) off the Russian and the Gualala Rivers. For the northern coast the north-flowing currents of October and December were the most rapid, reaching speeds of about 25 km/day (29 cm/sec) off Redwood Creek and the Klamath and Smith Rivers.

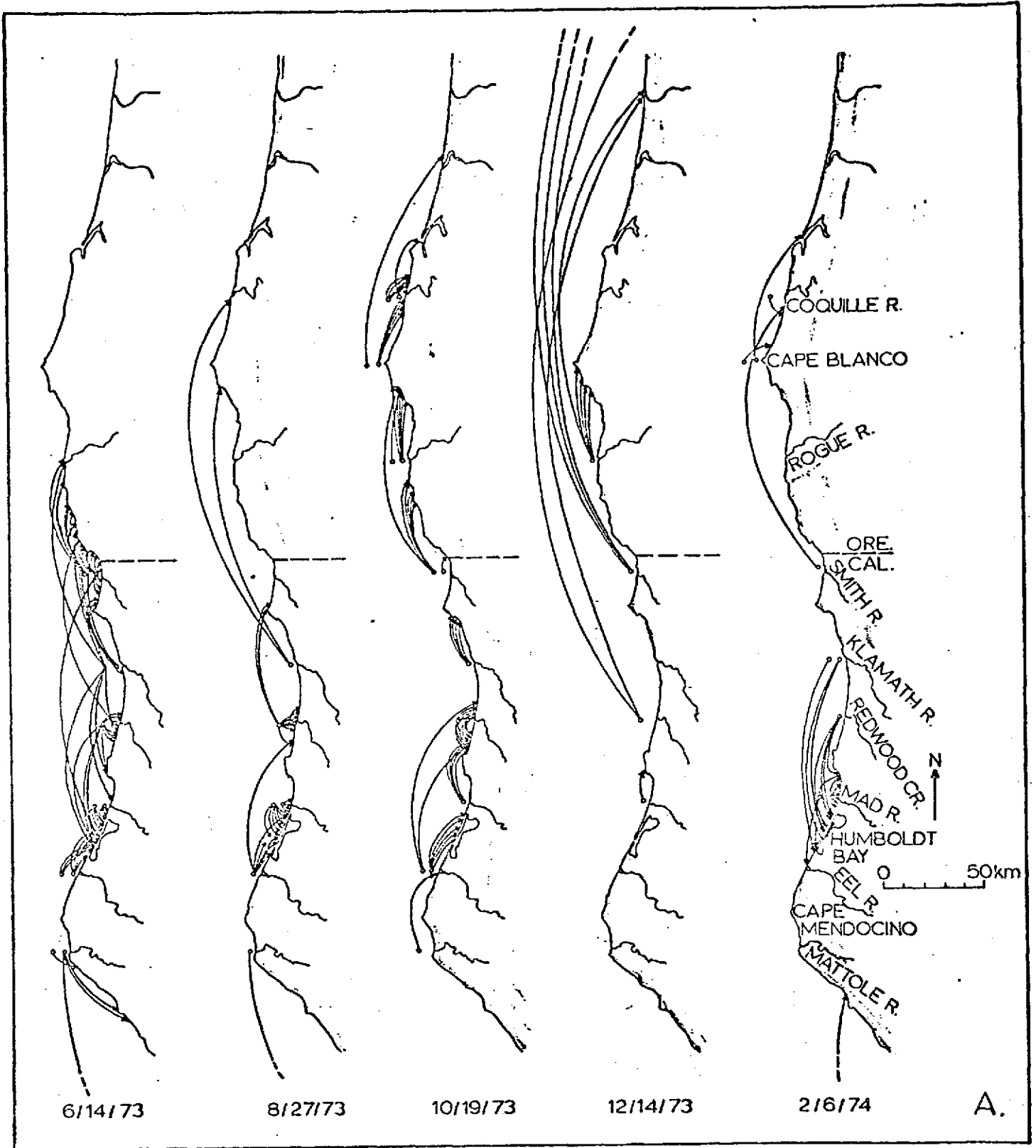


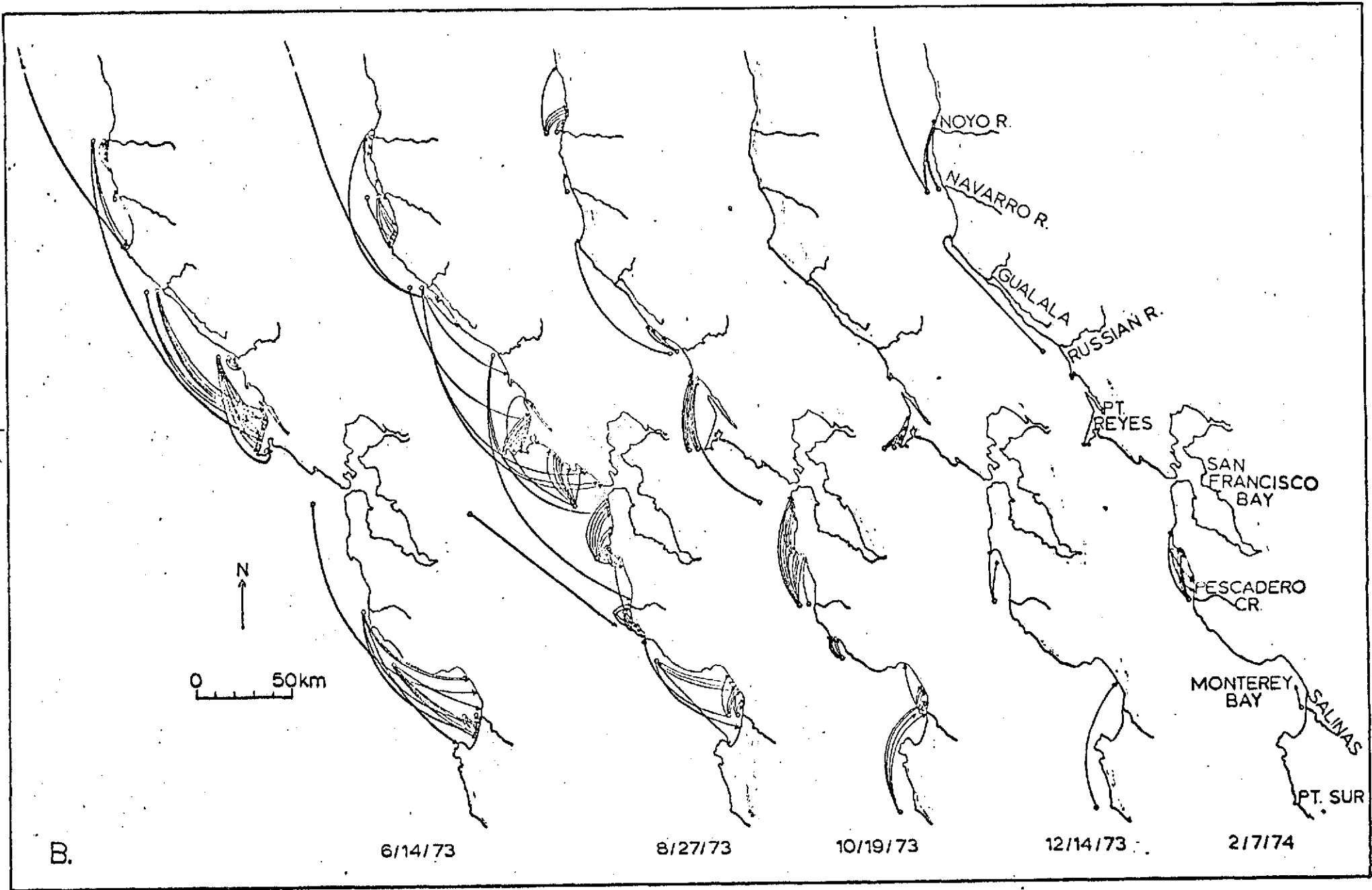
Figure 18. Seasonal differences in nearshore currents based on drift card returns.

a. Northern California and southern Oregon coast.

b. Central California coast.

Dates below each strip map are deployment dates; cards were air-dropped at positions of small circles. Arrows indicate generalized paths of drift cards and arrowheads indicate where the cards were found. Returns are limited to those cards found within two months of drop date.

122



B.

6/14/73

8/27/73

10/19/73

12/14/73

2/7/74

Table 3. Mean speeds and directions of nearshore surface currents along the northern and central California coast. Release and recovery points of drift cards shown on Figure 18.

<u>Flow direction</u>	<u>Northern coast</u>				
	<u>6/14/73<sup>a</sup></u>	<u>8/27/73</u>	<u>10/19/73</u>	<u>12/14/73</u>	<u>2/6/74</u>
north	11 <sup>b</sup> (13) <sup>c</sup>	4 (5)	16 (19)	20 (23)	6 (7)
south	9 (10)	5 (6)			11 (13)
	<u>Central coast</u>				
north		8 (9)	12 (14)	5 (6)	7 (8)
south	22 (25)	5 (6)			

<sup>a</sup> Release date of drift cards

<sup>b</sup> mean speed - km/day

<sup>c</sup> mean speed - cm/sec

Table 4. Long term average wind velocities along the Pacific Coast at Eureka, California and Astoria, Oregon.

Duration of records: Astoria-speed 19 yrs., and direction 10 yrs.; Eureka-speed and direction 54 yrs. (U.S. Dept. of Commerce, 1972).

Month	<u>Astoria</u>		<u>Eureka</u>	
	<u>Mean speed (knots)</u>	<u>Prevailing direction*</u>	<u>Mean speed (knots)</u>	<u>Prevailing direction</u>
Jan.	9.2	E	6.9	SE
Feb.	8.9	ESE	7.2	SE
Mar.	8.8	SE	7.6	N
Apr.	8.6	WNW	8.0	N
May	8.4	NW	7.9	N
June	8.2	NW	7.4	N
July	8.5	NW	6.8	N
Aug.	7.8	NW	5.8	NW
Sept.	7.3	SE	5.5	N
Oct.	7.4	SE	5.6	N
Nov.	8.2	SE	6.0	SE
Dec.	9.0	ESE	6.4	SE

---

\*Direction from which wind is blowing

- Dodimead, A. J., Favorite, F., and Hirano, T., 1963, Review of Oceanography of the Subarctic Pacific region, in Salmon of the North Pacific Ocean: International North Pacific Fisheries Comm. Bull. 13, Part II, 195 p.
- Frederick, M. A., 1970, An atlas of Secchi disc transparency and measurements and Forel-Ule color codes for the oceans of the world: M. S. Thesis, Monterey, Naval Postgraduate School, 179 p.
- Honey, F. R., and Lyons, R. J. P., 1974, STANSORT-a, simplified, low cost pattern recognition technique for ERTS spectral signatures: Summary papers of Ninth Internat. Symp. on Remote Sensing of Environ., Ann Arbor, Mich., p. 99.
- Reid, J. L., Roden, G. I., and Wylie, J. G., 1958, Studies of the California Current system, in Calif. Co-op Fisheries Investig. Progress Report, 1 July 1956 to January 1958: Marine Research Comm. Calif. Dept. of Fish and Game, p. 27-56.
- Reid, J. L., and Schwartzlose, R. A., 1963, Direct measurement of the Davidson Current off central California: Jour. Geophys. Research, v. 67, p. 2491-2497.
- Ross, D. S., 1973, Water depth estimation with ERTS-1 imagery: Symp. on Signif. Results Obtained from ERTS-1, NASA/Goddard Space Flight Center, Greenbelt, Maryland, p. 1423-1427.
- Schemel, L. E., 1975, A performance evaluation of the Turner Designs model 10 fluorometer/nephelometer for turbidity studies in natural waters, in Principle sources and dispersal patterns of suspended particulate matter in nearshore surface waters of the northeast Pacific Ocean and the Hawaiian Islands, Carlson, P. R., Conomos, T. J., Janda, R. J., and Peterson, D. H., eds: ERTS-1 Final Report, Natl. Tech. Info. Service, p. 92-99
- Sverdrup, H. U., Johnson, M. W., and Fleming, R. H., 1942, The Oceans: Prentice-Hall Inc., Englewood Cliffs, N. J., 1087 p.
- Uda, M., 1963, Oceanography of the Subarctic Pacific Ocean: Jour. Fisheries Resources Board of Canada, v. 20, p. 119-179.
- U.S. Dept. of Commerce, Natl. Oc. and Atmos. Admin., 1972, Local climatological data, for Eureka, Calif., Annual summary, Natl. Climatic Center, Ashville, N.C.

PRECEDING PAGE BLANK NOT FILMED

## ERTS IMAGERY OF THE WEST-CENTRAL COASTAL ZONE OF MEXICO

by

Deborah R. Harden, Erk Reimnitz and Paul R. Carlson

The study area extends along the west coast of Mexico from Mazatlan to Acapulco (Fig. 1). Included in the area are two major rivers, Rio Grande de Santiago and Rio Balsas. The purpose of the study was to observe patterns of sediment dispersal from these and other rivers using ERTS imagery (Fig. 2). We received imagery during late September 1972, from December 1972 until June 1973, and from mid-September until mid-December 1973.

The climate of the area is tropical. The area receives about 75-100 cm of rain annually, with 80-90 percent of the precipitation occurring from late May through October (Roden, 1964). Rainfall thus is less than that of the coastal zone of northern California (about 200 cm), but slightly greater than that of the San Francisco Bay area (about 75 cm).

Many factors determine sediment dispersal patterns at the mouth of a river. The river discharge rate, bottom configuration near the river mouth, ocean currents, and the direction, duration, and speed of wind are important. In addition, nearshore waters may be protected from wind and currents by protruding lands. Such headlands may also provide barriers to sediment transport. Planktonic activity, which depends on sunlight, often creates large amounts of suspended material in nearshore waters, especially near rivermouths, where nutrient supplies are high.

The amount of sediment supplied to the river mouth is influenced by many factors especially the nature of the drainage basin; i.e., its steepness and size, and the resistance of its underlying materials. In addition, the presence of dams and reservoirs will restrict the amount and size of material which reaches the river mouth. For instance, the presence of two major dams on the Rio Balsas may account, at least in part, for the almost total lack of sediment plumes off its mouth. Finally, the amount of precipitation influences the discharge of the river and thus its competence.

Almost no data concerning the parameters mentioned above are available for the study area. Any comparison between the rivers of northern latitudes with these more tropical streams in order to determine the climatological influences would necessitate selection of basins of comparable size, geology, and offshore topography. Other factors complicating a comparison are vegetation and land use by man.

Distinct sediment plumes can be seen at the river mouths in mid-June, early in the rainy season (Fig. 2) and in mid-September, late in the rainy season (Fig. 3 and 4). These plumes are considerably less extensive



Figure 1. ERTS study area, west-central coastal zone of Mexico.

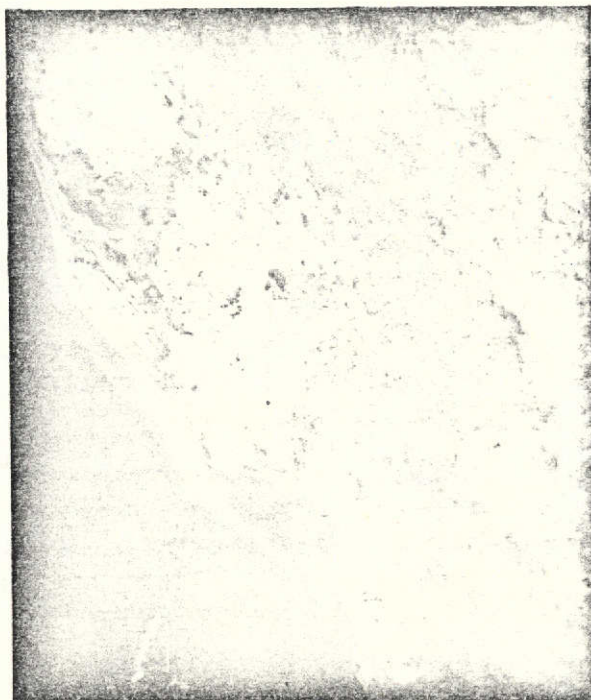


Figure 2. ERTS image of suspended sediment plume off the Rio Grande de Santiago, June 18, 1973 (no. 1330-16563). Note also the well developed beach ridges north of the river.

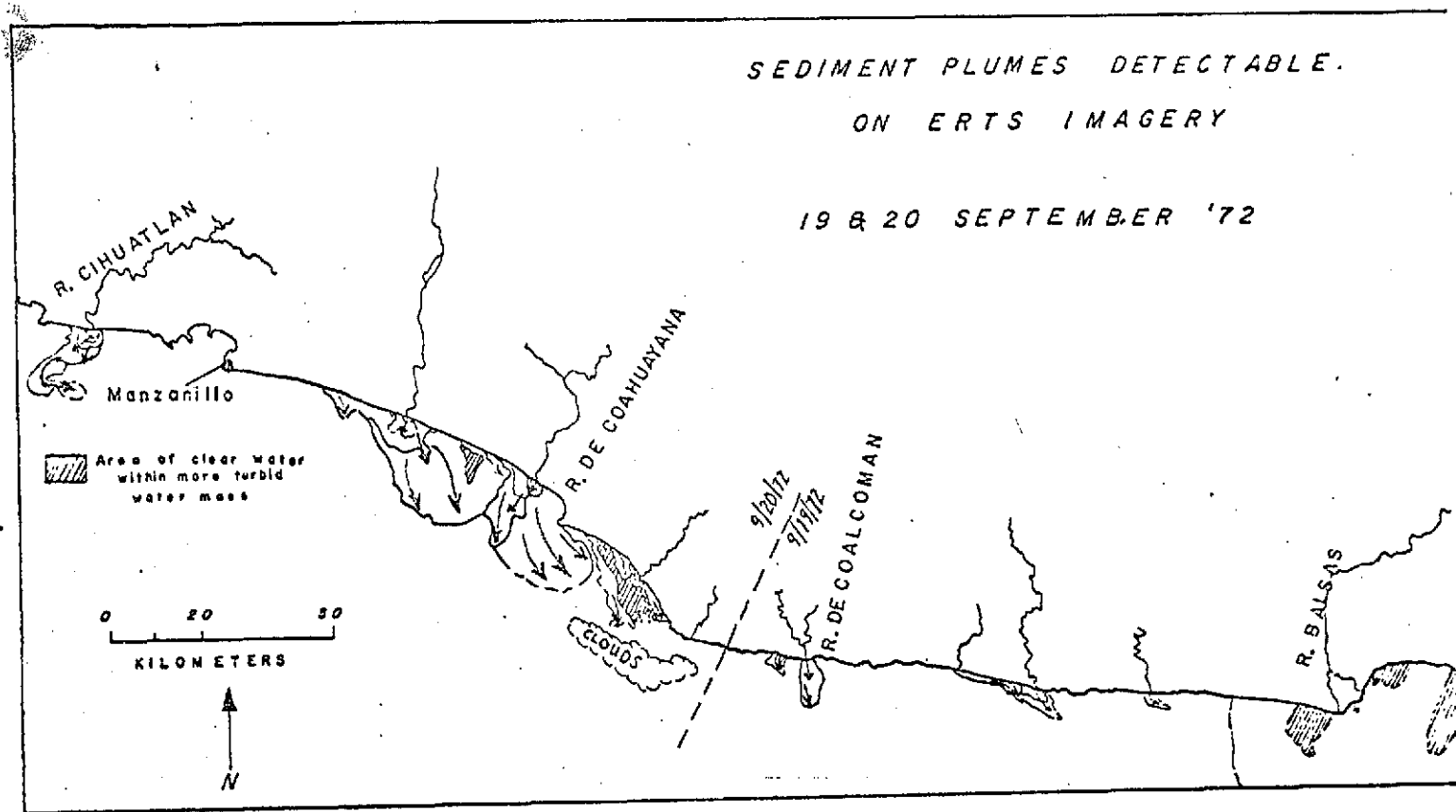


Figure 3. Dispersal patterns of suspended sediment visible on ERTS band 4 imagery of September 19 and 20, 1972 (nos. 1058-16451 and 1059-16510). Arrows indicate flow directions of surface currents as interpreted from ERTS images.

129

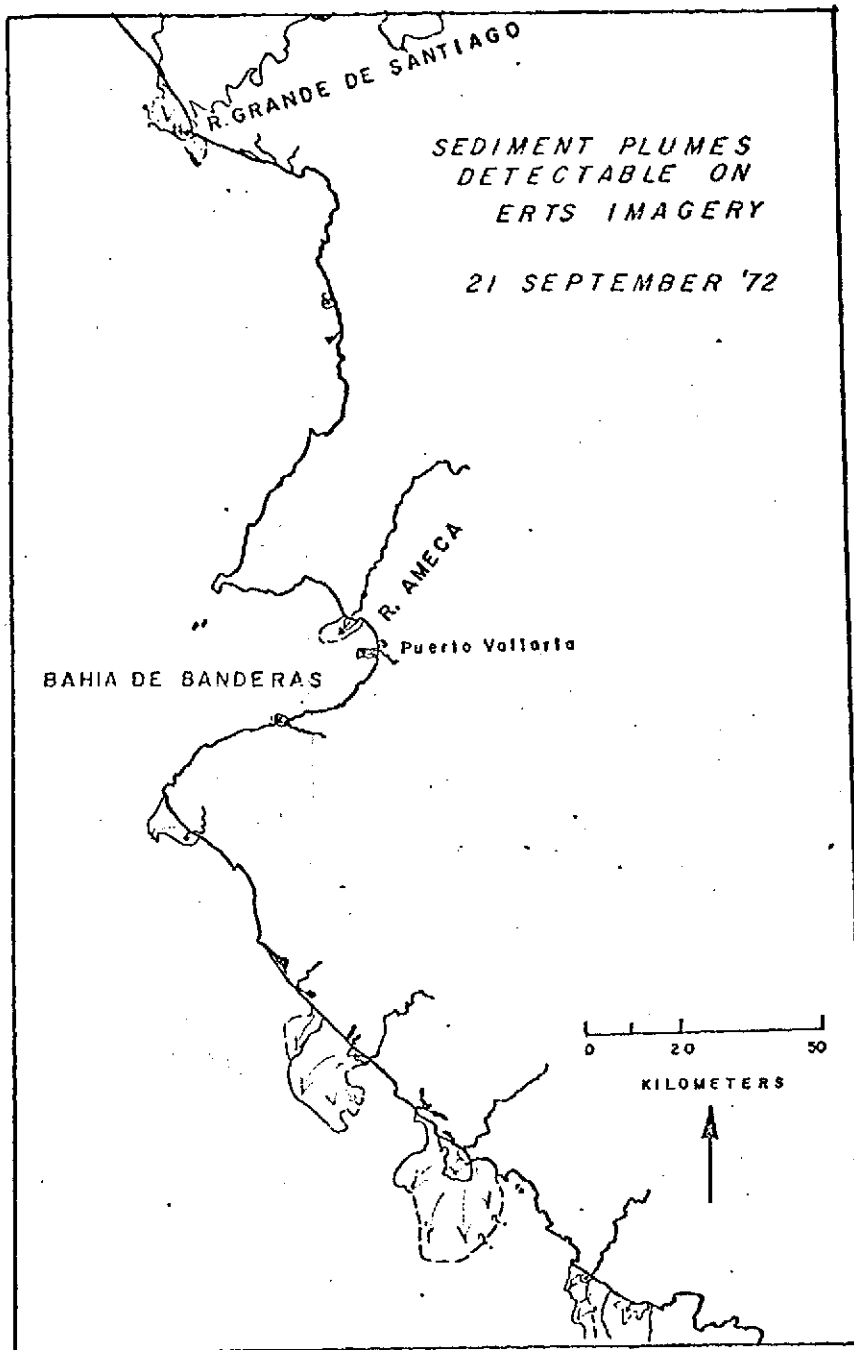


Figure 4. Dispersal patterns of suspended sediment visible on ERTS band 4 imagery of September 21, 1972 (nos. 1060-16555 and 16562). Arrows indicate flow directions of surface currents as interpreted from ERTS images.

than those of northern California rivers (see Carlson and Harden, 1975, Chpt. 9, this report) despite the fact that the drainage areas of the latter are about an order of magnitude smaller than those of the Rio Balsas and the Rio Grande de Santiago. Direction of surface transport as interpreted from the imagery showing summer plumes seems to be generally southward, which is the opposite of the reported summer drift. Drift currents are generally toward the south and southeast during winter and toward the northwest during summer (Reimnitz, 1968, Roden, 1964). However, current data are sparse, and southerly currents may not be abnormal for September.

Imagery obtained during December of 1972 and 1973 shows fairly distinct plumes at river mouths. The amount of suspended sediment visible on December imagery appears to be roughly the same as during September. Since the rainy season does not usually extend into the winter, this phenomenon may be due to factors other than seasonal rainfall variations and remains unexplained. We do not have sufficient imagery to determine the variation of plume size and shape before, during, and after the summer rains.

During April, bands of suspended matter appear more diffuse, but cover broader areas than in mid-September. The concentration of suspended matter during this time may be due to planktonic activity rather than to river discharge.

Imagery covering the Rio Balsas delta shows channel patterns which differ somewhat from those observed by Reimnitz and Gutierrez-Estrada (1969; Fig. 5). The easternmost tributary empties into the ocean west of its former mouth and the most westerly branch of the western distributary has been sealed off. Other shifts in the channel further upstream can also be observed. This may be related to construction activity on a dam, or to harbor dredging, which recently began. Comparison of the aerial photography and ERTS imagery also seems to show that some coastal erosion has taken place in recent years in the western part of the delta. This interpretation recently has been confirmed by conversations with Dr. A. Ayala-Castañares and Dr. R. Lankford (oral commun., 1974) in which they reported that 40-60 m/year of coastal retreat has been measured.

Imagery of the coastal region north of the mouth of the Rio Grande de Santiago shows striking parallel lineations (Fig. 2). These bands represent former beach lines approximately parallel to the present coastline. Places where the ridges trend at angles to the present beach are presumably those where the coastline has been realigned due to changes in the oceanographic and/or sediment supply regime. Curray and others (1969) ascribe their formation to the emergence of longshore bars to become new beach ridges. Former beaches thus become abandoned ridges, and lagoons between them are eventually filled. Areas of parallel beach ridges have also been described for the Rio Balsas delta (Reimnitz and Gutierrez-Estrada, 1969), but they are spaced too closely to be discernable on ERTS imagery.

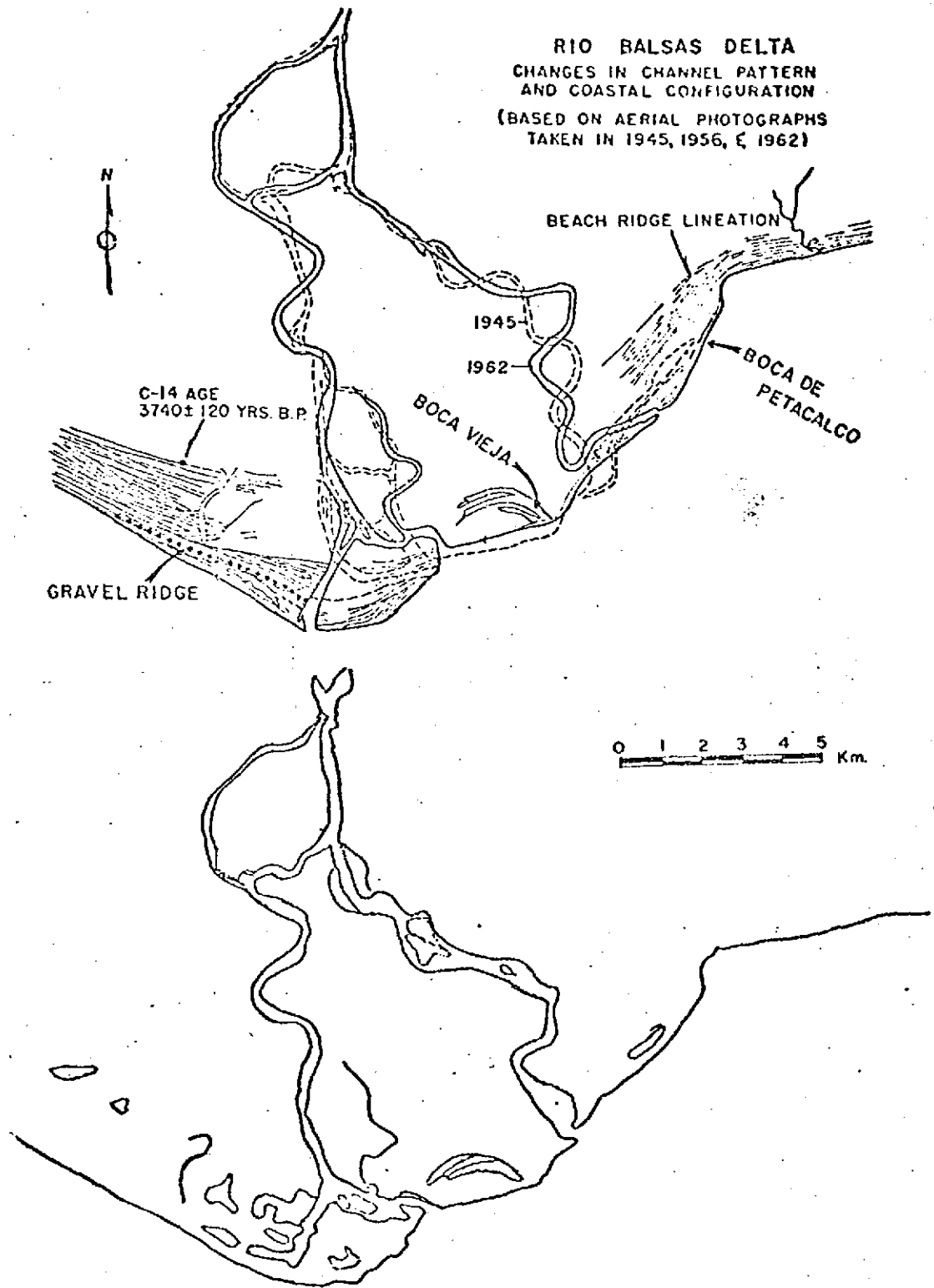


Figure 5. Changes in channel pattern and coastal configuration, compiled from (A) aerial photographs taken over a period of 17 years (1945-1962) - taken from Reimnitz and Gutiérrez-Estrada (1969), and (B) ERTS imagery obtained September 19, 1972 (no. E-1058-16451). Also shown (A) is beach-ridge lineation. Note gravel ridge, which probably is contemporaneous with the time at which the Boca de Petacalco was active, and location of shell sample, collected at a depth of 5 m below the oldest beach ridge.

In conclusion, ERTS imagery of the coastal zone of west-central Mexico may provide useful information about coastal morphology and dispersal of suspended sediment. However, more imagery and concurrent meteorological and oceanographic data must be obtained before meaningful interpretations can be made.

#### References Cited

- Carlson, P. R., and Harden, D. R., 1975, ERTS observations of surface currents along the Pacific Coast of the United States, in Principle sources and dispersal patterns of suspended particulate matter in nearshore surface waters of the northeast Pacific Ocean, Carlson, P. R., Conomos, T. J., Janda, R. J., and Peterson, D. H., eds.: ERTS-1 Final Report, Natl. Tech. Info. Service, p. 100-126.
- Curry, J. R., Emmel, F. J., and Crampton, J. J. S., 1969, Holocene history of a strandplain, lagoonal coast, Nayarit, Mexico: Lagunas Costeras, Un Simposio, Mem. Int. Symp. on Coastal Lagoons, UNAM-UNESCO, p. 63-100.
- Reimnitz, E., 1968, The Rio Balsas Submarine Canyons; Processes, History and Origin: Inst. Geol., Univ. Nacional Autonoma de Mexico, Interim Rept., 72 p.
- Reimnitz, Erk, and Gutierrez-Estrada, Mario, 1970, Rapid changes on the head of the Rio Balsas submarine canyon system, Mexico: Marine Geol., v. 8, p. 245-258.
- Roden, Gunnar I., 1964, Oceanographic Aspects of Gulf of California, in van Andel, T. H., and Shor, G. G., Marine Geology of the Gulf of California: AAPG Memoir 3, p. 30-58.

## Conclusions

ERTS imagery provides the synoptic, large area coverage important in the study of regional coastal zone problems. Knowledge gained from ERTS will be useful in control action vital in the event of large oil spills along the west coast between the port of origin in Prince William Sound and the port of destination be it Seattle, Portland or San Francisco-Oakland. The imagery is of sufficient resolution to allow the monitoring of plumes of suspended sediment which are discharged from the major west coast rivers. The dispersal patterns of these suspended sediments provide important details about movements of nearshore waters and transport of suspended matter introduced from natural or man-made sources, knowledge that is important for sediment budget studies. These studies are needed to properly locate waste effluent dischargers, to determine "safe" dump sites for dredge spoil, and to better understand erosional and depositional processes which will affect coastal construction and harbor dredging projects. In addition, knowledge of the coastal currents is of great importance to the marine biologists studying dispersal of larvae, fish roe, plankton and other marine organisms that have important roles in the food chain.

The 18-day cycle of ERTS imagery is useful for seasonal studies of circulation of coastal water. However, the rapid changes in the marine environment that result from severe storms would only be observed by ERTS fortuitously.

Resolution of ERTS imagery is less than 50 meters for linear features and is therefore useful to the geologist in reconnaissance mapping of large areas. This large areal coverage often can provide a perspective that will permit delineation of faults or other lineaments that are not observable on large scale aerial photographs. However, the limited resolution of ERTS imagery restricts its use in geologic mapping to that of a useful tool adjunct to conventional aerial photography.

All four bands of the multispectral scanner are valuable, but for different purposes. Band seven (0.8-1.1  $\mu\text{m}$ ) most clearly delineates water and land boundaries and is the most useful for distinguishing geologic features. Band four (0.5-0.6  $\mu\text{m}$ ) because of its better water penetrating capability provides the most complete picture of plumes of turbid river water discharged into ocean water. Band five (0.6-0.7  $\mu\text{m}$ ), however, is superior to four in delineating circulation patterns when the turbidity level is extremely high as is common in estuaries or at the mouths of rivers in flood. Band five also shows the best enhancement of snow boundaries. Band six (0.7-0.8  $\mu\text{m}$ ) was used the least in our

studies. However, when used in conjunction with the other three bands it sometimes provided reinforcement to suspended sediment patterns seen on bands four and five in that it allowed us to determine the exact effluent point of plumes of water when the turbidity was very high and the effluents were relatively close together.

## Appendix

### Papers associated with ERTS experiment

- Carlson, P. R., 1972, Principal sources and dispersal patterns of suspended particulate matter in nearshore surface waters of the northeast Pacific Ocean and the Hawaiian Islands: Type I Progress Rept., Natl. Technical Information Service E 72-10271, 4 p.
- \_\_\_\_\_, 1973, Principal sources and dispersal patterns of suspended particulate matter in nearshore surface waters of the northeast Pacific Ocean and the Hawaiian Islands: ERTS Type I Progress Rept., Natl. Technical Information Service E 73-10314, 5 p.
- \_\_\_\_\_, 1973, Principal sources and dispersal patterns of suspended particulate matter in nearshore surface waters of the northeast Pacific Ocean and the Hawaiian Islands. ERTS Type I Progress Rept., Natl. Technical Information Service E 73-10788, 9 p.
- \_\_\_\_\_, 1974, Surface currents along the California coast observed on ERTS imagery: Summary papers of Ninth International Symposium on Remote Sensing of Environment, Ann Arbor, Michigan, April, 1974, p. 138.
- \_\_\_\_\_, 1974, Turbid nearshore waters of the Northeast Pacific: Tracers of surface current flow, in Selective guide to operational and scientific uses of ERTS, Williams, R. S., Jr., and Carter, W. D., eds.: Washington, U.S. Dept. of Interior (In press).
- \_\_\_\_\_, 1974, ERTS imagery of northern California coastal currents: Photo Interpretation, Paris, France, Juillet-Août, TECHNIP (In press).
- \_\_\_\_\_, 1974, Surface currents along the California coast observed on ERTS imagery: Proceedings of the Ninth Int. Symposium on Remote Sensing of Environment, Ann Arbor, Univ. of Michigan press (In press).
- Carlson, P. R., Conomos, T. J., Janda, R. J., and Peterson, D. H., 1973, Principal sources and dispersal patterns of suspended particulate matter in nearshore surface waters of the northeast Pacific Ocean and the Hawaiian Islands: ERTS Type II Progress Rept., Natl. Technical Information Service E 73-10487, 9 p.
- Carlson, P. R., and Harden, D. R., 1973, Principal sources and dispersal patterns of suspended particulate matter in nearshore surface waters of the northeast Pacific Ocean and seasonal variation in snow cover in the Sierra Nevada: ERTS Type I Progress Rept., Natl. Technical Information Service E 73-11099/WR, 14 p.
- Carlson, P. R., and Janda, R. J., 1974, Principal sources and dispersal patterns of suspended particulate matter in nearshore surface waters of the northeast Pacific Ocean: ERTS Type II Progress Rept., Natl. Tech. Info. Servid E 74-10186, 12 p.

- Carlson, P. R., Janda, R. J., and Conomos, T. J., 1973, Observations of suspended particle patterns in nearshore northeastern Pacific Ocean waters by ERTS-1 imagery: Symposium on Significant Results Obtained from ERTS-1, NASA/Goddard Space Flight Center, Greenbelt, Maryland, p. 145.
- Carlson, P. R., and McCulloch, D. S., 1974, Aerial observations of suspended-sediment plumes in San Francisco Bay and the adjacent Pacific Ocean: U.S. Geol. Survey Jour. Research, v. 2, no. 5, p. 519-526.
- Carlson, P. R., and Reimnitz, Erk, 1973, Study of river effluents and coastal water circulation off the west coast of North America using ERTS-1 data, GSA-Cordilleran Section, Portland, Oregon, March 1973: Geol. Soc. America Abs. with Programs, v. 5, p. 20.
- Clifton, H. E., 1974, Storm deposits off a high-energy coast: Geol. Soc. America Abs. vol. (In press).
- Clifton, H. E., Hunter, R. E., and Phillips R. L., 1972, Depositional models from a high-energy coast: Am. Assoc. Petroleum Geologists Bull. 56, p. 609.
- Clifton, H. E., Phillips, R. L., and Hunter, R. E., 1973, Depositional structures and processes in the mouths of small coastal streams, Southwestern Oregon, in Coaster, D. A., ed., Coastal Geomorphology, Chpt. 6, published in Geomorphology: State Univ. N.Y., Binghamton Press, p. 115-140.
- Conomos, T. J., 1974, Movement of spilled oil as predicted by estuarine nontidal drift: Limnology and Oceanography (In press).
- Conomos, T. J., and Peterson, D. H., 1973, Seasonal circulation and suspended particle transport patterns, San Francisco Bay, California: Program and abs., Symposium: Internat. Relations Sedimentaires of Entre Estuaires et Plateaux, Institut de Geologie du Bassin d'Aquitaine, July 1973, p. 26-27.
- Conomos, T. J., and Peterson, D. H., 1974, Chemical and biological features of the San Francisco Bay turbidity maximum: 37th Annual Meeting, American Society of Limnology and Oceanography, Seattle, June 1974, p. 17.
- Conomos, T. J., Peterson, D. H., and McCulloch, 1973, Seasonal non-tidal drift patterns, San Francisco Bay, California [abs.]: Am. Geophys. Union Trans., v. 54, no. 4, p. 303.
- Janda, R. J., 1971, An evaluation of enhancement of light intensity differences on color aerial photographs and thermal infrared imagery for the Ozette Island-Cape Alava Area of the Olympic Coast of western Washington: Interagency Report NASA-187, 17 p and 7 fig. (Forwarded to NTIS).

- \_\_\_\_\_, 1972, Sedimentation, erosion and man - Coastal southwestern Oregon [abs.]: Program of 68th Annual Meeting Cordilleran Section of Geol. Soc. America, Honolulu, Hawaii, p. 179.
- \_\_\_\_\_, 1972, Testimony concerning stream sediment loads in northern California and southern Oregon presented in public hearings before the California Regional Water Quality Control Board, north coast region in Eureka, California on July 19, 1972: Mimeographed report on file with State Board and other interested parties, 24 p.
- \_\_\_\_\_, 1974, A geologic look at the soils of the Douglas-Fir region, in U.S. Forest Service, Soils of the Douglas-Fir Region, 9 p. (in press).
- \_\_\_\_\_, 1974, Preliminary report on natural and man-induced threats to the Redwood Creek corridor of Redwood National Park, Humboldt County, California: U.S. Geological Survey Open-file report, approx. 50 p. (In press).
- MacLeod, N. S., 1972, Coastline and geology of the area between Port Valdez, Alaska, and west coast ports, in Final environmental impact statement, proposed trans-Alaska pipeline, U.S. environmental setting between Port Valdez, Alaska, and west coast ports, p. 6-65.
- Nelson, C. Hans, 1973, Sediment and mercury dispersal through estuary, shoreline, and epicontinental shelf environments of the northeast Bering Sea: Symposium International, Relations Sedimentaires Entre Estuaries Et Plateaux Continentaux, Bordeaux, France, p. 65.
- Nelson, C. H., Larson, B. R., and Rowland, R. W., 1973, Late Holocene sediment dispersal in northeastern Bering Sea: Transactions, Am. Geophys. Union, v. 54, p. 1122.
- Nelson, C. H., McManus, D. A., Venkatarathnam, Kolla, and Hopkins, D. M., 1974, Yukon River sediment on the northernmost Bering Sea shelf: Jour. Sed. Petrology (In preparation).
- Peterson, D. H., Conomos, T. J., and Broenkow, W. W., 1973, Seasonal distribution of dissolved silica in temperate estuaries: Second International Estuarine Conference, October, 1973, p. 3.
- Peterson, D. H., Conomos, T. J., Broenkow, W. W., and Doherty, P. C., 1973, Location of density-current stagnation, San Francisco Bay estuary [abs]: Am. Geophys. Union Trans., v. 54, no. 4, p. 302.
- Peterson, D. H., Conomos, T. J., Broenkow, W. W., and Doherty, P. C., 1974, Location of the non-tidal null zone in San Francisco Bay: Estuarine and Coastal Marine Science (In press).
- Peterson, D. H., Conomos, T. J., Broenkow, W. W., and Scrivani, E. P., 1974, Processes controlling the dissolved silica distribution in San Francisco Bay: Second Internat. Estuarine Conf. (In Press).

Snively, P. D., Jr., MacLeod, N. S., and Wagner, H. C., 1973, Miocene Tholeiitic basalts of coastal Oregon and Washington and their relations to coeval basalts of the Columbia Plateau: Geol. Soc. America Bull., v. 84, p. 387-424.

Snively, P. D., Jr., Tiffin, D. L., MacLeod, N. S., and Curry, R. G., 1974, Preliminary gravity and magnetic maps of the Strait of Juan de Fuca, British Columbia, Canada, and Washington, United States: U.S. Geol. Survey Open-file report, 10 p. 3 figs.